

**ENGINEERING A NOVEL CYP119 WITH HIGH  
BIOCATALYTIC EFFICIENCY BY  
OPTIMIZATION OF PROTEIN INTERACTIONS  
AND ELECTRON TRANSFER**

**A Thesis Submitted to  
the Graduate School of Engineering and Sciences of  
İzmir Institute of Technology  
in Partial Fulfillment of the Requirements for the Degree of**

**DOCTOR OF PHILOSOPHY**

**in Bioengineering**

**by  
Akbotu KAKIMOVA**

**July 2024  
İZMİR**

We approve the thesis of **Akbota KAKIMOVA**

**Examining Committee Members:**

---

**Assoc. Prof. Dr. Nur Bařak SÜRMEĻİ ERALTUĐ**  
Bioengineering Department, İzmir Institute of Technology

---

**Assist. Prof. Dr. Hümeıra TAŐKENT SEZGİN**  
Bioengineering Department, İzmir Institute of Technology

---

**Assist. Prof. Dr. Yavuz OKTAY**  
Department of Medical Sciences, Dokuz Eylül University

---

**Assoc. Prof. Dr. Ali OĐuz BÜYÜKKİLECI**  
Food Engineering Department, İzmir Institute of Technology

---

**Assoc. Prof. Dr. Burcu KAPLAN TÜRKÖZ**  
Food Engineering Department, Ege University

**09 July 2024**

---

**Assoc. Prof. Dr. Nur Bařak  
SÜRMEĻİ ERALTUĐ**  
Supervisor, Bioengineering Department,  
İzmir Institute of Technology

---

**Assoc. Prof. Dr. Sinan GÜVEN**  
Co-Supervisor, Department of Medical  
Sciences, Dokuz Eylül University

---

**Assoc. Prof. Dr. Ceyda ÖKSEL KARAKUŐ**  
Head of Bioengineering Department

---

**Prof. Dr. Mehtap EANES**  
Dean of Graduate School of  
Engineering and Science

## ACKNOWLEDGEMENTS

I would like to first and foremost thank my advisor, Assoc. Prof. Dr. Nur Bařak SÜRMEĻİ ERALTUĐ. Joining your lab changed the trajectory of my life forever and I am thankful to have been given the opportunity to work with you. Your continuous support, wisdom, guidance helped me through challenging path in my graduate career. I could not have imagined having a better advisor and mentor for my PhD studies. This work would not have been possible without your tutelage, your invaluable insights and supervision.

I would like to express my sincere gratitude to my thesis committee members, Assist. Prof. Dr. Hümeyra TAŐKENT SEZĐİN and Assist. Prof. Dr. Yavuz OKTAY, and my co-advisor, Assoc. Prof. Dr. Sinan GÜVEN, for your time and contribution to my research. Your immense expertise and very delicate approach have encouraged me and kept me focused on my goals. It was absolute pleasure to share my progress with you and get inspired by you throughout my studies.

I must also express my heartfelt thanks to YTB Scholarship Program for graduate study opportunities and sponsorship, for experience to work with the brightest people. Additionally, I want to thank Prof. Dr. Engin ÖZÇİVİCİ, Prof. Dr. Volga BULMUŐ, Assoc. Prof. Dr. Hüseyin Cumhuri TEKİN, Prof. Dr. Almagul KUSHUGULOVA for their mentorship and support during my studies. As well as Prof. Dr. Erdal BEDİR, Assist. Prof. Dr. Hümeyra TAŐKENT SEZĐİN, Prof. Dr. ÇaĐlar KARAKAYA, Assoc. Prof. Dr. Burcu KAPLAN TÜRKÖZ, Assoc. Prof. Dr. Alper ARSLANOĐLU, Assoc. Prof. Dr. Muse OKE, Assoc. Prof. Dr. Ali OĐuz BÜYÜKKİLECİ, who helped me by providing the lab equipment and reagents that were necessary.

I also wish to convey my appreciation to my lab mates, Ekin KESTEVUR DOĐRU, TuĐçe SAKALLI, Burçin KARABEY and Alper őAHİN for a cherished time spent together in the lab.

I also thank my parents, Bayan KOISHUYEVA, Berikzhan KOISHUYEV, parents-in-law, Altyn ASSANGALIYEVA, Alibek AGLAKOV and my sisters, Balzhan KARIMOVA, Nadira KAKIMOVA, my sister-in-law Aryana ALBOVA, my brothers-in-law, Daniyar KARIMOV, Dmitry ALBOV, my aunt Karima KOICHIYEVA, and my grandmother for the unceasing encouragement, support and attention.

I am grateful to my husband and my best friend, Aibek ALIBEKULY who supported me through this journey, for his endless love, patience and unwavering support. I am indebted to you for everything, for your emotional support, steadfast belief in me during downs. Thank you for being my comfort person, for lending an ear to my complains, for the right words, for unconditional love and for being my inspiration.

Finally, I wish to acknowledge my precious baby. I am blessed to have my son, Amir AIBEKULY, my constant source of motivation, my unique, brave, gentle baby. I am extremely thankful and sorry for all of the sacrifices that you have made on my behalf. I love you so much and I am so proud of you. Being your mom is my most important and rewarding title.

## ABSTRACT

### ENGINEERING A NOVEL CYP119 WITH HIGH BIOCATALYTIC EFFICIENCY BY OPTIMIZATION OF PROTEIN INTERACTIONS AND ELECTRON TRANSFER

Cytochrome P450s are the perfect choice for many biotechnological applications. The requirement for costly electron donors (NAD(P)H), redox partners, and uncoupling, the process of formation of reactive oxygen species instead of desired products, are limitations of P450s' extensive utilization. By selecting the best redox partners, and utilizing site-directed mutagenesis to improve protein-protein interaction, a novel P450 enzyme with increased activity can be obtained.

Thermophilic CYP119 obtained from *Sulfolobus acidocaldarius* has a high potential as biocatalyst. In the current research, protein-protein interaction between electron transfer partner of P450cam, putidaredoxin (Pdx) and CYP119 was examined and their electron transfer efficiency was improved by rational design. Using PyRosetta Software, 14 mutants were created, using Rosie Docking Server, docking analysis were performed. The best models, N34E, D77R and N34E-D77R mutations were performed with site-directed mutagenesis method. Difference spectroscopy of substrate (lauric acid) binding to WT and mutant CYP119 revealed  $K_d$  values of 19  $\mu\text{M}$ , 35  $\mu\text{M}$ , 23  $\mu\text{M}$  and 87  $\mu\text{M}$  in WT CYP119, N34E, N34E-D77R and D77R mutant, respectively.

The reported  $K_d$  for Pdx binding for WT is 2100  $\mu\text{M}$ . Difference spectra of Pdx binding to WT CYP119 and mutants were followed to obtain dissociation constants. The observed  $K_d$  values for WT CYP119 and N34E, D77R, N34E-D77R mutants were 2390  $\mu\text{M}$ , 112  $\mu\text{M}$ , 797  $\mu\text{M}$  and 200  $\mu\text{M}$ , respectively.

These outcomes offer solid evidence that the N34E, N34E-D77R mutants bind to Pdx with higher affinity, thus, showing an increase in electron-transfer rate for 21-fold in N34E and 12-fold N34E-D77R mutation in CYP119-Pdx-PdR system.

## ÖZET

### PROTEİN ETKİLEŞİMLERİNİN VE ELEKTRON TRANSFERİNİN OPTİMİZASYONU YOLUYLA YÜKSEK BİYOKATALİTİK VERİME SAHİP YENİ BİR CYP119 MÜHENDİSLİĞİ

Sitokrom P450 enzimleri, birçok biyoteknolojik uygulama için mükemmel bir seçimdir. P450 sistemlerinin daha geniş uygulamalarını sınırlayan çeşitli zaafı vardır; redoks partner proteinleri yoluyla NAD(P)H'den elektron transferine duyulan ihtiyaç nedeniyle bu sistemlerin karmaşıklığı, NAD(P)H oksidasyonu ile ürün oluşumu arasındaki kopukluk gibi. Yüksek aktiviteye sahip rekombinant P450 enzim sistemleri, optimum redoks partnerleri seçilerek, bölgeye yönelik mutajenez kullanılarak veya farklı redoks ortakları denenerek elde edilebilir.

P450'ler arasında ısıya dayanıklı asidotermofilik *Sulfolobus acidocaldarius* arkesinden elde edilen CYP119 enziminin biyokatalizör olarak potansiyeli yüksektir. Bu çalışmada, elektron transfer partneri, putidaredoxin (Pdx) ve termofilik CYP119 enzimi arasındaki protein-protein etkileşim incelenmiş ve rasyonel tasarımla elektron transfer verimliliği iyileştirilmiştir. On dört çeşit mutantlar tasarımı, PyRosetta Yazılımı kullanılarak, Rosie Docking Server ile docking yapıldı. Elde edilen sonuçlara göre, deneysel işlemler için N34E, D77R, N34E-D77R mutasyonları seçildi. CYP119 ve N34E, N34E-D77R ve D77R mutantların laurik asitle bağlanmasının ayrışma sabitleri ( $K_d$ ) fark spektroskopisi ile 19  $\mu$ M, 35  $\mu$ M, 23  $\mu$ M ve 87  $\mu$ M olarak belirlendi.

CYP119 için Pdx bağlanmasına ilişkin literatürde bildirilen  $K_d$  değeri 2100  $\mu$ M. CYP119 ve N34E, N34E-D77R ve D77R mutantların Pdx ile bağlanmasının fark spektroskopisi ayrışma sabitleri ise 2440  $\mu$ M, 112  $\mu$ M, 200  $\mu$ M ve 797  $\mu$ M değerleri olarak gözlemlendi. Böylece N34E mutasyonunda elektron transfer hızı 21 kat, N34E-D77R mutasyonunda ise 12 kat artıyor. D77R mutasyonu Koo (2002) tarafından önerildiği gibi bağlanmada yaklaşık 4 kat artışı doğruladı.

Bu sonuçlar N34E ve N34E-D77R mutasyonlarının Pdx'e daha yüksek afiniteyle bağlandığına dair doğrudan kanıt sağlar. Bu CYP119-Pdx-PdR sisteminde elektron transfer hızında artış sağlar.

# TABLE OF CONTENTS

LIST OF FIGURES.....	x
LIST OF TABLES.....	xiii
LIST OF EQUATIONS.....	xiv
CHAPTER 1. INTRODUCTION .....	1
1.1. Cytochrome P450 Enzymes.....	1
1.1.1. Reactions Catalyzed by P450 Enzymes.....	3
1.1.2. Catalytic Cycle and Mechanism for Most Cytochrome P450 Enzymes.....	4
1.1.3. Structure of P450s: Active Site and Substrate Binding.....	7
1.1.4. Electron Transfer Systems in Cytochrome P450 Enzyme.....	11
1.1.5. Redox Partner Proteins.....	17
1.2. Biotechnological Applications of Cytochrome P450 Enzymes.....	23
1.2.1. Limitations of Cytochrome P450 Enzymes.....	26
1.3. Thermostable P450 Enzymes – CYP119.....	28
1.3.1. Reactions Catalyzed by CYP119.....	30
1.3.2. Secondary Structure of CYP119.....	32
1.3.3. Previous Studies on CYP119.....	35
1.3.4. Lauric Acid Hydroxylation.....	37
1.4. Cytochrome P450cam and Putidaredoxin Complex.....	39
1.4.1. Electron Transfer Pathway from Pdx/PdR to P450cam and CYP119.....	45
1.5. Protein Engineering and Design .....	46
1.5.1. Directed Evolution of Proteins.....	47
1.5.2. Rational Design of Proteins.....	48
1.6. Scope of the Study. Aims and Purposes.....	50
CHAPTER 2. METHODOLOGY.....	52
2.1. Bioinformatics Analysis.....	52
2.1.1. Structural Alignment of Proteins.....	52

2.1.2.	Design of CYP119 Mutant Enzymes .....	53
2.1.3.	Protein-Protein Docking .....	57
2.2.	Experimental Methods.....	60
2.2.1.	Site-Directed Mutagenesis Method for Construction of CYP119 Mutants.....	61
2.2.2.	Expression and Purification of WT and Mutant CYP119 Enzymes.....	65
2.2.3.	Expression and Purification of Redox Partner Proteins – Putidaredoxin (Pdx) and Putidaredoxin Reductase (PdR).....	67
2.2.4.	UV-Visible Spectral Analysis of WT and Mutant CYP119 Enzymes .....	70
2.2.5.	UV-Visible Spectral Analysis of Putidaredoxin and Putidaredoxin Reductase.....	71
2.2.6.	Lauric Acid Binding to WT and Mutant CYP119s: N34E, D77R, and N34E-D77R .....	73
2.2.7.	Putidaredoxin Binding to WT and Mutant CYP119s.....	74
2.2.8.	Assessment of Electron Transfer from Pdx to WT and Mutant CYP119s and Coupling Efficiency.....	75
2.2.9.	CO-binding to WT CYP119 and N34E, D77R Single Mutants and N34E-D77R Double Mutant.....	76
CHAPTER 3. RESULTS .....		78
3.1.	Structural Alignment of Proteins: CYP119 and P450cam .....	78
3.2.	Design of CYP119 Mutant Enzymes using PyRosetta Software.....	81
3.3.	Protein-Protein Docking using RosettaDock Server Rosie.....	83
3.4.	Construction of CYP119 Mutants using Site-Directed Mutagenesis Method.....	89
3.5.	Expression and Purification of WT and Mutant CYP119 Enzymes...	90
3.6.	Cloning, Expression and Purification of Redox Partner Proteins – Putidaredoxin (Pdx) and Putidaredoxin Reductase (PdR).....	92
3.7.	UV-Visible Spectral Analysis of WT and Mutant CYP119s.....	96
3.8.	UV-Visible Spectral Analysis of Putidaredoxin and Putidaredoxin Reductase.....	97



3.9. Lauric Acid Binding to WT and Mutant CYP119s.....	99
3.10. Putidaredoxin Binding to WT and Mutant CYP119s.....	101
3.11. Assessment of Electron Transfer from Pdx to WT and Mutant CYP119s and Coupling Efficiency.....	103
3.12. CO-binding to WT CYP119 and N34E, D77R Single Mutants and N34E-D77R Double Mutant .....	107
 CHAPTER 4. DISCUSSION.....	 110
 CHAPTER 5. CONCLUSION .....	 113
 REFERENCES .....	 116
 APPENDICES	
Appendix A.....	132
Appendix B.....	137
Appendix C.....	141

## LIST OF FIGURES

<u>Figure</u>		<u>Page</u>
Figure 1.1.	A. Three-dimensional CYP119 enzyme structure (PDBID: 1I07).....	2
Figure 1.2.	A fundamental catalytic cycle of P450s (Shaik & Dubey, 2021).....	5
Figure 1.3.	Helices of CYP119.....	8
Figure 1.4.	Cytochrome P450 system of transfer of electrons. Class I (Hannemann et al., 2007).....	12
Figure 1.5.	Cytochrome P450 electron transfer system. A. Class II B. Class III (Hannemann et al., 2007b).....	13
Figure 1.6.	Cytochrome P450 electron transfer system. A. Class IV, B. Class V, C. Class VI, D. Class VII (Hannemann et al., 2007b).....	14
Figure 1.7.	Cytochrome P450 electron transfer system. A. Class VIII, B. Class IX (Hannemann et al., 2007b).....	15
Figure 1.8.	Cytochrome P450 electron transfer system. Class X. (Hannemann et al., 2007b).....	16
Figure 1.9.	Putidaredoxin Cys73Ser/Cys85Ser mutant.....	18
Figure 1.10.	A. Putidaredoxin reductase.....	20
Figure 1.11.	A. Putidaredoxin and putidaredoxin reductase binding.....	22
Figure 1.12.	Lauric acid molecule (PubChem CID 3893).....	37
Figure 1.13.	CYP119 PDBID: 1I07. Hydroxylation reaction starts with substrate binding.....	38
Figure 1.14.	NADH oxidation/reduction.....	39
Figure 1.15.	A. P450cam (in purple)-Pdx (in gold) complex.....	41
Figure 1.16.	Directed evolution and rational design are compared.....	49
Figure 2.1.	Absorbance of WT Pdx and cysteine mutants of Pdx.....	72
Figure 2.2.	Absorbance of WT (solid) and His6 (dashed) PdR.....	73
Figure 3.1.	A. Structural alignment of proteins: CYP119 (PDB ID:1I07) in blue, Pdx (PDB ID:1XLN) in purple and P450cam-Pdx (PDB ID: 4JWS) in brown.....	79
Figure 3.2.	Interface score and RMSD values of WT and 14 mutant CYP119s.....	84
Figure 3.3.	Total energy and RMSD values of WT and 14 mutant CYP119s.....	85

<b><u>Figure</u></b>	<b><u>Page</u></b>
Figure 3.4. Distances between important residues of mutant CYP119s and Pdx complex.....	87
Figure 3.5. PCR products with mutated primers in 1% agarose gel.....	90
Figure 3.6. A. N34E single mutation; B.D77R single mutation; C. N34E-D77R double mutation.....	90
Figure 3.7. A. Expression of WT CYP119 observed by SDS-PAGE.....	91
Figure 3.8. A. Isolation of WT CYP119 was monitored by SDS-PAGE.....	92
Figure 3.9. Confirmation of obtained plasmids by digestion and agarose gel.....	93
Figure 3.10. Colonies obtained after transformation of plasmids containing genes coding for Pdx (A) and PdR (B).....	93
Figure 3.11. Expression of Pdx followed by SDS-PAGE.....	94
Figure 3.12. Expression of PdR followed by SDS-PAGE.....	94
Figure 3.13. Purification of Pdx followed by SDS-PAGE.....	95
Figure 3.14. Purification of PdR followed by SDS-PAGE.....	96
Figure 3.15. UV-Visible Spectra of WT and mutant CYP119s.....	97
Figure 3.16. A. UV-Visible spectra of Pdx.....	98
Figure 3.17. UV-Visible spectra of PdR obtained in the current study.....	98
Figure 3.18. Lauric acid binding to WT and mutant CYP119s.....	100
Figure 3.19. Difference spectra of Pdx binding to WT CYP119 (A); N34E CYP119 (B); N34E-D77R CYP119 (C); D77R CYP119 (D) .....	101
Figure 3.20. The binding of Pdx to WT, N34E, N34E-D77R and D77R CYP119 enzymes observed by difference spectra. Non-linear fitting of $\Delta$ Abs and Pdx concentration .....	102
Figure 3.21. NADH consumption by WT CYP119 (orange), N34E (pink), N34E-D77R (blue), D77R (green) mutations over time.....	104
Figure 3.22. NADH consumption by Control 1 – in the absence of CYP119 (orange), Control 2 – in the absence of lauric acid (pink), Control 3 – in the absence of Pdx (blue) over time.....	104
Figure 3.23. H <sub>2</sub> O <sub>2</sub> formation in a reaction with WT CYP119 (orange), N34E (pink), N34E-D77R (blue), D77R (green) mutations over time, 570 nm was followed for resorufin production.....	105

<b><u>Figure</u></b>	<b><u>Page</u></b>
Figure 3.24. H <sub>2</sub> O <sub>2</sub> formation in a reaction with Control 1 – in the absence of CYP119 (orange), Control 2 – in the absence of lauric acid (pink), Control 3 – in the absence of Pdx (blue), over time, 570 nm was followed for resorufin production.....	106
Figure 3.25. Reduced CO-bound WT and mutant CYP119s. WT (orange); N34E (pink); N34E-D77R (blue); D77R (green); Dithionite reduced sample (purple).....	108
Figure B.1. Sequencing analysis results of mutated DNA A. N34E mutant B. N34E-D77R mutant C. D77R mutant.....	140
Figure C.1. Plasmid map of pPdx (catalog numbers #85084) (Suzuki, 2014).....	141
Figure C.2. Plasmid map of pPdR (catalog numbers #85083) (Suzuki, 2014).....	142

## LIST OF TABLES

<b><u>Table</u></b>	<b><u>Page</u></b>
Table 2.1. Primers' melting temperatures, molecular weights, total nmols.....	62
Table 2.2. PCR reaction mixture use: concentration and volumes of reactants ( <a href="https://www.neb.com/en/protocols">https://www.neb.com/en/protocols</a> ).....	63
Table 2.3. PCR cycling conditions ( <a href="https://www.neb.com/en/protocols">https://www.neb.com/en/protocols</a> ).....	63
Table 2.4. KLD reaction mixture: concentration and volumes of reactants ( <a href="https://www.neb.com/en/protocols">https://www.neb.com/en/protocols</a> ).....	64
Table 2.5. Buffers used in CYP119 protein purification.....	66
Table 2.6. Single digestion reaction components.....	67
Table 2.7. Buffers used in PdR and Pdx proteins purification.....	69
Table 3.1. The list of mutations selected for mutant design process.....	80
Table 3.2. Amino acids that were used for creating mutations.....	81
Table 3.3. Total energies (REU) of WT CYP119 and created CYP119 mutants.....	82
Table 3.4. Docking results of Pdx and WT/mutants CYP119 using Rosie Docking Server.....	83
Table 3.5. Distances between key residues of docked Pdx with mutants of CYP119, compared to docked Pdx with wild type CYP119, as well as compared to crystal structure of P450cam-Pdx complex (PDB ID: 4JWS).....	88
Table 3.6. $K_d$ values of substrate (lauric acid) binding to WT and mutant CYP119s.....	99
Table 3.7. Effect of Mutations on binding Pdx to CYP119.....	102
Table 3.8. Reaction mixture for NADH consumption and hydrogen peroxide formation reaction.....	103
Table 3.9. Concentrations of NADH consumed and formed $H_2O_2$ in reaction.....	107
Table 3.10. Concentrations of CO-complexed reduced CYP119 proteins.....	108
Table A.1. The list of bacterial culture mediums used in current research .....	132
Table A.2. The list of proteins and their PDBIDs used in alignment analysis.....	133
Table A.3. The list of antibiotics used in current research.....	133
Table A.4. The list of Buffers used in current research.....	134

## LIST OF EQUATIONS

<u>Equation</u>	<u>Page</u>
Equation 1.1. The most typical reaction catalyzed by P450 enzymes. SH depicts Substrate, NAD(P)H – electron donor, SOH – oxidized product (Guengerich, 2018).....	4
Equation 1.2. The P450 system's rate of transferring of electrons via its redox components (Lewis & Pratt, 1998).....	7
Equation 2.1. <b>A</b> is the absorbance (for instance $A_{280}$ ); $\epsilon$ is extinction coefficient, unit $M^{-1}cm^{-1}$ ; <b>c</b> is concentration of protein in M; <b>l</b> is the length of the cuvette/microplate in cm.....	72
Equation 2.2. Calculation of $K_d$ and $A_{max}$ values.....	75
Equation 2.3. Formula for calculation of reduced and CO-complexed CYP119 concentration. Where $(\Delta A_{450} - A_{490})_{reduced, CO}$ – absorbance at (450 – 490 nm) when reduced using dithionite reduced, CO sample (Stresser, 2021).....	78

# CHAPTER 1

## INTRODUCTION

### 1.1 Cytochrome P450 Enzymes

Cytochrome P450s are remarkably complex enzymes functioning as an external monooxygenase that utilize an external reductant in their reactions (Bernhardt & Urlacher, 2014). Cytochrome P450s (CYPs or P450s) contain heme B as a cofactor and obtain the P450 name from their exceptional spectral properties (Bernhardt & Urlacher, 2014). P450s show a Soret band, an absorption peak at 450 nm when its reduced and bound with carbon monoxide (CO) (Bernhardt, 2006). While all hemoproteins show the maximum band of absorbance within 380-420 nm (Bernhardt, 2006), in binding of thiolate sulfur to the iron and significant perturbation of heme causes the shift in Soret band of about 30 nm. Whilst P denotes pigment (Guengerich, 2018).

Presently, the cytochrome P450 superfamily has a large number of identified members, according to Bernhardt and Urlacher (2014), there are more than 21,000 members (Bernhardt & Urlacher, 2014). Almost 4000 cytochrome P450 genes are identified in total (Denisov et al., 2005) and 57 genes have been discovered to code human cytochrome P450s (Sutcliffe et al., 2005; Winkler et al., 2018). Around 822 X-ray crystal structures are currently available (Guengerich, 2018). The Nelson website provides sequence information for all the hemoproteins belonging to the cytochrome P450 superfamily (<http://drnelson.utmem.edu/CytochromeP450.html>) (Nelson, 2009).

These exceptional P450s can be found in almost all kingdoms of life and in almost any tissue: liver, kidney, lungs, intestinal wall, plasma and even brain, but they have not been yet found in *Escherichia coli* (Denisov et al., 2005; McDonnell, 2013; Miller et al., 2023). In eukaryotes the endoplasmic reticulum membrane contains the predominant part of the cytochrome P450s, with the enzyme's catalytic domain located in the cytosol.

Beside these, mitochondrial P450s have also been reported to be attached to the inner membrane of mitochondria (Winkler et al., 2018).

Every member of the cytochrome P450s family share the same three-dimensional structure, yet they have only 20% resemblance in their sequence (Denisov et al., 2005). Figure 1.1 illustrates the 3D structure of CYP119 (PDBID: 1I07).

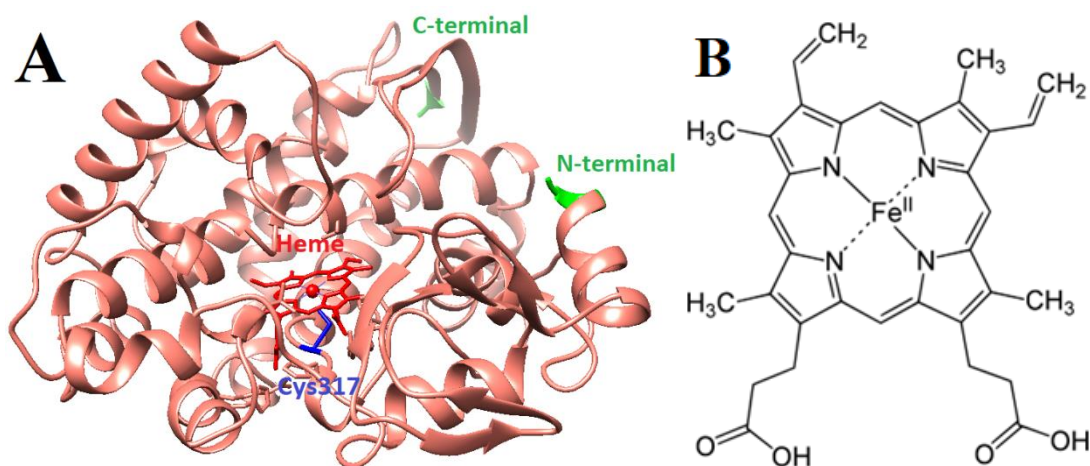


Figure 1.1. A. Three-dimensional CYP119 enzyme structure (PDBID: 1I07). CYP119 contains heme cofactor (shown in red), that binds the thiolate group of the Cys residue (shown in blue) in the proximal side of protein. N-terminal and C-terminal are shown in green. The image was created with UCSF Chimera. B. Chemical structure of Heme B cofactor.

P450s can be categorized by resemblance in their DNA sequences and they are differentiated by their family number (CYP101, CYP119), then subfamily letter (CYP101A, CYP3A), and also by an isoform quantity or specific enzyme (CYP3A37, CYP6A8) (McDonnell, 2013). One of the members of this broad superfamily, cytochrome P450 BM3 from *Bacillus megaterium*, which is referred as CYP102A1, is the most well-studied cytochrome P450 enzyme (Li et al., 2007).

Cytochrome P450s catalyze over 95% of known oxidation and reduction reactions; most P450 processes involve oxidation and necessitate the presence of molecular oxygen (Guengerich, 2018). The reductive cleavage of oxygen molecules (O<sub>2</sub>) attached to iron of cytochrome P450 and the subsequent transport of single electron twice



to the heme iron at specific times during the catalytic cycle are characteristics of the monooxygenase activity of enzymes (McLean et al., 2015).

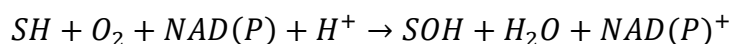
### **1.1.1. Reactions Catalyzed by P450 Enzymes**

Numerous endogenous and exogenous substances can be activated or inactivated by oxidative transformations and the cytochrome P450s, or CYPs, catalyze these processes (Goldstone et al., 2010). In the broadest terms, P450 oxygenases have two primary functional tasks as reported by Denisov et al., (2005). One is the metabolism of exogenous compounds – xenobiotics and drug metabolism, as a protective function of breakdown or as a preparation before excretion. The second major functional purpose is the creation of vital signaling molecules that regulate development and homeostasis, for instance, the production of steroid hormones, the metabolism of fat-soluble vitamins, as well as the transformation of polyunsaturated fatty acids into physiologically active compounds, the breakdown of herbicides and hormone biosynthesis in plants, and in insects – the improvement of resistance to pesticides. An expansive range of challenging biotransformations can be effectively catalyzed by P450s (Denisov et al., 2005). P450s are crucial for homeostasis of bile acid, synthesis of steroids, vitamin D formation, and the synthesis of numerous hormones (Goldstone et al., 2010).

P450s can efficiently regioselectively and stereoselectively catalyze enormous variety of oxidative processes (McLean et al., 2015; Wei, 2019). The most common 21 different reactions catalyzed by cytochrome P450 have been summarized (Bernhardt & Urlacher, 2014), these exceptional catalysts are involved in many significant reactions such as carbon hydroxylation, epoxidations (Bernhardt & Urlacher, 2014; Niemeyer, 2008), dealkylations and heteroatom oxygenations, as well as other atypical reactions such as reductions, desaturations, and isomerization (Niemeyer, 2008; Winkler et al., 2018), oxidative phenolic coupling (Niemeyer, 2008).

P450s are capable of catalyzing metabolism of drugs (McDonnell, 2013; Winkler et al., 2018), steroid biosynthesis (Denisov et al., 2005; Beilen et al., 2003; Winkler et al., 2018), metabolism of xenobiotics (Denisov et al., 2005; McDonnell, 2013; Winkler et al., 2018), synthesis of valuable drugs such as progesterone, cortisone, pravastatin (Beilen et

al., 2003; Winkler et al., 2018), 4-hydroxyproline (Beilen et al., 2003), and are crucial for the synthesis of other substances that are vital to physiological processes (Winkler et al., 2018). P450s are also involved in the conversion of polyunsaturated fatty acids and vitamins into physiologically active substances (Bernhardt & Urlacher, 2014; Denisov et al., 2005), herbicide and insecticide degradation (Denisov et al., 2005), oxyfunctionalization of antibiotics, terpenes, alkanes and alkaloids (Bernhardt & Urlacher, 2014) and many more. P450s catalyze hydroxylation reactions, additionally N-, O-, and S-dealkylation reactions (Bernhardt & Urlacher, 2014), sulfoxidation (Beilen et al., 2003), epoxidation (Beilen et al., 2003), N-oxide reduction, peroxidation, deamination, desulfuration, and dehalogenation (Denisov et al., 2005). A large number of P450 enzymes take part in the production of secondary metabolites, These enzymes require nicotinamide adenine dinucleotide phosphate hydrogen (NADPH) (Beilen et al., 2003). Commonly, P450s catalyze the addition of a single oxygen atom of O<sub>2</sub> to both endogenous and exogenous substrates for a variety of oxidative processes via the traditional two-electron oxo-transfer pathway (Wei, 2019). Most commonly P450s catalyze the reaction shown in Equation 1.1 (Guengerich, 2018).



Equation 1.1. The most typical reaction catalyzed by P450 enzymes. SH depicts Substrate, NAD(P)H – electron donor, SOH – oxidized product (Guengerich, 2018).

### **1.1.2. Catalytic Cycle and Mechanism for Most Cytochrome P450 Enzymes**

Cytochrome P450's common catalytic cycle was first proposed in 1968 and the existence of intermediates and as well as the successive two-electron reduction of these enzymes were first reported in bacterial cytochrome P450 CYP101, commonly known as P450cam (Denisov et al., 2005). The cytochrome P450 catalytic mechanism primarily

considers the condition of oxygen and heme iron (Denisov et al., 2005). A fundamental catalytic cycle of P450s is represented in Figure 1.2.

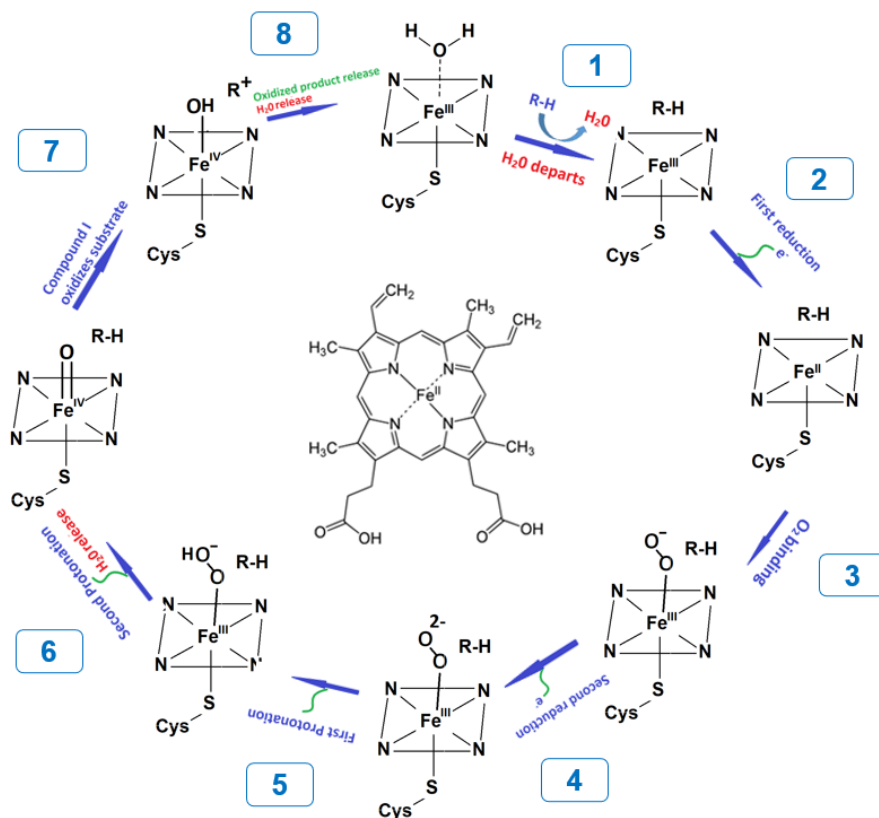


Figure 1.2. A fundamental catalytic cycle of P450s. I. Substrate Binding. II. First reduction and formation of  $\text{Fe}^{2+}$ . III. Oxygen Binding and formation of  $\text{Fe}^{3+}\text{-OO}^-$  (Autoxidation may occur here). IV. Second reduction and formation of  $\text{Fe}^{3+}\text{-OO}^{2-}$ . V. First protonation and formation of  $\text{Fe}^{3+}\text{-OOH}^-$  (Hydrogen peroxide can be formed here). VI. Second protonation and formation of Compound I (Two water molecules can be formed here). VII. The process involves removing a H atom from R–H and transforming it into a ferrohoxo intermediate. The next step, VIII, the latter then produces alcohol (R–OH) through R rebound. A water molecule replaces the R–OH as it leaves the pocket region via one of the distal side exits. The enzyme now returns to its resting state and prepares for a new turnover (Shaik & Dubey, 2021).

1. According to McIntosh et al., (2014), the catalytic cycle starts with the resting state of the enzyme, the ferric enzyme in low-spin state. A water molecule is bound to the iron from distal side as the sixth ligand. In the first step ferric enzyme binds the substrate displacing water molecules (McIntosh et al., 2014). As reported by Wang et al., (2007), substrate binding leads to the changes in the spin state: from low-spin state to the high-spin state, which has more positive reduction potential. CYP101 with the high spin  $\text{Fe}^{3+}$  is able to be reduced to a ferrous state considerably more easily. Yet, shifting of a spin state is not a necessary aspect of the first cycle (Wang et al., 2007).

2. Shaik and Dubey (2021) reported that ferrous state quickly binds an  $\text{O}_2$  molecule and which then changes into the oxyferrous complex. Binding of oxygen with ferrous heme iron leads to a relatively stable intermediate – oxy-P450 complex or oxygenated heme  $\text{Fe}^{2+}\text{-OO}$  or  $\text{Fe}^{3+}\text{-OO}^-$  (Shaik & Dubey, 2021).

3. The reduction of oxy-P450 complex forms several intermediates: a)  $\text{Fe}^{3+}\text{-OO}^2$ , peroxo-ferric intermediate and b)  $\text{Fe}^{3+}\text{-OOH}^-$  hydroperoxo-ferric intermediate, the state of an “a)” when protonated (Krest et al., 2013).

4. The latter  $\text{Fe}^{3+}\text{-OOH}^-$  complex is protonated second time at the oxygen atom from distal side and generate an unsteady transitory  $\text{Fe}\text{-OOH}_2$ , then subsequently occurring of O-O bond heterolysis and Compound I and  $\text{H}_2\text{O}$  are formed (Wang, 2007);

5. The last step of the cycle is the oxygenation of the substrate to yield a product complex (Denisov et al., 2005; Lewis & Pratt, 1998; McLean et al., 2015).

The heme iron–oxygen complex generally termed Compound I, formally  $\text{FeO}^{3+}$  have a high oxidation–reduction potential. The majority of P450 oxidations are considered to happen through Compound I (Denisov et al., 2005). The mechanism of P450 is a complex reaction, that involves supporting proteins that are redox partners and consumption of reducing agents, and most of cytochrome P450 enzymes use pyridine nucleotide usually NADH or NAD(P)H as a cofactor (Guengerich, 2018).

Multiple side reactions could, nevertheless, occur (Guengerich, 2018). Three major reactions are:

1. Autoxidation shunt. The first unproductive pathway in P450 catalysis is called autoxidation, in which the enzyme produces a superoxide anion instead of products and then returns to its ferric resting state (Luthra et al., 2011). For majority of P450s, the primary unproductive pathway is the autoxidation shunt (Luthra et al., 2011).

2. Peroxide shunt: the inefficient double reduction of electrons of oxygen that occurs when coordinated peroxide or hydroperoxide anion separates from iron to form

hydrogen peroxide (Shoji & Watanabe, 2014). Hydrogen peroxide can also be used as an oxidant for generating the active species through a “shunt reaction” (Shoji & Watanabe, 2014).

3. An oxidase shunt, wherein two water molecules are formed as a result uncoupling, instead of oxygenation of the substrate (Denisov et al., 2005). Generally speaking, these procedures have been grouped together and called uncoupling (Denisov et al., 2005; Meunier et al., 2004; Modi & Dawson, 2015).

Although the protein redox partner facilitates the heme iron reduction, it is essential that the P450 enzyme be able to facilitate the two protons transport towards the oxygen atom in distal side (Lewis & Pratt, 1998). In the P450 system, the rate of transferring of electrons via redox proteins can be expressed through equation given in Equation 1.2.

$$\text{Reduction rate} = K_a k_{ET} [P450] [Fpt]$$

Equation 1.2. The P450 system's rate of transferring of electrons via its redox components (Lewis & Pratt, 1998).

Where, the binding affinity constant of P450s and the reductases is represented by  $K_a$ , whereas  $k_{ET}$  is the rate constant of transferring of electrons. “[P450]” and “[Fpt]” are concentrations of proteins (in M), of P450 and the reductase, respectively (Lewis & Pratt, 1998).

### **1.1.3. Structure of P450s: Active Site and Substrate Binding**

Although P450 enzyme family has only 20% resemblance in their sequence (Denisov et al., 2005); the overall P450 family conserve its folding, because no non-P450 structure is known similar to the folding type of P450 enzymes. Thus, P450s have a unique folding to obtain the heme-thiolate that is needed for activation of molecular

oxygen, also for the interaction with redox proteins, and the stereochemical prerequisites for recognition of substrate (Kemper, 2004; Poulos & Johnson, 2015). Helices of CYP119 is represented as an example in Figure 1.3.

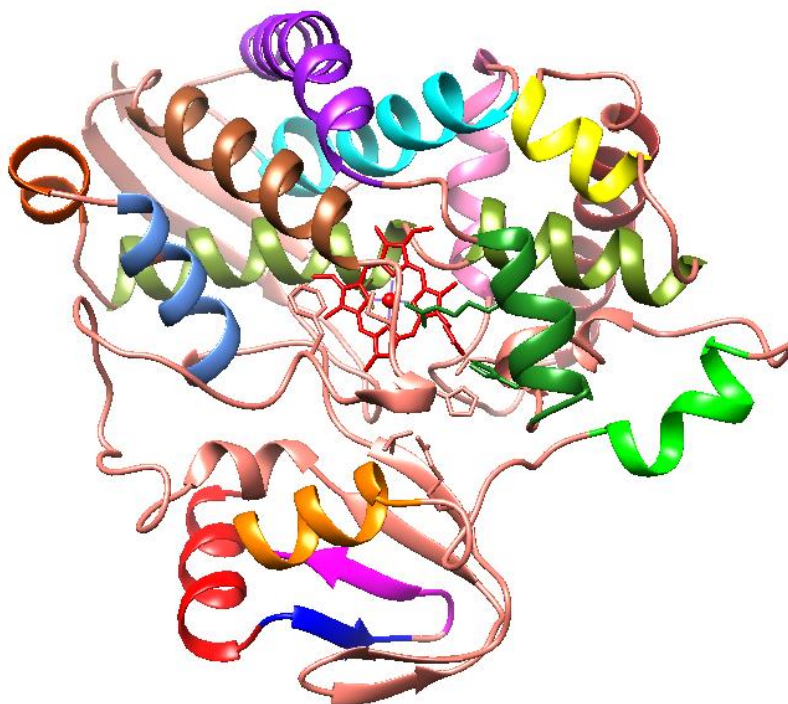


Figure 1.3. Helices of CYP119. Conserved residues of helices shown in parentheses: A-helix 1-12 (red); B-helix 26-35 (orange), B-B' loop 36-44 (Ser40-Lys260), B'-helix (green) (SRS1), B1-helix 62-66 and B2-helix 67-71 (Leu69); C-helix 73-81 (dark green) (Arg80), C-D loop 82-87; D-helix 88-109 (purple); E-helix 117-121, E'-helix (cyan); F-helix 140-151 (pink), F-G loop 151-164 (Phe153); G-helix 164-179 (brown); H-helix 183-191 (yellow); I-helix 195-209 (Ala 209) and I'-helix 210-228 (olive); J-helix 230-238 (orange-red); K-Helix 239-251 (light blue); K2-helix 284-286 (light pink); L-helix 319-336 (light brown).

The structure exhibits greater conservation in regions closer to the heme (Ortiz De Montellano, 2005), especially helices which directly contact conserved heme structure, D, L and I that are parallel and helix E that is antiparallel with each other

(Kestevur Doğru, 2019). The enzyme's prosthetic group is connected with a Cys residue and is situated in the vicinity of the proximal L helix and distal I helix (Denisov et al., 2005).

Cysteine residue is the ligand in the structure of heme at the “fifth” coordination of iron and it is absolutely conserved (Unno et al., 1997). To enable receiving hydrogen bonds from amino groups of peptide, the Cys ligand must be held in place and protected by its rigid architecture (Ortiz De Montellano, 2004).

As in reported review article by Denisov et al., (2005), the proximal Cys forms two hydrogen bonds with adjacent backbone amides. The long I helix forms the wall of the heme pocket. The active site contains the highly conserved threonine, which is thought to be important in the catalytic reaction (Denisov et al., 2005).

Amino acid residues, Thr252 of P450cam is among the most conserved amino acids of the P450 family (Unno et al., 1997). Cys357 and Thr252 residues are crucial for enzymatic oxygen activation. Cys357 coordinates the heme iron to donate electrons (Tani et al., 2002). A network of hydrogen bonds, formed by Thr252's hydroxyl group and a few water molecules, transfers protons to the terminal oxygen atom (Tani et al., 2002).

The P450's active site is situated close to the heme prosthetic group and is frequently completely separated from the solvent environment as reported by Wade et al., (2004) (Wade et al., 2004). The protein's isolated active site implies that for substrates entry and products to escape, the protein needs to move dynamically. For the majority of P450s, the widely recognized ligand route travels across the  $\beta$ 1 sheet, the B' helix/BC loop area, and the F/G loop section. However, there are significant differences in the substrate specificities and dynamics of the various P450s (Wade et al., 2004).

Denisov et al., (2005) reported that there are six sites that recognize substrate, in other words substrate recognition sites or SRS. They provide the recognition and binding of substrates: SRS1 corresponds to the B' helix region, whereas SRS2 and SRS3 corresponds to the regions of the F and G helices, respectively, SRS4 is a part of the I helix, while connecting region of SRS6 is the K helix  $\beta$ 2 and SRS5 is the  $\beta$ 4 hairpin line in the P450 active site (Denisov et al., 2005).

Denisov et al., (2005) reported that point mutations in SRSs significantly affect substrate specificities since the cytochrome P450 specificity for a substrate is established in advance by SRS. Because SRSs are flexible, an induced-fit mechanism can be enabled, allowing the catalytic reaction to happen after the substrate binds to the enzyme (Denisov et al., 2005).

In the reactions catalyzed by P450s, a molecule of substrate receives a single molecular oxygen atom in a regioselective, stereoselective (Winkler et al., 2018) and chemoselective manner (Van Beilen et al., 2003).

The process by which substrate binds to cytochrome P450s is sophisticated (Syed et al., 2014). In the resting state, cytochrome P450s have a comparatively low reduction potential, which is frequently within a certain range of -400 and -170 mV, it is controlled by proximal thiolate ligand that has a negative charge (Bernhardt & Urlacher, 2014; Guengerich, 2007; Syed et al., 2014; Van Beilen et al., 2003).

Substrate binding is able to change the spin state in the heme iron (Guengerich, 2009). Change occurs from low spin state to high spin state and cause the alteration in the reduction potential ranging from -300 to 100 mV more positive (Guengerich, 2007; Syed et al., 2014).

As reported by Guengerich (2007), Bernhardt and Urlacher (2014), Syed (2014) and other authors, the water molecule that is coupled to  $\text{Fe}^{3+}$  is often displaced as a result of substrate binding, it is discernible from the change in the heme's midpoint potential to positive values as well as the shift of the spin state from low spin state to high spin state. The reduced enzyme is impacted by the same factors. Strong ligands for the  $\text{Fe}^{2+}$  heme, CO and  $\text{O}_2$  cause the directly measured reduction potential to shift to greater positive values; ferric iron porphyrins, on the other hand, are not bound by them (Bernhardt & Urlacher, 2014; Syed et al., 2014). Additional factors, involving: temperature, pH, and the presence of cosolvents, could potentially alter the characteristics of the detected high-spin-low-spin changes (Bernhardt & Urlacher, 2014; Guengerich, 2007; Syed et al., 2014; Van Beilen et al., 2003).

Cytochrome P450s can employ as substrates a broad variety of small molecules and larger molecules in their enzymatic reactions with variable degrees of specificity (Bernhardt & Urlacher, 2014; Guengerich, 2007; Syed et al., 2014; Van Beilen et al., 2003). Generally, P450's substrates are poorly soluble in water and hydrophobic. However many other organic compounds, including as alcohols, phenols, and detergents, are also metabolized by these enzymes (Denisov et al., 2005).

Substrates examples can be fatty acids, ethanol, prostaglandins, pesticides and carcinogens, compounds such as drugs, anesthetics, organic solvents, steroids (Guengerich, 2007). P450s can also utilize a wide variety of chemicals as substrates, including aromatic, hetero-aromatic, polycyclic aromatic, and aliphatic (Syed et al.,



2014). Cytochrome P450s, in their oxygenation of substrate, are highly regio- and stereospecific (Denisov et al., 2005).

NAD(P)H serves as the reducing agent in majority P450 systems for the catalytic cycle. Midpoint potential of NAD(P)H is -320 mV (Denisov et al., 2005). According to Denisov et al., (2005) the supplemental redox protein partners have potentials for reduction that are basically in the identical range. This indicates that P450s, in order to avoid an inefficient turnover and the wasteful consuming of reducing agent NAD(P)H, furthermore formation of the toxic superoxide or peroxides formation, should be reduced only slowly before substrate binds (Denisov et al., 2005).

After substrate binding, NADPH-P450 reductase transfers one electron, then O<sub>2</sub> is bound to the ferrous form Fe<sup>2+</sup> of the enzyme, and second electron is delivered (Bernhardt & Urlacher, 2014). Places the substrate close the periphery of the protein; the substrate then moves towards the heme, where the protein changes one more time before reaching its final conformation (Guengerich, 2007).

As described above, a Compound I species is involved in the mechanism of P450s, its known as an intermediate that results from the oxidative processes of other various enzymes that contain heme as well (Wei, 2019). The protein environment controls the metabolic profile and substrate selectivity, which are determined by the bioinorganic chemistry of the heme iron and oxygen (Denisov et al., 2005).

#### **1.1.4. Electron Transfer Systems in Cytochrome P450 Enzymes**

Cytochrome P450s require electrons for activation of oxygen and conversion of substrate (Denisov et al., 2005). According to Denisov et al., (2005) as monooxygenases, P450s rely on an electron transport system. Electrons are usually received from NAD(P)H donors and are transported utilizing supplementary proteins – redox partners (Denisov et al., 2005).

The process may involve one or two electron transport proteins (Sevrioukova et al., 2003). Putidaredoxin reductase (PdR), containing an flavin adenine dinucleotide (FAD), and putidaredoxin (Pdx), comprising an [2Fe–2S] type iron-sulfur protein, are

proteins involved in transferring electrons from NAD(P)H electron donor to CYP101 (P450cam) enzyme (Sevrioukova et al., 2003).

According to Bernhardt and Urlacher (2014), eukaryotic P450s are divided into two classes: 1. P450s that interact with a protein: a ferredoxin and a ferredoxin reductase and 2. P450s that interact with a cytochrome P450 reductase, CPR systems. The selection of the electron transfer partner has a major impacts on the activity of human P450s (Bernhardt & Urlacher, 2014).

According to Hannemann and coworkers (2007), there are ten classes of electron transfer systems in P450s, including some unusual electron transfer systems (Hannemann et al., 2007). Class I is characterized for most bacterial P450 systems and several eukaryotic mitochondrial P450s, which contains three distinct proteins: first is reductase containing an FAD. This reductase accepts the electron from NAD(P)H, ferredoxin which reduces the P450 enzyme (Hannemann et al., 2007b).

Hannemann et al., (2007) reported that Class II is related to P450s mostly found in eukaryotes and contains two integral membrane proteins: P450s and NAD(P)H-dependent cytochrome P450 reductases (CPR). CPR consists of the prosthetic groups flavin adenine dinucleotide (FAD) and flavin mononucleotide (FMN) (Hannemann et al., 2007). Reductase and P450 are membrane-bound in eukaryotes only ferredoxin is soluble, whereas all of the three proteins are soluble in bacteria, as can be seen in Figure 1.4.

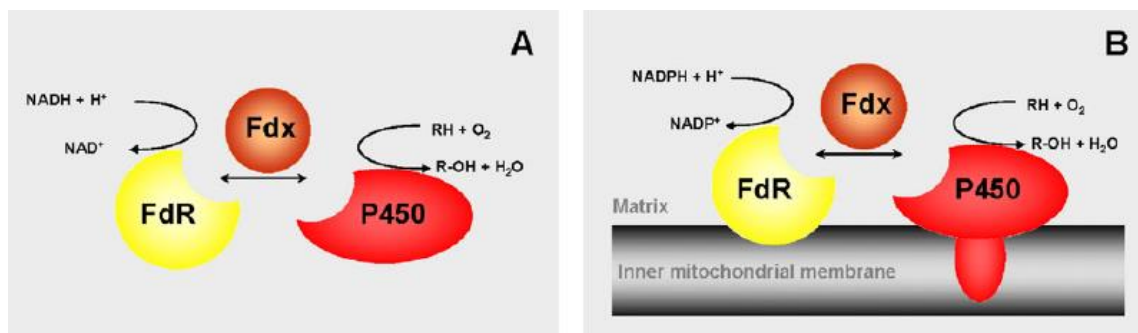


Figure 1.4. Cytochrome P450 system of transfer of electrons. Class I represents two distinct systems: A. Bacterial system. B. Mitochondrial system. (Source: Hanneman et al., 2007).

Schematic representation of Class II and Class III can be seen in Figure 1.5.

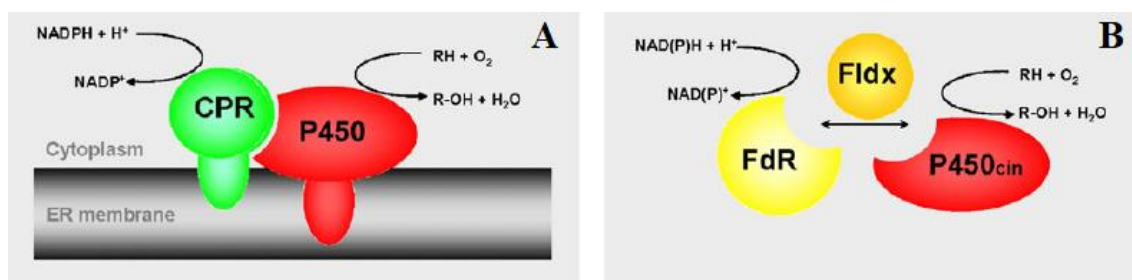


Figure 1.5. Cytochrome P450 electron transfer system. A. Class II represents microsomal system. B. Class III represents bacterial system. (Source: Hannemann et al., 2007b).

Prosthetic groups play a key role in transferring of electrons from NAD(P)H to P450s. CYP105A3 (P450sca) is the only member of prokaryotic class II monooxygenase system (Serizawa, 1989). It has been shown that *Streptomyces carbophilus* contains P450 reductase that accepts electrons from NAD(P)H and contains both FAD and FMN. It is involved in the hydroxylation of mevastatin to yield pravastatin (Serizawa, 1989). Endoplasmic reticulum (ER) of eukaryotes is the location where the class II of monooxygenase system can be observed (Hannemann et al., 2007b).

Class III is a novel class of electron transfer system which was reported by Hawkes and coworkers (2002). This group is related to Class I, with a significant difference. Electrons are transferred by three protein system: 1. ferredoxin reductase. These proteins utilize NAD(P)H, reductases contain FAD as part of protein; 2. redox protein to the cytochrome P450 is putidaredoxin from *Pseudomonas putida* in Class I. while in class II it has been proposed that it is a flavodoxin known as cindoxin from *Citrobacter braakii* (Hawkes et al., 2002).

As Puchkaev and Ortiz de Montellano (2005) reported, example of P450 enzymes for Class IV is thermophilic CYP119 enzyme. CYP119 does not employ NAD(P)H-dependent flavoprotein to be reduced in enzymatic reactions. CYP119 reactions are supported by surrogate mesophilic electron donors (Puchkaev & Ortiz De Montellano, 2005). For example, a thermostable ferredoxin, or a 2-oxoacid-ferredoxin oxidoreductase,

getting the origin of reducing agents, these are utilizing pyruvic acid instead of NAD(P)H (Hannemann et al., 2007).

Schematic representation of Class IV, Class V, Class VI, Class VII can be seen in Figure 1.6.

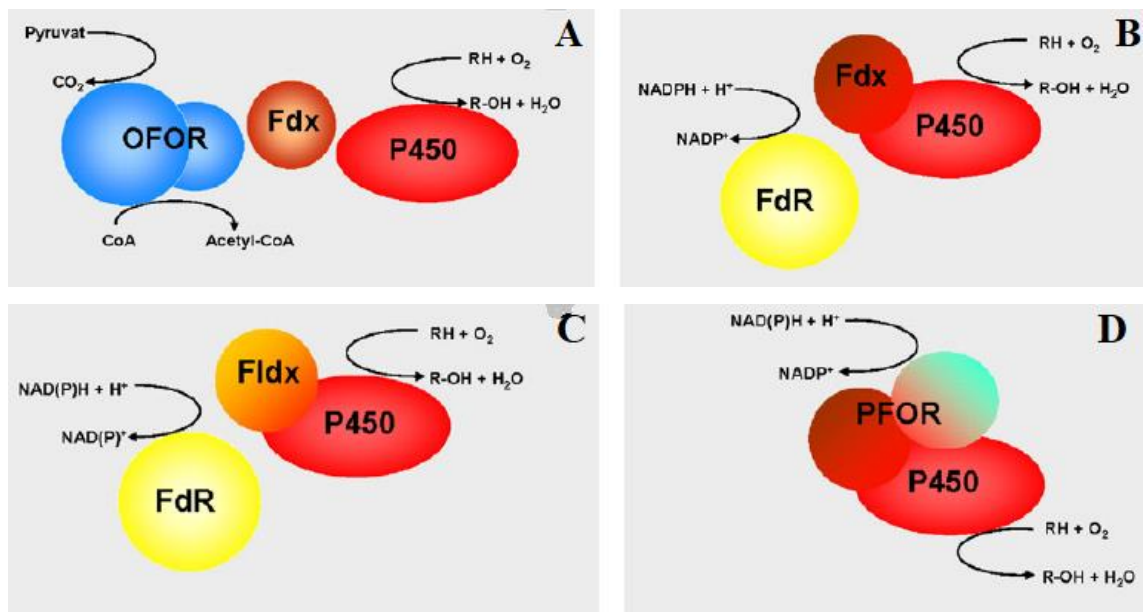


Figure 1.6. Cytochrome P450 electron transfer system. A. Class IV signifies bacterial thermophilic system. Whereas, B. Class V signifies bacterial Fdx-P450 fusion system. C. Class VI suggests bacterial system of the fusion of Fldx-P450. While, D. Class VII reflects bacterial PFOR-P450 fusion system. (Source: Hannemann et al., 2007b).

In Class V of CYPs electron transfer systems contain unknown estimated reductase, which is also utilizes NAD(P)H as donor and a cytochrome P450 protein fused together with ferredoxin (Hannemann et al., 2007). CYP51 derived from *Methylococcus capsulatus*, participating in a reaction of sterol 14 $\alpha$ -demethylase, is the sole known example of this group (Jackson et al., 2002). Authors reported that a ferredoxin domain which contains [3Fe-4S] cluster is bound to the P450 heme monooxygenase at the C-terminus through linker region rich with alanine residues. This group has close

relationship with class I because of redox center, iron-sulfur of ferredoxin involved (Hannemann et al., 2007b; Jackson et al., 2002).

A hypothetical flavoprotein reductase that is dependent on the reducing agent NAD(P)H and a flavodoxin-P450 fusion protein constitute the class VI cytochrome P450 system (Hannemann et al., 2007). The cytochrome P450-like gene obtained from strain 11Y of species of *Rhodococcus rhodochrous* is the initial representation of the novel class VI cytochrome P450s. Cytochrome P450 and a flavodoxin domain are fused to each other in this system (Hannemann et al., 2007).

The Class VII constitutes is unique bacterial fusion system, example of which is the P450 superfamily member CYP116B2 from *Rhodococcus sp.* A cytochrome P450 and a reductase domain are fused in C-terminal, only a small 16-amino acid linker sequence divides proteins from one another (Xie et al., 2020). Moreover, it has a [2Fe–2S] ferredoxin site, a site for binding of FMN, and a site for binding of NADH (Xie et al., 2020).

Schematic representation of Class VIII and Class IX can be seen in Figure 1.7.

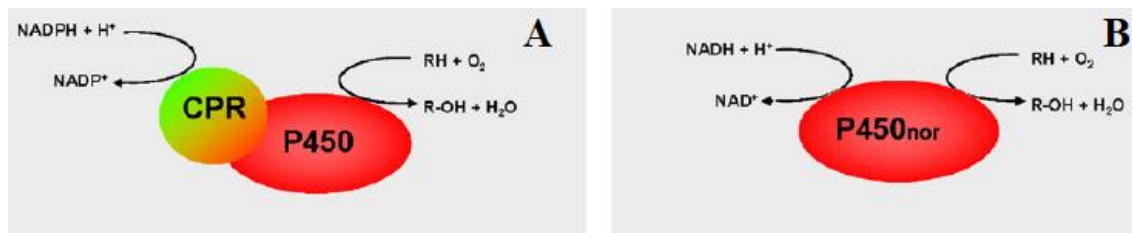


Figure 1.7. Cytochrome P450 electron transfer system. A. Class VIII represents bacterial CPR-P450 fusion system. B. Class IX indicates soluble eukaryotic P450nor system. (Source: Hannemann et al., 2007b).

P450 proteins found in Class VIII are fused in a single polypeptide chain to cytochrome P450 reductase (CPR), its eukaryotic-like diflavin reductase partner as reported by Li et al., (2020). The most extensively researched member of this family is CYP102A1 (P450BM3). It is derived from the soil bacteria *Bacillus megaterium*. P450BM3 catalyzes the cytosolic fatty acid hydroxylation, this flavocytochrome has been found in a variety of prokaryotes and lower eukaryotes (Li, 2020).

Thus far, Class IX has only included nitric oxide reductase, which is a specific type of cytochrome P450 (Hannemann et al., 2007a). A member of this category, *Fusarium oxysporum*'s CYP55 is found in the cytosolic and mitochondrial parts of the cells (Nakahara et al., 1993). To date, CYP55 is the only soluble P450 protein that exists in eukaryotes (Hannemann et al., 2007b; Nakahara et al., 1993). NADH is an electron donor for P450<sub>nor</sub> and it functions independently of other electron-transport proteins to catalyze the converting of the two nitric oxide molecules into nitrous oxide, it is unique reductive process for P450s (Hannemann et al., 2007b; Nakahara et al., 1993).

As demonstrated in Figure 1.8, Class X of P450 systems that contain the independent P450s. There is no requirement for the electron source NAD(P)H, O<sub>2</sub>, or a cytochrome P450 reductase that uses NAD(P)H, instead utilize the acyl hydroperoxide of the substrate as O<sub>2</sub> donor, for example CYP74 (Itoh & Howe, 2001).

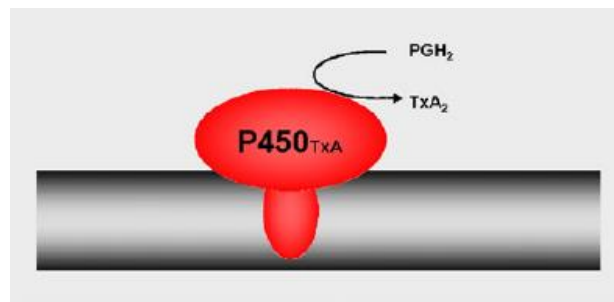


Figure 1.8. Cytochrome P450 electron transfer system. Independent eukaryotic system encompasses the Class X. (Source: Hannemann et al., 2007b).

As a result, CYP74 form additional carbon-oxygen linkages in the final products (Itoh & Howe, 2001). Other than mentioned above there are many more artificial systems reported (Hannemann et al., 2007b). Recent studies reveal that there is much more complex scenario: for instance, P450s are inherently connected to either one of their redox proteins or a protein that makes up their electron transfer mechanism, and fused P450s enzyme's partners that are non-redox (McLean et al., 2015).

In addition, there are two main empirical classes: 1. diflavin enzyme NAD(P)H-dependent P450 oxidoreductase in eukaryotes, and 2. NAD(P)H-dependent ferredoxin reductase and ferredoxin proteins that are bacterial/mitochondrial (McLean et al., 2015).

NAD(P)H-dependent cytochrome P450 reductase (CPR) is the redox partner of the P450 enzymes, that participate in the metabolism of drugs and xenobiotics (Winkler et al., 2018). In case of mitochondrial P450s, they interact with a two-component system: 1) consists of ferredoxin with [2Fe-2S] cluster and 2) ferredoxin reductase with FAD cofactor, dependent on reducing agent NAD(P)H (Winkler et al., 2018).

Nagamune and coworkers (2014) assembled the elements of CYP101A1 catalyzing camphor hydroxylation systems using heterotrimeric ring-shaped proliferating cell nuclear antigen (PCNA) (Suzuki et al., 2014). The three PCNA subunits were fused to either the appropriate monooxygenase, putidaredoxin reductase (Pdr), or Pdx. The "PUPPIT" complex exhibited significantly more activity in the conversion of camphor compared to when free proteins CYP101A1, Pdx, and Pdr was used in the equimolar concentrations (Hirakawa & Nagamune, 2010; Suzuki et al., 2014).

### 1.1.5. Redox Partner Proteins

Redox partners are supporting proteins that affect the transfer of electrons in P450s catalytic reactions (Suzuki, 2014). Usually they are two-iron two-sulfur, [2Fe-2S] containing ferredoxins and FAD-containing NAD(P)H-dependent ferredoxin reductases (Suzuki, 2014).

The prototype of ferredoxins in bacterial P450 systems and putidaredoxin (Pdx), adrenodoxin (Adx), in addition to a few well-studied bacterial flavodoxins and bacterial ferredoxins, are the most efficient electron transfer proteins studied for the present (Suzuki, 2014). Many bacterial soluble cytochrome P450s, accept electrons from electron donor for complex formation employing specific ferredoxins that are in their turn are reduced by specific reductases (Suzuki, 2014).

Ferredoxins contain two-iron two-sulfur cofactor, [2Fe-2S] cluster and take part in a variety of crucial biologically oxidation-reduction processes (Sevrioukova et al., 2003). According to Sevrioukova et al., (2003), NADH-dependent oxidoreductases reduces the bacterial [2Fe-2S] proteins then the latter transfers electrons to cytochrome P450s in order to catalyze hydroxylation reactions. A form of ferredoxin with the [2Fe-2S] cofactor is putidaredoxin (Pdx). They originated from the *Pseudomonas putida*, which is a type of protein that functions as a "one-electron carrier". Pdx transfers electrons

to the terminating oxygenase cytochrome P450cam from the NADH-dependent putidaredoxin reductase (PdR), which contains FAD as a cofactor (Sevrioukova et al., 2003).

Redox partner proteins used in current research are putidaredoxin (Pdx, MW 11.4 kDa) and putidaredoxin reductase (PdR, MW 46.6 kDa) from *Pseudomonas putida*. Crystal structures of both P450cam-Pdx and Pdx-PdR are available and were used in this project.

Gunsalus laboratory discovered putidaredoxin or Pdx for the first time in 1968, that is a component of the trimeric system of camphor hydroxylase (Sevrioukova et al., 2003). In all variedly used buffers Pdx was found to be extremely unstable, after few days it changes its color from dark brown color to colorless, suggesting that within a few days, the Pdx was losing the 2Fe-2S metal cluster (Sevrioukova et al., 2003). Pdx 3D structure is illustrated in Figure 1.9.

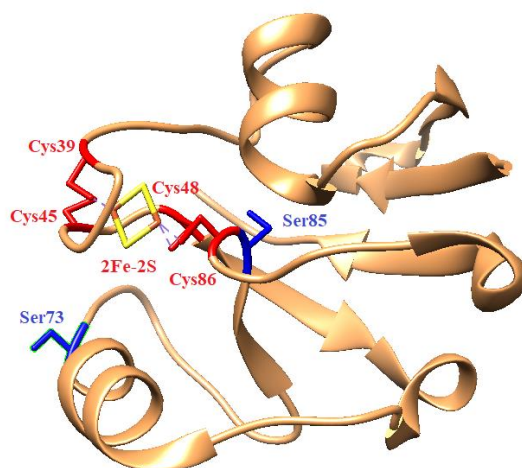


Figure 1.9. Putidaredoxin Cys73Ser/Cys85Ser mutant. Mutated residues of Cys replaced with Ser are depicted in blue. Conserved Cys residues are shown in red. 2Fe-2S cluster is depicted in yellow-orange. The image was created using UCSF Chimera PDBID: 3LB8.

Sevrioukova et al., (2003) studies suggest that the stability of Pdx is highly unstable caused by losing the metal cluster (Sevrioukova et al., 2003). Pdx has six cysteine residues: 2Fe-2S metal cluster of Pdx has four cysteine ligands (Cys39, Cys45,



Cys48, and Cys86). However Cys73 and Cys85 residues are not forming bonds and therefore, may be reactive. Free cysteine residues form disulfide bridges with molecules which inactivates Pdx, that leads to subsequent loosing of structure and therefore the [2Fe-2S] iron–sulfur cluster is separated from the whole structure (Sevrioukova et al., 2003).

To enhance the stability of Pdx by avoiding the process of development of disulfide bond between residues, Sevrioukova et al., (2003) replaced two residues, Cys73 and Cys85 with serine residue. The potential of Pdx to preserve the iron-sulfur cofactor was significantly enhanced by this mutation (Sevrioukova et al., 2003).

Sevrioukova et al., (2003) also solved the crystal structures of Cys73Ser/Cys85Ser mutants of Pdx, showing the similar absorbance spectra to WT Pdx (Figure 1.9). This indicates that the surroundings of the 2Fe-2S metal cofactor of mutant Pdx was not perturbed. Pdx extinction coefficient at  $\epsilon_{412nm} = 11.0 \text{ mM}^{-1}\text{cm}^{-1}$  was used in calculation of concentration of protein (Sevrioukova et al., 2003).

Pdx contains 106 residues. Cofactor of Pdx the [2Fe-2S] iron–sulfur and hydrogen bonds, sulfur ligands of Pdx are highly conserved (Sevrioukova et al., 2003). As reported by Sevrioukova et al., (2003), positioned on the surface, His49 residue of Pdx is also conserved. The only charged residues in putidaredoxin are Asp38 and Arg66 residues that are located close to the metal center (Sevrioukova et al., 2003), furthermore Asp38 plays a key role in electron transfer pathway. Cys73 residue is crucial for binding interactions with putidaredoxin reductase. 103-106 residues of Pdx are flexible (Sevrioukova et al., 2003).

Trp106 residue is an another important residue in Pdx and it serves a function in the electron transfer processes between PdR and Pdx, then Pdx and P450cam to mediate electron transfer, particularly the indole ring of it (Sevrioukova et al., 2003).

Putidaredoxin reductase, frequently shortened as PdR, is a NADH-dependent ferredoxin reductase and bacterial oxygenase-coupled (Peterson et al., 1990). Molecule of putidaredoxin reductase contains three different domains: the first, domain that binds FAD cofactor, corresponding to residues from 1 to 114 and from 248 to 325, the second is an NAD-binding domain corresponding to residues from 115 to 247, and the third is a C-terminal domain consisting of residues from 326 to 422 (Peterson et al., 1990; Sevrioukova et al., 2010).

Sevrioukova (2010) reported that the most conserved region of the protein is FAD-binding domain. The binding conformation of the FAD cofactor is expanded and it

has surface residues such as Pro46, Ser301, Val302, and Trp330. The Lys50 amino acid and corresponding hydrogen bonding constitutes one of the crucial components of the active site. Lys50 and Glu163 residues makes a salt bridge, moreover Lys50 binds with O4 of FAD with hydrogen bonds and Pro46 (Figure 1.10).

Schematic representation of PdR and its key residues are shown in Figure 1.10.

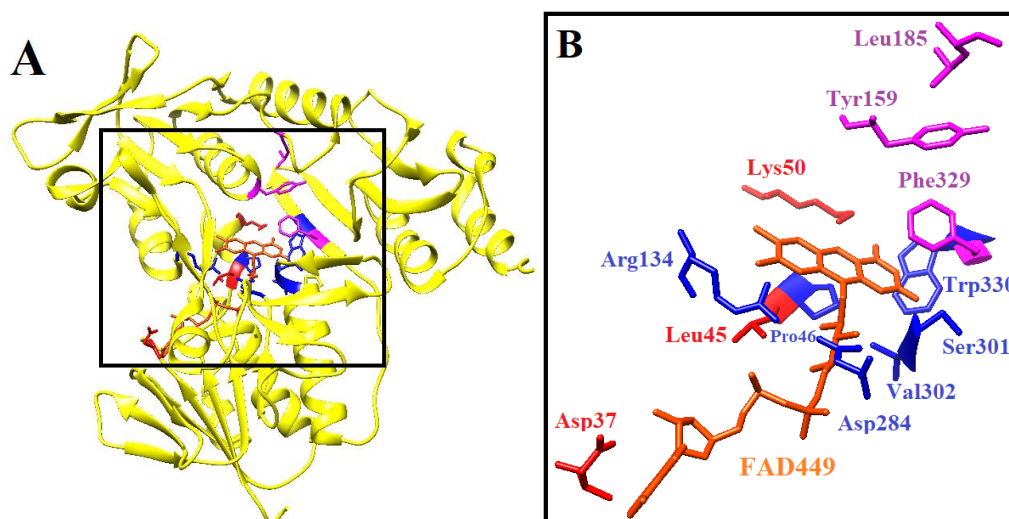


Figure 1.10. A. Putidaredoxin reductase is depicted in yellow. B. Conserved residues of FAD-binding domain depicted in blue: Pro46, Arg134, Asp284, Ser301, Val302, Trp330. Conserved residues of NAD-binding domain depicted in magenta: Tyr159, Leu185, Phe329. Other highly conserved residues depicted in red: Asp37, Leu45, Lys50. FAD cofactor depicted in orange. The image was created using UCSF Chimera PDBID: 3LB8.

Important residues for FAD binding are Leu45 and Ala38. The 13 Å length and 7 Å width tunnel which forms up the FAD-binding region containing His43 and His44 residues along the wall of the tunnel. It is known that cofactor of putidaredoxin reductase, the flavin complex exhibits an oxidation-reduction value of 285 mV and that the protein is extremely specific for NADH (Sevrioukova et al., 2010).

Side chain of aromatic residue Tyr159 occupies NAD-binding site of putidaredoxin reductase, meanwhile protecting FAD from environment of solvent in

ligand-free protein. Leu185 and Phe329 residue's side chains are separated by a tyrosine ring (Unno et al., 1996).

There are more residues that are critical, such as Glu163 for pyridine nucleotide binding, Asp 179 and Glu300 binds with hydrogen bonds with the ribose moieties through the hydroxyl groups, while Arg187 establishes hydrogen binds with both the ribose and for NADH via the pyrophosphate group of it, as well as multiple residues Arg115, Arg187, Arg284, and Arg298 located in the NAD-binding channel's opening of putidaredoxin reductase. Gly157 is conserved residue (Sevrioukova et al., 2010; Unno et al., 1996).

The crystal structure of recombinant FAD-containing NADH-dependent flavoprotein putidaredoxin reductase (PdR) derived *Pseudomonas putida* has been determine to 1.90 Å resolutions by Sevrioukova et al., (2004) (Sevrioukova et al., 2004).

Domains for the binding of cofactor FAD and NAD are separated by the compact C-terminal domain of PdR, which has two  $\alpha$ -helices and a five-stranded  $\beta$ -sheet (Sevrioukova & Poulos, 2011). Flavin has the pyridine component that are protected by residues of this domain from solvent (Sevrioukova & Poulos, 2011; Sevrioukova et al., 2010).

The PdR-Pdx reaction is the starting reaction of the whole electron delivery process. NADH donates 2 electrons to FAD of PdR protein which is followed by two electron transfers one at a time to [2Fe-2S] redox center of Pdx (Sevrioukova & Poulos, 2011). Pdx after accepting the electron from PdR molecule, then dissociates from it and deliver the electron to P450 monooxygenase, while another Pdx binds to PdR (Sevrioukova & Poulos, 2011; Sevrioukova et al., 2010).

Both PdR and P450cam binds Pdx at the same surface region (Sevrioukova & Poulos, 2011). According to authors, Pdx has retained massive Tyr33, Arg66, and Trp106 residues that hinder its tight attachment to the proteins and enable in dissociation upon reduction. In Pdx and PdR complex, Trp328 and Trp330 residues of PdR are about in 3.7 Å distance regarding to the Cys ligands of [2Fe-2S] in Pdx. It forms a straight link amid the FAD, the cofactor of PdR and iron-sulfur cluster, the cofactor of Pdx (Sevrioukova & Poulos, 2011; Sevrioukova et al., 2010).

Some important residues located on the surfaces of PdR and Pdx, such as Arg310, forming salt bridge with residue Asp38, and Arg65, are important in binding of PdR and Pdx (Sevrioukova & Poulos, 2011).

Figure 1.11 represents binding of PdR and Pdx molecules and key residues in electron transfer.

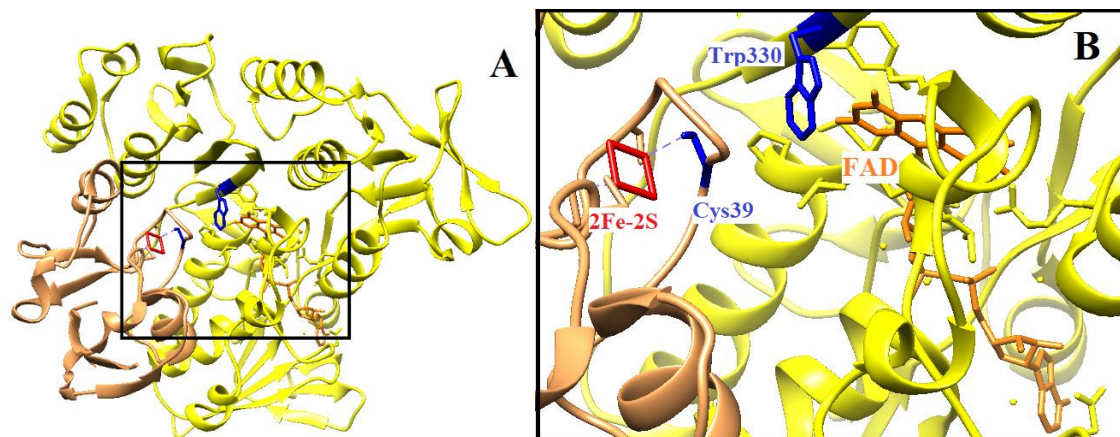


Figure 1.11. A. Putidaredoxin and putidaredoxin reductase binding. Putidaredoxin is depicted in brown and putidaredoxin reductase in yellow. B. Conserved residues of FAD domain depicted in orange. Conserved residues of PdR, Trp330 in blue. Conserved residues of Pdx, Cys39 in blue and Fe-S cluster is depicted in red. Images were created using UCSF Chimera PDBID: 3LB8.

Arg65 hydrogen bonds with Val28 residue in Pdx, backbone atom of Val28 with its guanidine group of Arg65. The rate of electron transfer may be decreased if mutate these residues (Sevrioukova & Poulos, 2011; Sevrioukova et al., 2010).

Molecular recognition between the partners involves Tyr33, Asp38, Arg66, Glu72, and Cys73 residues of Pdx (Aoki et al., 1998). The PdR-Pdx complex's surface area is comparably tiny, measuring about  $365 \text{ \AA}^2$  for each protein and there are 20 surface residues in putidaredoxin reductase, nine of them are hydrophobic, four polar, and five having positive charge (Sevrioukova & Poulos, 2011; Sevrioukova et al., 2010).

In case of Pdx, 14 surface residues including four hydrophobic, four polar, and three charged (Sevrioukova et al., 2010). Therefore, hydrophobic interactions as well as polar interactions are fundamental for the protein-protein complex. Besides the cross-linked pair Lys409 of PdR and Glu72 of Pdx, there is only one bidentate salt bridge between Arg310 of PdR and Asp38 of Pdx (Sevrioukova et al., 2010).

Protein-protein interactions tend to occur by means of hydrogen bonding, electrostatics, and/or hydrophobicity effects (Chen et al., 2021). PdR accepts electron from reducing NAD(P)H agent and Pdx receives one electron at a time in two steps through FAD- PdR<sub>Trp330</sub>-Pdx<sub>Cys39</sub>-Pdx<sub>FeS</sub> route from NADH-dependent putidaredoxin reductase (Sevrioukova et al., 2010).

## 1.2. Biotechnological Applications of Cytochrome P450 Enzymes

Cytochrome P450 enzymes are outstanding biocatalysts with large number of substrates, and different types of catalyzed reactions, with broad applicability (Bernhardt & Urlacher, 2014). Cytochrome P450 enzymes are very appealing as catalysts in practical applications because of their versatility and ability to activate O<sub>2</sub> and to introduce one oxygen atom into the substrate, whereas the second one is reduced to water. All these findings make cytochrome P450 enzymes such enormous potential for various applications in biotechnology (Bernhardt & Urlacher, 2014).

Cytochrome P450s are flexible enzymes that catalyze oxyfunctionalization of a broad spectrum of chemical substances when molecular oxygen prevails, components for instance xenobiotics, terpenes, antibiotics, alkaloids, steroids, alkanes, fatty acids, and many others (Bernhardt & Urlacher, 2014). They can biodegrade existing chemical compounds and execute hydroxylations of complex molecules in a stereo- and regio-selective manner. Since no other set of enzymes has the same range of accepted substrates and types of catalyzed reactions, they have enormous potential for use in biotechnology (Bernhardt & Urlacher, 2014). P450 enzymes are extremely adaptable catalysts due to their capacity to catalyze a wide variety of conversions and processes, their active sites are capable of binding many different kinds of irrelevant structures (Koo et al., 2000). Cytochrome P450 enzymes are applied widely on industrial scale (Winkler et al., 2018).

Cytochrome P450 enzymes known as frequently employed enzymes in the synthesis of drug metabolites (Bernhardt & Urlacher, 2014). Recombinant hosts expressing approaches are a promising tool for human drug metabolizing P450s to produce metabolites of drug (Bernhardt & Urlacher, 2014). An extensive number of

enzymes for the manufacture of structurally differed drug metabolites may be available through microbial recombinant CYPs (Bernhardt & Urlacher, 2014).

Although oxygenases have a broad variety of biological functions, their applications fall into two main types: 1) the commencement of the process of biodegradation and detoxification of potentially hazardous substances and carbon sources; 2) the production of hormones, signaling molecules, secondary metabolites, and many other chemicals through biosynthesis (Van Beilen et al., 2003).

Ro et al., (2006) published that one of the great examples is artemisinic acid production. The antimalarial medication artemisinin originates from this acid in CYP-involved artificial multi-enzyme-cascade. This pathway was modified to include CYP71AV1 from *Artemisia annua* in order to oxyfunctionalize amorpha-4,11-diene and produce artemisinic acid. Utilizing engineered strain of *S.cerevisiae*, artemisinic acid 100 mg/L or more might be obtained (Ro et al., 2006). Artemisinin is one of the components of the artemisinin-based combination treatments of malaria. Clearly, a reliable and affordable source of artemisinin was needed to enable an affordable treatment (Ro et al., 2006).

According to Sakaki et al., (2012) important ingredients in the flavor and scent industries are oxygenated terpenes. P450s are the majority of the enzymes that catalyze the terpenes hydroxylation in a regio- and enantioselective way. Steroids are widely used as important medicines (Sakaki, 2012). Microbial steroid bioconversions are established techniques in the steroid biotechnology. For instance, P450<sub>11β</sub>-dependent 11 $\beta$ -hydroxylation was the catalyst for the immobilized *Curvularia lunata mycelium* to produce cortisol from substrate of 11-deoxycortisol. In the adrenal cortex, hydroxylation processes that are catalyzed by CYP11A1, CYP17A1, CYP21A2 (or CYP21B2), and CYP11B1 are involved in the process of steroidogenesis from cholesterol to cortisol (Sakaki, 2012).

Another example reported by Szczebara et al., (2003) is the hydrocortisone production, the primary mammalian adrenal glucocorticoid and a significant steroid drug metabolism intermediate, recombinant *Saccharomyces cerevisiae* strains serves as a simple carbon source. Adrenodoxin (Adx), adrenodoxin reductase (AdR), mitochondrial versions of CYP11B1 and Adx, CYP17A1, and CYP21A1 are all involved in biosynthesis (Szczebara et al., 2003). Hydrocortisone, a mammalian steroid (11 $\beta$ ,17 $\alpha$ ,21-trihydroxy-4-pregnene-3,20-dione), is the ideal precursor when synthesizing drugs. The steroid has a slight glucocorticoid effect, but it also possesses potent anti-inflammatory, abortive, or

antiproliferative characteristics (Szczepara et al., 2003). The steroidogenic tissues that express the CYP11, CYP17, CYP19, and CYP21 families include the adrenal gland, testis, ovary, and placenta (Hiroi et al., 2001). The biosynthesis of endogenous steroid molecules is facilitated by these isoforms; progesterone hydroxylation activities are exhibited by the human isoform CYP2D6 (Hiroi et al., 2001).

Commercial potential of CYPs is obvious: other examples can be the microbial progesterone hydroxylation to yield 11 $\alpha$ -hydroxyprogesterone which is catalyzed by *Rhizopus arrhizus*, steroid oxygenations including the 11 $\beta$ -hydroxylation of deoxy cortisone conversion to hydrocortisone with *Curvularia sp.* (Bernhardt & Urlacher, 2014). Moreover, the utilization of CYP-expressing microbial strains to oxidize compactin to pravastatin, which is employed in widespread commercial uses, and *Rhizopus sp.* to convert progesterone to cortisone (Bernhardt & Urlacher, 2014). CYP105A3 which is also called P450sca-2 catalyzes compactin's 6 $\beta$ -hydroxylation (Bernhardt & Urlacher, 2014). Pravastatin is a statin that lowers cholesterol levels to reduce the risk of cardiovascular illnesses and one of the first available statins on the market (Bernhardt & Urlacher, 2014).

Bacterial P450s are involved in several steps of the manufacture of antibiotics. P450eryF (CYP107) is needed for the synthesis of erythromycin and tetracenomycin (Kumar, 2010). In another example, CYP153 expressed in *Pseudomonas putida* produced the anti-cancer medication perillyl alcohol from limonene with a yield of 6.8 g/L (Kumar, 2010).

Preemergence herbicides called chloroacetamide are used to suppress annual grasses and broadleaf weeds when producing rice, soy beans, corn, and numerous other crops (Liu et al., 2021). Authors reported that they are broadly used and chemically stable, hence have been discovered in numerous countries' drinking water, furthermore in ground surface waters. Herbicides containing chloroacetamide showed to be extremely harmful to a variety of species and to cause cancer in people (Liu et al., 2021).

Chloroacetamide herbicides' breakdown process is great concern (Liu et al., 2021). A bifunctional enzyme from the cytochrome P450 family was reported by Liu et al., (2021), derived from *Rhodococcus sp. B2*. They catalyze the N-dealkoxymethylation and O-dealkylation of chloroacetanilide herbicides (Liu et al., 2021).

Kumar et al., (2010) reported the three primary groups of industrial pollutants that are widely distributed around the world and can be found in soil, water, and air are:

1. polycyclic aromatic hydrocarbons (PAHs),

2. polychlorinated dibenzo-p-dioxins (PCDDs), and
3. polychlorinated biphenyls (PCBs).

It is known that PAHs are metabolized by CYP101, CYP102, CYP1A1, CYP1A2, and CYP1B1. While CYP1A1 mutant F240A observes activity toward 2,3,7,8-tetra-chloro-DD, CYP1A1 has strong activity toward dibenzo-p-dioxin (DD) and mono-, di-, and tri-chloro-DDs. CYP2B11 is capable of metabolizing PCBs (Kumar, 2010).

### **1.2.1. Limitations of Cytochrome P450 Enzymes**

Despite the enormous practical potential of P450 enzymes, the redundancy of P450 systems can restrict the use of the enzymes in manufacturing processes (Koo et al., 2002). Main limitations of these enzymes are: a) the need for specific electron transfer partners; b) the need of costly and unstable electron donor such as NAD(P)H; c) low activities and instability; d) low substrate solubility; e) substrate and product toxicity; f) uncoupling of a process during oxidation employing NAD(P)H as an electron source without yielding a product, as well as additional problems may occur such as NAD(P)H depletion, an incomplete knowledge of the regarding factors that determine of P450 substrate specificity (Bernhardt & Urlacher, 2014; Koo et al., 2002).

As an external monooxygenase most cytochrome P450 enzymes require electrons from NAD(P)H donors for oxygen activation and substrate conversion (Sevrioukova & Poulos, 2002). Redox partner proteins are needed for electron transfer, in general, the process comprises one or two proteins (Sevrioukova & Poulos, 2011). Efficient oxygen activation and generation of products depend on interactions between two proteins and by optimizing of electron flow, improving in substrate conversion can be obtained (Bernhardt & Urlacher, 2014).

According to Bernhardt and Urlacher (2014), interactions between two proteins and transferring of electron optimization, enhanced efficiency and development of selectivity of catalytic processes can help to solve at least some of these problems. It will be possible to identify the ideal redox system and produce biocatalysts with sufficiently high productivities by combining different CYPs with different redox partners (Bernhardt & Urlacher, 2014). Given that they are often composed of various components, some of



which could possibly be membrane-bound, and due to that certain enzymes may need expensive cofactors comprising NADPH and have intricate electron-transfer mechanisms, oxygenases are often unstable (Van Beilen et al., 2003; Wei, 2019).

The costly cofactor NAD(P)H need is a significant barrier to the use of CYP (Wei, 2019). Surrogate oxygen donors such as hydroperoxide or other peroxides are used without NAD(P)H and redox protein partners to make reaction much simpler, so-called shunt pathway. Yet excess of peroxides damages heme, which make it not productive (Wei, 2019). Furthermore, Compound I synthesis through the hydrogen peroxide shunt pathway is inhibited by the size and shape of the substrate-binding pocket of the P450s, allowing alternative competing radical species to induce subsequent substrate oxidation (Wei, 2019). Enzymatic regeneration systems can be an approach to overcome the stoichiometric need of electron donors NADPH and NADH (Bernhardt & Urlacher, 2014). For example, glycerol dehydrogenase could be effectively utilized for NADH regeneration as demonstrated by Michizoe et al., (2005) (Michizoe et al., 2005).

Low productivity limits industrial implementation of cytochrome P450 enzymes. It is possible to get significantly better biocatalytic system overall productivities by optimizing strain engineering (Bernhardt & Urlacher, 2014). The catalytic efficiency ( $k_{cat}/K_M$ ) of CYPs can be increased and be improved significantly by using protein engineering methods such as directed evolution, likewise site-directed and saturation mutagenesis method (Bernhardt & Urlacher, 2014). Obstacles in the substrate rate of transformation can be overcome by applying rational design of cytochrome P450 enzymes or subjecting them to directed evolution methods (Bernhardt & Urlacher, 2014). Due to their limitations as thermostability and improper substrate-active site pocket docking, these enzymes' practical applicability in industrial processes has been limited (Zhang, 2014). Substrate toxicity and toxic product may have a negative effect on the use of P450s in biotechnology (Donova et al., 2007). According to Donova et al., (2007), low substrate solubility in water is another limitation because the majority of the P450s substrates are hydrophobic. By adding a solubility enhancers for example cyclodextrins can help to overcome this problem by solubilizing hydrophobic molecules of substrates in order to facilitate their cellular absorption (Donova et al., 2007).

Coupling of a reaction is a degree of processivity indicating that all steps of reaction cycle occurred, or a substrate was converted into a product (Van Beilen et al., 2003). Van Beilen (2003) reported that numerous monooxygenases reduce molecular oxygen by two or four electrons without also oxidizing the substrate, producing water or

hydrogen peroxide as a result, respectively. This process is called uncoupling, reasons for that may be the lack of substrate, another reason is the occurrence of chemicals that are not appropriate to active site. It also happens when essential protein residues are altered or when the compound is unable to be oxidized (Van Beilen et al., 2003). Uncoupling of a process during oxidation employing NAD(P)H as an electron source without yielding a product is an additional factor that may restrict CYPs' potential for use in biotechnological techniques (Bernhardt & Urlacher, 2014). Bernhardt and Urlacher (2014) reported, that on the substrate binding step  $\text{Fe}^{3+}\text{O}_2^-$  and  $\text{Fe}^{3+}\text{O}_2^{2-}$ , reactive oxygen species can arise as a result of possible electron leaking. Furthermore, two water molecules can be formed and four electrons can be consumed without simultaneous substrate hydroxylation. As a result, no hydroxylated product is observed, but the costly cofactor NAD(P)H is having been utilized (Bernhardt & Urlacher, 2014).

Moreover, the heme cofactor may become unstable and the apoprotein degrade due to the generation of harmful hydrogen peroxide or active oxygen species (Bernhardt & Urlacher, 2014). The turnover number of the propane hydroxylation process was boosted by the site-directed and saturation mutagenesis while combined with the directed evolution of CYP102A1, which also improved the coupling effectiveness (Bernhardt & Urlacher, 2014). When considered collectively, despite the difficulties in applying cytochrome P450 systems for biotechnological processes, they represent highly promising and demanding enzyme systems for future applications (Bernhardt & Urlacher, 2014). Their exceptional adaptability and the chances they offer to advance and get around obstacles already make them excellent models for biotechnological applications in the present day (Bernhardt & Urlacher, 2014).

### **1.3. Thermostable P450 enzymes – CYP119**

Thermostable P450s are resistant to harsh industrial conditions, including high temperatures, high of pH levels and organic solutions, therefore they are good choices for the purposes of the field of biotechnology (Syed et al., 2014). The protein's capacity to withstand harsh conditions is enhanced by thermal stability (Koo et al., 2000). There aren't many thermostable P450s known to exist and the most well-studies thermostable

members of P450 family are CYP175A1 from bacteria and CYP119 from archaea (Li et al., 2007). CYP119 is the very first discovered and the well-characterized thermostable enzyme derived from *Sulfolobus acidocaldarius* as reported by Nishida and Ortiz de Montellano (2005). CYP175A1 from *Thermus thermophilus* is the well-studied thermophilic P450 from bacterial origin. P450 enzyme from *Sulfolobus tokodaii* sp. strain 7 is also thermophilic P450 enzyme. All of them are crystalized and their structures were determined (Nishida & Ortiz De Montellano, 2005). In addition to these natural thermostable P450s, *Bacillus megaterium* P450 CYP102A1 was used to develop 44 new thermostable P450s with novel catalytic activity (Li et al., 2007). From both *M. thermophila* and *T. terrestris*, two thermophilic ascomycetes that degrade biomass, there are a plenty of thermophilic P450s with biotechnological promise, as described by (Syed et al., 2014).

The enzyme of interest of current work is thermophilic CYP119 of the P450 superfamily. CYP119 is the first identified and cloned thermophilic member of the P450 superfamily (Koo et al., 2000) and the most thoroughly investigated acidothermophilic proteins from CYP superfamily (Niemeyer, 2008), derived from archaebacteria *S. acidocaldarius*, which was initially thought to be isolated from *Sulfolobus solfataricus* (Niemeyer, 2008). *Sulfolobus* grows best in environments with temperatures between 78 and 86°C and pH levels between 3 and 4 (Koo et al., 2000). CYP119 from archaea *S. acidocaldarius* resists extended cultivation at extreme temperatures, as well as at a pH level of 6.0 and has a melting temperature of 90°C (Chang & Loew, 2000; Koo et al., 2000). These enzymes have compact structure with typical P450-fold, the crystal structure of CYP119 is available (Koo et al., 2002). As reported by Koo et al., (2002) CYP119 is a soluble protein it does not have a hydrophobic tail. Simultaneously, CYP119 has a significant degree of similarity in the region of heme binding with other P450 enzymes of mammalian and bacterial nature (Nair et al., 2016). Compare to P450 CYP101, CYP119 showed similarity in optical spectra of ferric form, likewise ferrous form and ferrous-carbonmonoxy states of these two proteins (Denisov et al., 2001). It refers that CYP119 is an acidothermophilic enzyme, because CYP119 shows high degree of thermo- and baro-stability due to several factors (Paine et al., 2006). Aromatic regions are major impact on thermostability, whereas the presence of a linked polar hydrogen bonding and general assembling characteristics can be the reason of barostability of CYP119 (Liu et al., 2018; Paine et al., 2006). Another property of CYP119 is that it can bear pressure higher than 200 MPa (Jiang et al., 2019).

Thermo- and barostability of CYP119 is related to its small and compact packing having a higher quantity of ion pairs and aromatic residues (Koo et al., 2002). According to Koo et al., (2002), CYP119 shows the stability at up to 85°C, at higher temperatures, the enzyme only slightly transitions in spin state, from the low to the high. Changing in spin states depends on losing the distal water ligand. The change in the maximum Soret band from 415 nm to 390 nm implies the shift of the low spin state to the high spin state. The shift of P450 spin state depends on the ionic strength, pH, and temperature (Koo et al., 2000). Interior structure of protein, the stacking of aromatic residues, internal salt links, salt links on the surface and hydrogen bonds can all contribute to CYP119's thermostability as reported by Park et al., (2002). A portion of CYP119's shorter loops and lack of residues before the helix A, perhaps, are responsible for the thermostability. Compared with the majority of other mesophilic CYPs, CYP119 enzymes have a somewhat greater amount of aromatic stacking linkages per residue. Ten of the 22 pairs in CYP119 (11O7) are arranged for optimal stacking with rings between 70 and 90 degrees. Of the total 22 pairs, 15 have been discovered in the two large clusters (Park et al., 2002).

According to Hannemann et al., (2007) in relation to the homology model and CYP119's crystal structures, the protein's interior has a significant proportion of isoleucine amino acids and a relatively small amount of alanine amino acids, which improves side-chain packing and contributes to the protein's thermal stability. Further investigations revealed that CYP119's thermostability may be mostly determined by its aromatic clusters (Hannemann et al., 2007b). F/G region of CYP119 is subjected to conformational alterations while substrate binding (Wei, 2019). The expansive aromatic cluster along with entropic impact increases the thermal stability of CYP119, the substrate-binding pocket, which is not affected by the iron spin state or the active site architecture dictated by the threonine residues (Koo et al., 2000; Wei, 2019).

### **1.3.1. Reactions Catalyzed by CYP119**

The natural substrate for CYP119 remains unknown, likewise native partners of the CYP119 assisting in electron transfer nonetheless undetermined (Koo et al., 2002).

Although CYP119 is known to participate in binding lauric acid and styrene, and catalysis of the styrene epoxidation reaction and hydroxylation reaction of lauric acid (Koo et al., 2002). Moreover, CYP119 shown notable peroxidase activity and it was utilized for the electrochemical reduction of nitrite, nitric oxide, and nitrous oxide in addition to the electrochemical dehalogenation of  $\text{CCl}_4$  to produce  $\text{CH}_4$  (Blair et al., 2004; Ngcobo et al., 2023; Rabe et al., 2008).

CYP119 catalyzes fatty acid hydroxylation reaction utilizing of redox partner proteins, native for P450cam, Pdx and PdR (Niemeyer, 2008). As well, site-directed mutant CYP119 is able to hydroxylate lauric acid with redox partner proteins – Pdx and PdR utilizing NADH as reducing agent (Wei, 2019). As reported by Koo et al., (2002) T214V and D77R mutations increased hydroxylation of lauric acid for 15-fold and showing a  $k_{\text{cat}}$  value that is  $8.8 \text{ min}^{-1}$ . T214V mutation facilitated binding of substrate, as well as enhanced associated spin state change, as a result rate of hydroxylation reaction was increased, whereas D77R mutant bound to the redox partner tighter improving the electron transfer efficiency from Pdx to the heme iron of the enzyme (Koo et al., 2002).

CYP119 was also found to catalyze styrene epoxidation reaction, which characterized as an enantioselective  $\text{H}_2\text{O}_2$ -dependent (Koo et al., 2000). Reaction forms of the S- and R-enantiomers in a about 3:1 ratio (Zhang, 2014). Zhang et al., (2014) reported that the peroxide-dependent epoxidation of styrene at  $35^\circ\text{C}$  and  $70^\circ\text{C}$  in the presence of TBHP at pH 7.5 was enhanced by site-directed mutation of CYP119 of Thr213 to glycine, exhibiting  $k_{\text{cat}}$  values of  $51.2 \text{ min}^{-1}$  and  $346.2 \text{ min}^{-1}$ , respectively. Turnover rate was increased as a result of the T214V mutation's modified enantioselectivity ratio of the S- and R-epoxides due to a decrease in the steric restriction of the peroxide-dependent epoxidation of styrene and improved access of styrene and tert-butyl hydroperoxide (TBHP) to the catalytic site (Zhang, 2014). With a turnover number of up to  $308.8 \text{ min}^{-1}$  at  $35^\circ\text{C}$  and pH 7.5, as well as in the presence of TBHP, the quadruple mutant S148P/I161T/K199E/T214V created using the directed evolution approach shown enhancement in the epoxidation of styrene (Wang, 2018). Styrene modifies the spin state slightly (Koo et al., 2000). It was discovered that by utilizing TBHP, CYP119 catalyzes the sulfonation of sulfoxide and the sulfoxidation reaction of thioanisole (Wei, 2019). According to Wei et al., (2019) the F153G/T213G mutation led to a sulfoxide yield rise, a drop in sulfone yield, and a 2.4-fold increase in turnover rate. The F153G mutation may improve the specificity for the substrate. Furthermore, the K199E mutant with an acidic Glu residue and the S148P/I161T/K199E/T214V mutant improved the final product's

ratio of sulfoxide and sulfone (Wei, 2019). Furthermore, CYP119 can be employed for these reactions: electrochemical reduction of nitrite, nitrous oxide, and nitric oxide, as well as for the electrochemical dehalogenation of CCl<sub>4</sub> to produce CH<sub>4</sub> (Niemeyer, 2008).

CYP119 has a peroxidase activity, without the requirement for proteins or other oxidant cofactors, CYP119 can catalyze oxidation of AmplexRed using H<sub>2</sub>O<sub>2</sub> as an oxidant (Başlar, 2019). AmplexRed as the substrate can be used to monitor any potential peroxidase activity by fluorescence spectroscopy. At about 70°C, the CYP119 enzyme appeared highest in activity in the hydroxylation reaction of lauric acid to yield hydroxylauric acid. Similar assessment of peroxidase activity using AmplexRed was performed by Niemeyer et al., (2008) and a likely comparable activity peak in the vicinity of 75°C was observed (Niemeyer, 2008). A faster decrease in enzyme activity resulting from the increased levels of concentration of H<sub>2</sub>O<sub>2</sub> (5 mM) was noticed. CYP152A1 is recognized for its peroxidase activity. This protein demonstrated a consistent decline in peroxidase activity as temperature increased, suggesting that the increased reactivity of CYP119 at 75°C is actually caused by its thermostability rather than the acceleration of chemical reactions at higher temperatures. When the pH was raised to pH 8.5, CYP119 exhibited nearly consistent rise in reactivity, which was essentially nonexistent at lower pH values. Two electron acceptors was investigated by Niemeyer et al., (2008): cumene hydroperoxide (CHP) and tert- butyl hydroperoxide (TBHP). Under the circumstances of the oxidizing reaction, TBHP enhanced the enzyme's stability as well as its turnover rate. Thus, it would seem that TBHP is a very good choice for an oxidizing agent while screening. The epoxidation of styrene was carried out at 70°C and pH 8.5 with TBHP acting as the oxidant. In the presence of tert-butyl hydroperoxide (TBHP), the optimized reaction conditions at 70°C and pH 8.5 resulted in an increased turnover rate of 78 min<sup>-1</sup> (Niemeyer, 2008).

### **1.3.2. Secondary Structure of CYP119**

The P450-fold characteristics that are common to all crystallized P450 enzymes are preserved in the structure of CYP119 (Nishida & Ortiz De Montellano, 2005). However, CYP119 has a shorter sequence comparing to other P450 enzymes, this is due

to surface turns of CYP119 making it compact packing in contrast with the additional bacterial P450 enzymes (Nishida & Ortiz De Montellano, 2005).

CYP119 consists of 366 amino acids, 15  $\alpha$ -helices and 7  $\beta$ -sheets (Kestevur Dođru, 2019). According to Kestevur Dogru (2019), A-helix consists of residues 1-12,  $\beta$ 1A-sheet includes residues 13-17. Between  $\beta$ 1A and  $\beta$ 1B (19-25 residues) sheets Gly18 residue is located. This residue is conserved and it changes the rotation of  $\beta$ 1-sheet. B helix consists of residues 26-35 (Kestevur Dođru, 2019).

B-B' loop contain residues from 36 to 44. Residue Ser40 from this region makes a conserved hydrogen bond with Lys260 which is important for enzyme folding. B'-helix consists of residues 45-54. B'-helix and C-helix are separated with a loop region that has two small helices: B1-helix containing residues 62-66 and B2-helix containing residues 67-71. Leu69 is important for substrate binding. Following helix is C-helix with 73-81 residues. Arg80 is a conserved residue of this region that hydrogen bonds with D-ring propionate and Leu316 (Kestevur Dođru, 2019).

Regions that don't have any conserved residues are: the C-D loop with residue numbers 82-87, likewise D-helix containing residues 88-109, as well as E-helix, which consists of residues numbered 117-121 and E'-helix with residues 122-135 (Kestevur Dođru, 2019). As author reported, F-helix is flexible helix with 140-151 residues. The residues between 151 and 164 belongs to F-G loop. This loop region is the most flexible region of the enzyme and crucial for the process of binding to the substrate. The Phe153 residue belonging to the F/G loop is conserved. Its side-chain is positioned in the ligand-free architecture above and facing the heme. The residues in the G-helix are 164–179 and H-helix consists of residues 183-191. I-helix (residues 195-209) has Ala209 residue which is this helix's most significant residue. Utilizing Gly210 from the I'-helix, it serves for expanding the flexibility prolonged I-I' helices. Residue pair Glu212-Thr213 located I'-helix, containing residues 210-228 make this helix absolutely significant for the activities of enzymes. Arg154 of F-G loop and Glu212 also establishes a salt bridge. J-helix contains 230-238 residues and most critical residue of this helix is Ile234. A hydrogen bond formed between residue Ile234 and Leu239 of K-helix consisting of residues 239-251 is also crucial (Kestevur Dođru, 2019).

As Kestevur Dogru (2019) reported, ERR triad: Glu246 and Arg249 and Arg302 functions as a folding motif, therefore impacting heme-binding, also is important in binding of redox partner. ERR triad also play role in further maintaining the conserved linkage of Asp288 residue and Tyr26 of B-helix (Kestevur Dođru, 2019).  $\beta$ 3A-sheet

(residues 252-261) is structurally conserved. In the beginning of  $\beta$ 3A-sheet there is conserved sequence of four amino acids – PPVM or Pro252, Pro253, Val254, Met255 residues respectively. Hydrogen bonds between Pro 253-Asn355 of  $\beta$ 5B sheet and Met255-Val353 of  $\beta$ 5 sheet are important for folding. Conserved RTV (Arg256, Thr257, Val258) play key role in substrate recognition and enzymatic activity. C-ring propionate of heme and residue Thr257H are bound (Kestevur Dođru, 2019).

According to Kestevur Dogru (2019), heme group loss might result from the losing of this hydrogen bond, but since the Thr residue is not conserved, any other residue could take its place as long as the hydrogen bond is preserved. Heme binding arginine, also known as Arg259 residue, is a conserved  $\beta$ 3A-sheet residue that forms a hydrogen bond with the C-ring propionate of the heme group. Mutations at this location cause complete loss of activity because of the heme group is loss (Kestevur Dođru, 2019).

Kestevur Dogru (2019) published that, 262-274 residues belong to  $\beta$ 4-sheet and  $\beta$ 3B-sheet contains residues 257-283. Before the meander area with residues 287–318 there is a smaller K2-helix comprising residues 284–286. Of all the P450s, the meander region is extremely preserved. Phe310 is a residue that is effectively conserved and has a reduction potential of heme. Hydrogen bonds are preserved between His315 and the heme group's D-ring propionate (Kestevur Dođru, 2019).

Gly319 and Glu326 are two conserved residues of the L-helix that contain residues 319-336. Gly319 is required for heme-thiolate loop stabilization; and Glu326 is another conserved residue located in L-helix. The locations of following residues of Leu206, Leu207 and Gly210 are stabilized using hydrogen bonds.  $\beta$ 5A-sheet (residues 345-351) and  $\beta$ 5B-sheet (residues 355-365) altogether form broad and highly conserved hydrophobic surface of binding cavity, as well containing three residues that contact substrate; Glu352, Val353 and Leu354 which gives so called EVL sequence (Kestevur Dođru, 2019).

CYP119 includes two highly conserved residues in the active site: cysteine residue, Cys317 which is involved in heme coordination, as well as on the distal side, the I-helix of the protein includes the highly conserved threonine residue, Thr213 includes binding oxygen and ferrous prosthetic group, cleaving the attached oxygen molecule to produce the final active oxidized species, and coordinating a water ligand to the ferric heme (Koo et al., 2002; Park et al., 2002).

Highly conserved and catalytically important threonine residues are oxygen-activating Thr213, as well as extra threonine residues corresponded to 214 and 215.



Thr213 is important for catalysis, whereas Thr214 facilitates spin state regulation (Koo et al., 2000).

Additionally, they are essential for regulating the conformation of the active site and catalytic activity, but they are not necessary for maintaining the enzyme's thermal stability (Koo et al., 2000). In the studies of Koo et al., (2000) the H<sub>2</sub>O<sub>2</sub>-dependent styrene epoxidation at 30°C was shown to be three times more rapid, when Thr214 was modified to valine instead. However, the rate remained much lower than when Thr213 was mutated to any of these residues of phenylalanine or tryptophan residues with higher residue sizes (Koo et al., 2000).

Electron transfer is facilitated by the low spin to high spin shift that is promoted by the dissociation of the water ligand (Koo et al., 2002). Proximal Cys317 maintains ligation to heme residue. CYP119's ideal growing environments were associated with thermophilic and acidophilic sulfur-containing surrounding (Wei, 2019).

Nishida and Ortiz de Montellano (2005) reported that CYP119 don't have a hydrophobic tail and is thus a soluble protein. Mammalian, fungal, and bacterial CYP119 all have an identical binding site for the heme. Two molecules are joined together in the crystal structure of CYP119 by a zinc ion that coordinates to Glu139 and His178 in every one of the two molecules of protein. However, they don't describe an enzyme's functional aspect. A water molecule and iron form a bond with a separation of 2.27 Å between the iron and oxygen. An additional water at a distance of 2.93 Å is hydrogen-bonded to the water ligand. The proximal side's thiolate, sulfur, and iron exhibit a separation of 2.27 Å (Nishida & Ortiz De Montellano, 2005).

### **1.3.3. Previous Studies on CYP119**

Several mutations on CYP119 enzyme have been made and characterized in previous studies by Koo et al., (2002) such as mutations D77R and T214V (Koo et al., 2002). According to them, 15-fold increase in activity is achieved in reaction of fatty acid hydroxylation by T214V and D77R mutations. T214V mutation facilitated the binding of the substrate, as well as enhanced associated spin state change, as a result improving the rate of hydroxylation, whereas D77R mutation resulted in tighter binding to redox partner

putidaredoxin thus increasing the rate at which electrons are transferred from Pdx to the enzyme's heme iron (Koo et al., 2002).

F24L mutation was created by Park et al., (2002) to probe contribution of aromatic stackings to thermostability (Park et al., 2002). Phe24, Trp4, Phe5, Tyr15 and Trp281 are within 6 Å packed extremely high. Phe24Ser has 10.2°C lower melting temperature comparing to WT CYP119. Phe24Leu mutation possesses a 4°C lower melting temperature than WT CYP119 implying a significance in contribution to feature of thermostability of CYP119 (Park et al., 2002). Thr213 and Thr214 mutants were characterized by Koo et al. (Koo et al., 2000). Studies showed that these residues in enzyme are crucial for regulating the enzyme's catalytic activity, spin state, and active site conformation. However, they are not essential to its thermal stability (Koo et al., 2000).

Zhang et al., (2014) reported a T213G mutants, that greatly improves the turnover rate 4.4-fold to 346.2 min<sup>-1</sup> for the reaction of peroxide-dependent styrene epoxidation, and the S and R-enantiomers ratio of the epoxide yields increases twofold to 5.8 in the double T213G/T214V mutant (Zhang, 2014).

T213R/T214I was characterized by Başlar et al., (2020) with 5-fold greater  $k_{cat}$  for AmplexRed peroxidation (Başlar et al., 2020). The same mutant showed 2-fold greater  $k_{cat}$  for reaction of styrene epoxidation. Mutation demonstrated increased resistance to degradation of cofactor heme under influence of H<sub>2</sub>O<sub>2</sub>. However, effects on the  $K_m$  for styrene and H<sub>2</sub>O<sub>2</sub> was not observed of the T213R/T214I mutant, however binding affinity for lauric acid decreased 4-fold (Başlar et al., 2020).

Salt bridge that connects residues Arg154 and Glu212, likewise aromatic cluster residues Tyr2, Trp4, Trp231, Tyr250, Trp281 that are important for thermostability were investigated by Ortiz de Montellano (2003). Mutations on Glu212 to aspartate and glutamine amino acid residues have been reported, while Arg154 underwent mutations to either glutamine and alanine amino acid residues. These mutations did not affect the thermostability. R154A and R154Q mutants showed binding of the lauric acid approximately 3 and 10 times weaker than the WT. The E212D mutant showed no signs of catalytic activity. Also, W231A, W281A Y250A, and Y168A single mutants and Y2A/Y250A and W4A/W281A double mutants were created. Based on the mutants' melting temperatures, it was determined that a mutation of any residue in the hydrophobic patch reduced the stability of CYP119 by about 10°C (Ortiz de Montellano, 2003).

K176R-I329M, D52V-D72H, E273G-K348R, I272V-N367R-E368I, E114D, R80G, R259K, S40C-T67A-V118L, R235G-I282V, I299V-E352K, G313E, F24S mutations created by Maves and Sligar, showed decrease in thermostability (Maves & Sligar, 2001).

### 1.3.4. Lauric Acid Hydroxylation

Twelve carbons compose up the medium-chain saturated fatty acid lauric acid that is straight-chain and has potent bactericidal effects. In addition to being an algal metabolite, it also functions as an antimicrobial and plant metabolite. Lauric acid is an inexpensive easily handled, non-toxic material that is widely used in laboratory research. At room temperature, lauric acid has a solid structure, but in boiled water, it melts quickly.

Chemical formula of lauric acid is shown in Figure 1.12.



Figure 1.12. Lauric acid molecule (PubChem CID 3893).

Utilizing the redox partner molecules putidaredoxin (Pdx) and putidaredoxin reductase (PdR), CYP119 hydroxylates lauric acid. As reported by Zollner et al., (2009) the first electron transfer from the reductase protein occurs in the second phase of the process and oxygen binding to the iron of the heme (Zollner et al., 2009). Electron is donated by reducing agent, NADH molecule. NADH donates 2 electrons in total in the whole reaction by reducing putidaredoxin reductase, redox partner. Putidaredoxin reductase reduces putidaredoxin, which in its turn transfers electrons to CYP119 enzyme one at a time, reducing CYP119 enzyme into ferrous state. Whenever the ferrous state

promptly bonds an O<sub>2</sub> molecule, it converts into an oxyferrous complex (Zollner et al., 2009).

The first step of lauric acid hydroxylation reaction by CYP119 is substrate binding to the enzyme, e.g., lauric acid binds CYP119 as shown in Figure 1.13.

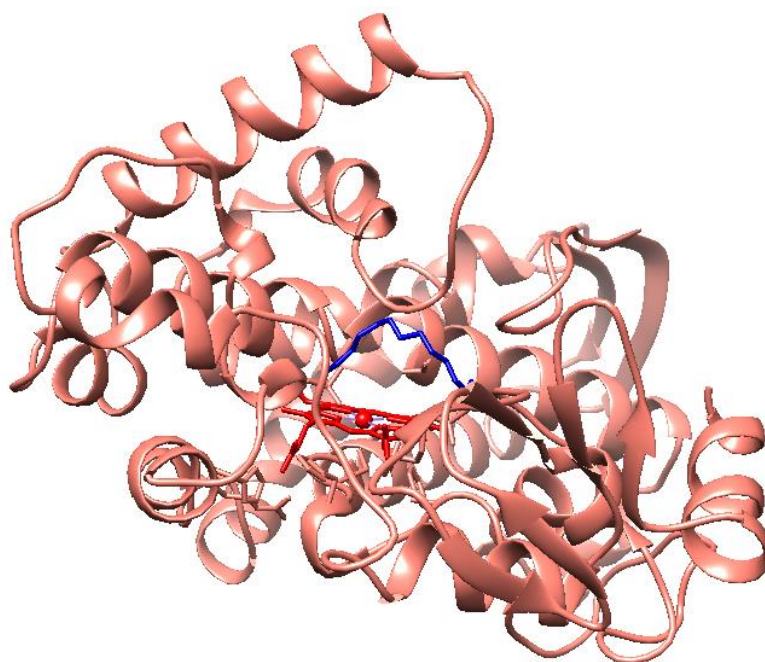


Figure 1.13. CYP119 PDBID: 1I07. Hydroxylation reaction starts with substrate binding. Lauric acid (in blue) binds CYP119 (in pink) in the region of active site from the distal side of the structure of heme (in red). The image was created with UCSF Chimera.

The following step is the second reduction of CYP119 and formation of Fe<sup>3+</sup>-OO<sup>2-</sup>. Following steps are: first protonation and formation of Fe<sup>3+</sup>-OOH<sup>-</sup> and Second protonation and formation of Compound I (Kim et al., 2014).

Compound I hydroxylate lauric acid and releases hydroxy lauric acid and H<sub>2</sub>O molecule. The enzyme at this point returns to its resting state and prepares for a new turnover (Sevrioukova et al., 2001).

Single electron is delivered by FeS of Pdx to the heme-center of P450cam through Pdx(Asp38)-P450cam(Arg112)-heme route through PdR(FAD)-PdR(Trp330)-

Pdx(Cys39)-Pdx(FeS) route from NADH-dependent putidaredoxin reductase and the enzyme becomes activated and binds oxygen (Sevrioukova & Poulos, 2011).

NADH oxidation/reduction is represented in Figure 1.14.

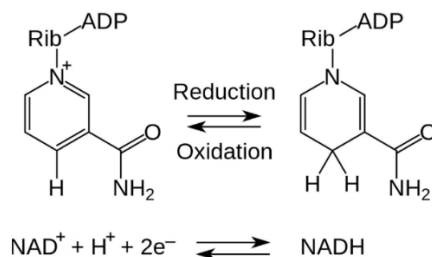


Figure 1.14. NADH oxidation/reduction.

CYP119 bound to lauric acid has a  $K_d$  value for Pdx binding of 2.1 mM. The D77R mutation decreases  $K_d$  value down to 500  $\mu\text{M}$ . The values reported in the literature for Pdx's binding to P450cam bound to camphor vary from 5 to 17  $\mu\text{M}$ . Pdx binds to CYP119 with a substantially larger dissociation constant than it does to P450cam. The D77R mutation decreased the  $K_d$  for Pdx and CYP119 by more than 4-fold, which is consistent with the protein's 5-fold enhancement in rate of electron-transfer over wild type CYP119 (Aoki et al., 1998; Koga et al., 1993; Koo et al., 2002).

#### 1.4. Cytochrome P450cam and Putidaredoxin Complex

Cytochrome P450cam (CYP101) is among the most extensively studied members of CYP family. P450cam is obtained from *Pseudomonas putida* bacterium, and catalyzes the hydroxylation reaction of its native substrate *d*-camphor, in the stereo- and regiospecific way (Unno et al., 1997) and it was the first cytochrome P450 for which a crystal structure was obtained (PDBID: 3L63) (Sibbesen et al., 1996). There is a crystal structure available of cytochrome P450cam and putidaredoxin (Pdx) complex (PDBID: 4JWS).

For the process to produce 5-exo-hydroxycamphor product and water by conversion of substrate, camphor, as well as molecular oxygen, P450cam demands a couple of electrons during its reaction cycle (Sevrioukova & Poulos, 2002). Two electrons are transported to P450cam through ferredoxin containing iron-sulfur (2Fe/2S) cluster, Pdx in two distinct stages. The latter accepts electron from putidaredoxin reductase (PdR) containing FAD cofactor (Harford-Cross et al., 2000; Tang et al., 2008).

Nagano et al., (2003) reported that ferric substrate-free enzyme binds to substrate, d-camphor, displacing six water molecules from the active site. The enzyme's ferric camphor-bound state then takes one electron from Pdx to produce a ferrous form that is bound to a substrate. O<sub>2</sub> is then bound to the ferrous form to form oxyP450cam, a derivative of ferrous O<sub>2</sub> bound to D-camphor. A second one-electron reduction by Pdx leads to the hydroxylation process of D-camphor, which yields 5-exo-hydroxycamphor and water, thereby recovering the ferric substrate-free resting state (Nagano et al., 2003).

Pdx is the physiological reductant of P450cam and effector (Pochapsky, 1996; Sibbesen et al., 1996; Zhang et al., 2008). According to authors, because Pdx carries a strong negative charge, it binds to P450cam from the proximal face and their interaction is dictated by charge-charge coupling. Furthermore, without Pdx, the oxygenated P450cam is unable to turnover. Therefore, Pdx also plays an effector role in P450cam catalysis and Pdx impacts the heme active site of P450cam (Pochapsky, 1996; Sibbesen et al., 1996; Zhang et al., 2008).

Unno et al., (1997) reported, that the camphor substrate is located in an internal active site pocket of P450cam near the heme distal face close to the location where ligands bind and displace waters from the distal pocket, shifting the heme iron from a 6C/LS (6 coordinate low spin) configuration that binds with water as a sixth ligand to a 5C/HS (5 coordinate high spin) configuration (Unno et al., 1997). According to Unno et al., (1997), Pdx binding to P450cam results in a six-coordinate low-spin species, with water likely acting as the sixth ligand. This alters P450cam's distal side and raises the pocket's water occupancy. The spin-state equilibria of ferric P450cam is shifted to the low-spin state by the complex formation of P450cam and Pdx; this change in spin state is characterized by a drop in absorbance at around 390 nm and an increase in absorbance at approximately 420 nm (Unno et al., 1997).

P450cam-Pdx complex and intermolecular salt-bridges identified in P450cam-Pdx combination is shown in Figure 1.15. (Pochapsky et al., 1996; Zhang et al., 2008).

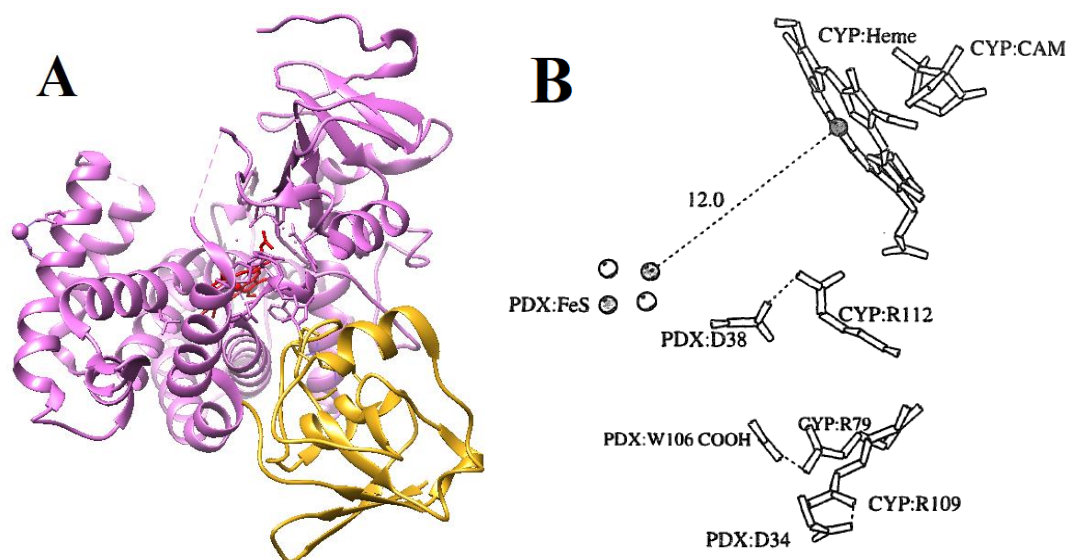


Figure 1.15. A. P450cam (in purple)-Pdx (in gold) complex. Image was created using UCSF Chimera. B. Intermolecular salt-bridges observed in P450cam-Pdx complex (Pochapsky et al., 1996).

P450cam-Pdx complex is 58 kDa. Pochapsky et al., (1996) suggested complex structure model of P450cam-Pdx, which is 12 Å Fe-Fe long, with three arginine residues of P450cam: Arg109, Arg112, and Arg79 that forms three salt bridges between Pdx Asp34, Asp38, and Trp106 residues, respectively. Pdx's C-terminal residue, Trp106, is required for Pdx to carry out its effector role and reduction function, and it may offer an architectural component for the binding surface (Pochapsky et al., 1996).

In the P450cam-Pdx complex, Arg72, Arg112, Lys344, and Arg364 participate to the electrostatic interactions (Unno et al., 1997). Previous investigation showed that mutation of Arg112 site causes a dramatic drop in enzymatic activity and 600-fold rise in dissociation constant for complex formation with Pdx (Unno et al., 1996). Sligar et al., (1989) demonstrated that replacing Arg72 and Lys344 residues to glutamate and glutamine residues, decrease the binding affinities (20-60%) between Pdx and P450cam (Sligar, 1989).

Role of Arg112 was reported by Unno et al., (1996) in detail. According to their research, by changing residue of Arg112 replacing with a neutral residue for instance Tyr, Cys, or Met led to decrease in affinity between P450cam-Pdx complex, as well as the oxidation and reduction potentials of cytochrome P450cam ( $\text{Fe}^{3+}$  ferric and  $\text{Fe}^{2+}$  ferrous

couple) declined in a manner identical to the decline in rate of electron transfer after amino acid replacement (Unno et al., 1996). Therefore, Unno et al., (1996), suggested replacement of amino acids at spot of 112 with a neutral amino acid influenced the rate of electron transfers within the two metal centers (Shimada et al., 2000; Unno et al., 1996). In P450cam, Arg112 engages in contact with heme and its surrounding area through a complex network of hydrogen bonds (Koga et al., 1993). Mutants of the ferrous P450cam having Gln109, Met112, Lys109, and Lys112 did not exhibit spectrum alterations that are typically seen during complex formation when reduced Pdx is complexed (Koga et al., 1993).

Sevrioukova et al., (2006) optimized the model by Pochapsky et al., (1996) (Pochapsky et al., 1996; Sevrioukova, 2006). According to Sevrioukova et al., (2006), key Pdx residues Tyr33, Asp38, Arg66, and Trp106 are anticipated to be crucial in redox protein recognition and electron transfer. Arg109 residue of P450 interacts with Trp106 residue of Pdx (COOH) and likewise Arg112 residue of P450 and Asp38 of Pdx form a highly conserved salt bridges. A salt bridge formed by interaction of Glu65 residue of Pdx and Lys344 residue of P450 residues is demonstrated as unimportant for the redox couple's activity. The first electron transfer route follows the route Cys39 residue of Pdx then Asp38 of Pdx passing the electron to Arg112 of P450cam (Sevrioukova, 2006).

As mentioned above, upon substrate binding to P450cam, the first electron is delivery by Pdx occurs. In order to achieve full activity second stage of electron transfer demands the presence of Pdx molecule, although P450cam is able to accept the initial electron from any additional donors if the reduction potential is appropriate (Zhang et al., 2008).

According to Zhang et al., (2008) electrostatic interaction occurs between residues of salt bridge Arg112 residue of P450cam and Asp38 residue of Pdx rendering binding of two proteins, as well as the Pdx's aromatic Trp106 residue's essence has been claimed to be very critical for binding to P450cam. Iron-sulfur cluster binding region of Pdx directly faces the heme of P450cam with distance 17.1 Å. The side chains of residues such as His352 and Arg72, Glu76, and in P450cam are located close to the side chains of Gln25, Val28, and Tyr33 in Pdx (Zhang et al., 2008).

Arg112 contacts the heme propionate directly, through backbone atoms of residue Cys39 and through a bond from the Fe1, Asp38 side chain passes one electron at a time to Arg112 of P450cam. Leu358 and Leu356, His361, Met121 residues of P450cam, together with residues of Pdx: Ile35, Val36, and Thr47 envelop Trp106 in a hydrophobic



pocket. Trp106 also has non-bonded interactions with the methyl groups of Leu356, Leu358, Met121, His361, and Thr47 residues of Pdx (Zhang et al., 2008). These interactions play influencing role in the formation of the complex (Zhang et al., 2008).

The substrate binding region and O<sub>2</sub> molecule at the distal side undergo structural alterations upon binding of Pdx, which "pushes" on the proximal side of the heme and positions the critical catalytic waters for appropriate proton transfer to the O<sub>2</sub> linked to Fe (Sevrioukova et al., 2010). Only the reduction of the Fe<sup>2+</sup> P450–O<sub>2</sub> complex, makes this effector role significant in the second electron transfer step (Sevrioukova et al., 2010).

Mutations of surface residues of Pdx showed that Asp38 to Ala nearly eliminates the second electron transfer and the second reductive process is also rendered inactive by the W106A mutation, whereas the W106F variation maintains roughly 60% of its activity. Therefore Asp38 and Trp106 are key residues in electron transfer (Sevrioukova et al., 2010).

Approximately 119 crystal structures of bacterial P450cam (CYP101A1) are accessible with open, closed, and intermediate conformational states according to Guengerich (2018). In these states, the movement of the F and G helices, surrounding the substrate binding channel, fluctuates (Guengerich, 2018).

According to Guengerich (2018), Pdx is the immediate electron donor to P450cam, and has also been found to perform a distinct "effector" function in catalytic processes, where it enhances product formation in addition to electron supply. But the exact mechanism is still unclear. In general, the reduced P450 Fe<sup>2+</sup>O<sub>2</sub> (or Fe<sup>3+</sup>–O<sub>2</sub><sup>–</sup>) bounds to the oxidized Pdx complex for sufficiently long for its structure to alter. Reduced P450cam is induced to shift to the open form by oxidized Pdx. However, this shift is somehow inhibited by carbon monoxide binding. Research findings suggest that Pdx appears to bind to the exact same P450cam region both in its open and closed state (Guengerich, 2018).

CYP101A1 from *Pseudomonas putida* (P450cam) has  $k_{cat}$  values of 1,000–3,000 min<sup>–1</sup>, most CYPs have  $k_{cat}$  values within the scope of about 1–300 min<sup>–1</sup> (Bernhardt & Urlacher, 2014). Thr252 is the conserved threonine in P450cam (Koo et al., 2000). The uncoupled reduction of oxygen to H<sub>2</sub>O<sub>2</sub> and H<sub>2</sub>O is greatly increased and the binding of substrates is affected when this residue has been altered to an Ala or Val (Koo et al., 2000).

Tripathi et al., (2013) solved the crystal structure of P450cam-Pdx complex, both oxidized and reduced P450cam to 2.2 and 2.09 Å, respectively. Depending on data they

published, it was anticipated that redox partner Pdx binds from the proximal face of the P450cam. Proton-coupled electron transfer necessitates the formation of a water-mediated H-bonded network, which is made possible by Pdx binding, which causes the P450cam to switch to an open state. Two key residues are Asp38 of Pdx which ion pairs with Arg112 of P450cam and the C-terminal Trp106 of Pdx. On top of that, Trp106 of Pdx establishes a hydrogen bond with Asn116 and nonbonded contacts with Ala113 of P450cam. In addition, Arg109 of P450cam interacts with the carboxyl group of Trp106 residue of Pdx. Trp106 of Pdx interactions perform a critical part in the conformational transition of P450cam from its closed state to its open state. Additionally, Trp106 is particularly significant for the second phase of electron transport process (Tripathi et al., 2013).

Redox partners' contact is guided and maintained by electrostatic interactions, while hydrophobic residues are essential for anchoring the relationship and promoting electron transport (Koo et al., 2002). Key Arg residues located in P450cam binding site are anticipated to interact with Asp residues of Pdx (Koo et al., 2002).

Studies by Sevrioukova (2006) showed that Arg109 of P450 is critical for P450cam-Pdx association. Another interaction with not much impact between P450cam and Pdx is a salt bridge connecting Glu65 residue of Pdx and Lys344 residue of P450, its shown very little influence in the activity of the P450cam-Pdx couple (Sevrioukova, 2006). P450cam and Pdx interact is very specific manner: electron transfer routes from Pdx to ferric P450cam and includes Asp38 on route (Sevrioukova, 2006).

According to Shimada et al., (2000) there are several arginine residues that are crucial in P450cam, they are located at the Pdx binding site, mutations of corresponded residues showed uncoupling between proteins (Shimada et al., 2000). These residues are Arg109 and Arg112. Cys39, that forming bond with 2Fe-2S cluster, is involved in electron transfer. Major pathway or route for electron delivery to P450cam from Pdx is defined to be the route containing essential residues such as Asp38 of Pdx and Arg112 of P450cam (Shimada et al., 2000).

Studies by Hiruma et al., (2013) showed, another essential interaction in P450-Pdx complex is a salt bridge formed between Asp38 of Pdx and Arg112 of P450cam showing significant impact on the binding of two proteins, likewise critically important in transferring of electrons (Hiruma et al., 2013).

Arg66 of Pdx is crucial that participate in salt bridge formation with Glu76 of P450cam, appears to play role in stabilization of the complex of proteins Pdx-P450cam

(Roitberg et al., 1998; Wallrapp et al., 2008). Apart from the strong electrostatic interactions, the Pdx–P450cam complex has been primarily anchored by hydrophobic and van der Waals interactions (Roitberg et al., 1998; Wallrapp et al., 2008).

Pochapsky et al., (2003) proposed the P450cam/Pdx complex structure based on the P450cam and Pdx structures already available. Three arginine residues of P450cam—Arg109, Arg112, and Arg79—create salt bridges with two aspartic residues and one tryptophan residue of Pdx: Asp34, Asp38, and Trp106, respectively. This representation shows a 12 Å Fe-Fe length of electron transfer route (Pochapsky et al., 2003).

#### **1.4.1 Electron Transfer Pathway from Pdx/PdR to P450cam and CYP119**

Pdx and PdR are native partner proteins of P450cam according to Sevrioukova et al., (2003). Pdx transfers electrons to P450 enzymes from oxidoreductases – PdR to perform hydroxylation reactions (Sevrioukova et al., 2003). PdR are dependent on reducing agents usually NAD(P)H, an contain FAD cofactor in their structure, which participate in electron transfer process. Pdx also plays a coupling effector role, however it is not fully understood yet (Sevrioukova et al., 2003).

Two different electron transfer steps from Pdx to P450 are required for the reaction to occur (Sevrioukova & Poulos, 2002). An electron delivery route starting from FAD cofactor of PdR and 2Fe-2S cluster of Pdx is predicted to be around 12Å-long (Sevrioukova et al., 2010).

According to Sevrioukova et al., (2010), PdR accepts electron from electron donor (NAD(P)H) and Pdx receives one electron at a time in two steps through PdR(FAD)-PdR(Trp330)-Pdx(Cys39)-Pdx(FeS) route from NADH-dependent putidaredoxin reductase. PdR-Pdx interface is 365 Å<sup>2</sup> of surface area, containing nine hydrophobic, four polar, and five positively charged residues from PdR side and four hydrophobic, four polar, and three charged residues from Pdx side and one Arg310(PdR)-Asp38(Pdx) salt bridge, that it is vital for docking and determining the ideal positions of PdR and Pdx for

transferring electrons. Steric affinities and hydrophobic forces are what propel the PdR-Pdx relationship (Sevrioukova et al., 2010).

Single electron is delivered by Fe-S of Pdx to the heme-center of P450cam, immediately after substrate binding to enzyme, through Asp38(Pdx)-Arg112(P450cam)-heme route and the enzyme becomes activated and binds oxygen (Sevrioukova, 2006). A single molecule of water is produced as a result of cleavage bonding between two oxygen molecules and the consumption of two protons (Sevrioukova, 2006). Water molecule subsequently released from the active site. Immediately following that, a single oxygen atom is added to the substrate to yield a product (Sevrioukova, 2006). Since formation of product can possibly be replaced with the formation of undesirable chemicals, uncoupling of the reaction cycle can happen (Morlock et al., 2018).

As reported by Morlock et al., (2018), examples of undesirable chemicals formed instead of products can be oxygen species, superoxide anion, or hydrogen peroxide. Moreover, hydrogen peroxide itself could also be further reduced to water. Despite the consumption of NAD(P)H, reaction does not give to the desired product, moreover, the enzyme can be made inactive by a reaction between reactive oxygen species and amino acids. Uncoupling can happen with or without a substrate and is very dependent on the circumstances of the reaction (Morlock et al., 2018).

## **1.5. Protein Engineering and Design**

Enzymes are biological catalysts responsible for cell metabolism processes. Many commercially available enzymes are manufactured and showed the developments in enzyme production industry in recent years, yet obtaining an enzyme with the most ideal characteristics is still difficult (Başlar, 2019). Protein engineering is a young discipline, used in improving functions of many enzymes for industrial catalysis. Two primary methods in protein engineering are rational design and directed evolution (Başlar, 2019).

Three processes are often involved in protein engineering: choosing the modifications to the protein's sequence, implementing these modifications, and assessing the protein variations for better properties (Başlar, 2019; Kestevur Doğru, 2019). Computational methods have become important recently in the prediction process

(Winkler et al., 2018). There are so many tools and software that can be used in designing a novel enzyme. As well as, the Protein Data Bank (RCSB PDB) comprises approximately 160,000 structural proteins with scientifically verified crystal data ([www.rcsb.org](http://www.rcsb.org)) can be useful toward goals in improving enzyme's activity or any other desired properties.

### **1.5.1. Directed Evolution of Proteins**

One of the strategies in protein engineering is directed evolution of proteins (Başlar, 2019). Traditionally, a repetitive two-step process is the foundation of directed evolution approach according to Lutz et al., (2010). First generating varieties of molecules by in vitro recombination and random mutagenesis. Secondly, using high-throughput screening or selection to identify individuals in the library with superior attributes in the intended phenotype (Lutz, 2010). To produce proteins with the desired characteristics, directed evolution imitates Darwinian evolution (Başlar, 2019).

Basically, in directed evolution, one or more initial genes are often randomly mutated, then a screening or selection phase is performed to find or isolate enzyme variants that have improved one or more desirable qualities (Dalby, 2011). Until the required degree of change is achieved, the procedure can be repeated (Dalby, 2011).

Error-prone PCR (epPCR) is the most frequently employed technique, which introduces random point mutations (Dalby, 2011). Furthermore, random recombination of non-homologous genes, random codon insertions and deletions, and the production of a library of random truncations were made possible by saturation or cassette mutagenesis, which targeted pre-selected sites or randomly dispersed sites (Dalby, 2011).

Studies involving directed evolution necessitate an assessment phase to determine the best mutant protein variants with particular attributes (Dalby, 2011). There are two types of assessment approaches: screening-based methods and selection-based methods (Başlar, 2019). Mutants in selection-based methods are examined for a desired characteristic. Screening-based techniques rely on the substrate turnover rate, which is determined by the applied assay (Kestevur Doğru, 2019). A limitation of directed evolution research is that it results in a large number of failed mutants for the intended

activity, which is expensive and time-consuming (Başlar, 2019; Dalby, 2011; Kestevur Dođru, 2019).

### **1.5.2. Rational Design of Proteins**

Rational design is another strategy for protein engineering that uses computational tools to design proteins. Knowing of protein structure, function and whatnot is very essential in order to rational design of proteins (Başlar, 2019).

A significant portion of rational engineering techniques are procedures that make use of high-resolution, three-dimensional structural data. It is possible to alter the specificity and affinity of protein interactions by rational design (Marshall et al., 2010). The principle behind the de novo design technique is to replicate the primary functional region of an enzyme and modify it alone to get the intended results (Kestevur Dođru, 2019).

Site-directed mutagenesis method is one of the effective ways to create specific targeted changes in DNA with various purposes (Hogrefe et al., 2002). For instance, previous research performed by Koo et al., (2002) showed 15-fold increase in activity is achieved in reaction of fatty acid hydroxylation by T214V and D77R mutations. T214V mutation facilitated binding of substrate, as well as enhanced associated spin state change, as a result enhancing the rate of hydroxylation, whereas D77R mutation bound to redox partner Pdx tighter improving the rate of electron delivery from Pdx to the heme group of the enzyme (Koo et al., 2002). Through applying the technique of site-directed mutagenesis, it is possible to increase both the delivery of electrons from Pdx to the CYP119 enzyme and the protein-protein surface affinity.

According to Kestevur Dogru (2019), the following residues are categorized as structurally significant and conserved structural elements of CYP119: residues producing conserved hydrogen bonds, ERR triad, residues participated in biding of substrates, heme binding regions, and thermostability associated regions (Kestevur Dođru, 2019).

Figure 1.16 demonstrates a comparison of rational design and directed evolution.

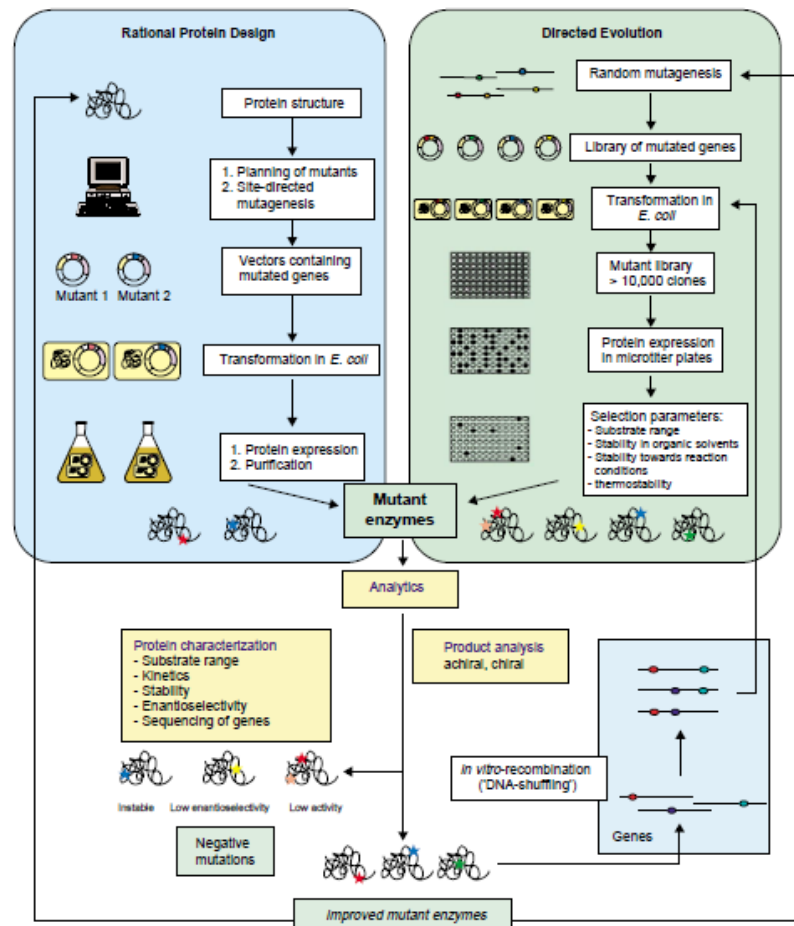


Figure 1.16. Directed evolution and rational protein design are compared. In the process of rational protein design, SDM is used to prepare mutants based on their protein structures. Following transformation in the host organism (such as *Escherichia coli*), the variation is purified, expressed, and its desired features are examined. Using random mutagenesis to create mutant gene libraries that are then expressed in the host organism is the first step in directed evolution. Typically, a variety of selection criteria are used in microtiter plates to screen protein libraries. Positive and negative mutations are distinguished by protein characterization and product analysis. For additional developments DNA shuffling in vitro recombination is one method that can be employed. It is possible to mix or repeat both protein engineering techniques until biocatalysts with the required characteristics are generated (Bornscheuer & Pohl, 2001).

The aromatic clusters I and II were also identified as residues relevant to thermostability (Kestevur Dođru, 2019). A crucial residue for substrate interaction in the B2-helix is Leu69. Along with Arg302 of the meander region, Glu246 and Arg249 create an ERR triad. They also make for the sole CYP conserved motif, EXXR. The ERR triad affects the binding of heme structure by acting as a folding motif, contributing to the binding of redox partners, and maintaining the conserved interaction between the B-helix (Tyr26) and the meander region (Asp288) (Kestevur Dođru, 2019). Important residues maintaining heme structure binding and keeping at the same position are Arg259, Thr257, His315, Cys317, Glu212 (Park et al., 2002). Arg259, also known as heme binding arginine, hydrogen bonds with heme group at a C-ring propionate position (Kestevur Dođru, 2019). By mutating of conserved residues mentioned above lead to total inactivity because of the heme group's loss, thermostability or appropriate folding etc. (Kestevur Dođru, 2019). Therefore, non-conserved residues on the surface of binding sites of proteins must be selected for the following mutagenesis studies.

## **1.6. Scope of the Study. Aims and Purposes**

Cytochrome P450 enzymes are outstanding versatile biocatalysts with large number of accepted substrates and catalyzed reaction types, with broad applicability (Bernhardt & Urlacher, 2014). Cytochrome P450 enzymes are very desirable as catalysts in practical applications because of their ability to carry out stereoselective and regioselective hydroxylation on complex molecules and all these findings make cytochrome P450 enzymes such enormous potential for application in biotechnology (Bernhardt & Urlacher, 2014). Cytochrome P450 enzymes are applied widely on industrial scale, for example progesterone hydroxylation to yield 11 $\alpha$ -hydroxyprogesterone which is catalyzed by *Rhizopus arrhizus*, CYP105A3 which is also called P450sca-2 catalyzes compactin's 6 $\beta$ -hydroxylation and etc (Winkler et al., 2018).

Limitations of these enzymes such as the necessity for specific electron transfer proteins and the requirement for electron donors such as costly cofactor NAD(P)H; as well as uncoupling which is the process of formation of reactive oxygen species instead of desired products (Bernhardt & Urlacher, 2014; Koo et al., 2002).



To overcome some of these limitations, various methods are currently used according to Bernhardt and Urlacher (2014). For example, a notable enhancement in product production can be achieved by enhancing the affinity of redox partner. As literature says (Bernhardt & Urlacher, 2014), truncation of Adx showed 20-fold increased efficiency in formation of bovine CYP11B1-dependent hydrocortisone, enhanced activity for 3-fold in formation of CYP11B1-dependent corticosterone and furthermore conversion of CYP11A1-dependent cholesterol was improved for a 75-fold (Bernhardt & Urlacher, 2014). These impressive examples clearly demonstrate that by optimizing the redox partner affinities, it is possible to substantially increase the production of products (Bernhardt & Urlacher, 2014).

In research of Koo et al., (2002) 15-fold increase in activity is achieved in reaction of fatty acid hydroxylation by T214V and D77R mutations were reported. According to this study, T214V mutation facilitated binding of substrate, as well as enhanced associated spin state change, as a result improving the rate of hydroxylation, whereas D77R mutant bound to redox partner putidaredoxin (Pdx) tighter improving the rate of electron delivery from Pdx to the heme group of the enzyme (Koo et al., 2002).

An enhanced electron transfer from Pdx to the CYP119 enzyme can be obtained by engineering an improved affinity and binding of the protein-protein interface (Koo et al., 2002). A structural alignment is an effective method to determine a region of the binding surface of Pdx on CYP119 enzyme (Koo et al., 2002).

Yet only around 10-20% of DNA sequence of P450 enzymes demonstrate resemblance, overall protein structures of these enzymes' superfamily are similar (Ortiz de Montellano, 2003). Therefore, CYP119 enzyme alignment with P450cam can be efficacious way to define a potential nonideal protein-protein interaction and docking site, in order to adapt the natural redox partners for P450cam – Pdx and putidaredoxin reductase (PdR) to CYP119 enzyme (Koo et al., 2002).

Aim of current project is engineering of a novel CYP119 enzyme that has higher biocatalytic activity, by using site-directed mutagenesis method, optimizing protein-protein interaction between CYP119 and redox partner protein, Pdx, thus increasing affinity between them, in order to achieve higher electron transfer rate.

Main purpose of current project is to obtain CYP119 mutants with enhanced electron transfer rate, efficiently working in a three-protein system with Pdx and PdR from *Pseudomonas putida*, by rational design strategy, using P450cam enzyme as a model structure.

## CHAPTER 2

### MATERIALS AND METHODS

#### 2.1 Bioinformatics Analysis

Protein design and computational prediction have proven to be effective in producing proteins with unique enzymatic activity, enhanced binding affinity, higher thermostability, and modified ligand specificity (Gromiha, 2019). Understanding the binding affinity and recognition process of protein-protein complexes, predicting complex structures, and analyzing and identifying binding sites and binding residues are all necessary for the engineering of protein-protein complexes (Gromiha, 2019).

##### 2.1.1 Structural Alignment of Proteins

By creating a more favorable protein-protein affinity, putidaredoxin can transfer electrons to the CYP119 enzyme more efficiently (Koo et al., 2002). According to Koo et al., (2002), a structural alignment is an effective method to determine a region of the binding site of putidaredoxin (Pdx) on CYP119 enzyme (Koo et al., 2002).

P450cam enzyme was used as a model structure in the current project, because putidaredoxin and putidaredoxin reductase are its natural redox partners (Sevrioukova & Poulos, 2011). P450cam's oxidized and reduced states' crystal structures associated with putidaredoxin (Pdx) were solved by Tripathi et al., (2013), to 2.2 Å and 2.09 Å, respectively (Tripathi, 2013).

UCSF Chimera Software was used in the current research for proteins alignment to analyze and compare two proteins: P450cam and CYP119, and to identify possible

binding sites of CYP119 with Pdx. UCSF Chimera is utilized for analysis and visualization of proteins structures in Python language that has various tools such as density mapping, molecular docking, as well as structure and sequence alignment (Goddard et al., 2005; Pettersen et al., 2004). The PDBIDs of proteins used in alignment can be seen in Appendix A.

### **2.1.2 Design of CYP119 Mutant Enzymes**

Protein design and computational prediction have proven to be effective in producing proteins with unique enzymatic activity, enhanced binding affinity, higher thermostability, and modified ligand specificity (Gromiha, 2019).

Rosetta is a well-known structural prediction and design software package (Le et al., 2020). Le et al., (2020) reported that Rosetta is a popular tool for several design objectives, including de novo folds, loop design, and interface design. In addition to algorithms for protein structure prediction, docking, and design, it includes algorithms for protein interactions with small molecules, nucleic acids, carbohydrates, or in a lipid bilayer (Le et al., 2020).

Rosetta can effectively perform protein structural design and prediction. PyRosetta is a Python library that provides the Rosetta techniques, making it simpler to comprehend and integrate them with other scientific coding libraries (Lyskov et al., 2011).

Rosetta follows the theory of thermodynamics to anticipate and create structures (Chaudhury et al., 2010). To approximate the free energy of a given structure or sequence, a scoring function is utilized and it uses mathematical representations of the primary biophysical forces—such as Van der Waals energies, hydrogen bonds, electrostatics, etc. (Chaudhury et al., 2010).

Rosetta offers modeling packages for small molecule docking (Lyskov et al., 2011), but it is more effective in protein folding studies (Davis & Baker, 2009), protein-protein docking (Surpeta et al., 2020), DNA/RNA – protein docking and antibody design (Leaver-Fay et al., 2011).

PyRosetta 3 was used in designing mutants in the current research. PyRosetta 3 is written in Python 2 scripting language (Lyskov et al., 2011), all codes written with Python 2.7.16 package (Chaudhury et al., 2010). In PyRosetta, a biomolecular system is symbolized as a “pose”, that contains in itself all the structure and sequence data, relative position and orientation (Chaudhury et al., 2010). Additionally, the side chain torsion angles  $\chi$  are included in the internal coordinates used for proteins, which also contain the backbone torsion angles,  $\phi$ ,  $\psi$ , and  $\omega$  (Chaudhury et al., 2010).

Creation of mutants were performed using codes referring to the project by Kestevur Dogru (2019). As Kestevur Dogru (2019) reported, “Pose” is read from Protein Data Bank by command:

```
pose=pose_from_rcsb("PDBID")
```

Using the “ScoreFunction” the energy of structure was calculated. A score function is created and set using following codes:

```
“from rosetta import*”  
“from toolbox import*”  
“init()”  
“scorefxn =create_score_function(score function name)”  
“scorefxn(pose)”  
“protocol_name.set_scorefxn(scorefxn)” (Kestevur Doğru, 2019).
```

As described in research by Kestevur Dogru (2019), following steps were performed. Clean PDB 1IO7 file was downloaded from RSCB. In order to create direct mutation of a residue of protein using PyRosetta, command: “mutate\_residue (pose, residue number, “letter code of mutation”)” can be given to Software.

Although code above creates a mutation, optimization of rotamers is not performed. Therefore, mutation can be created by using a specific file – “resfile”. It is possible to perform a single mutation, as well as double or triple mutations in a single resfile. Using following code, the pdb file can be converted to .resfile:

```
“generate_resfile_from_pose(pose, “mutant name.resfile”)”
```

Resfiles for all mutations were created from pose with the file names: N34E.resfile, N34D.resfile, N35E.resfile, N35D.resfile, K30D.resfile, K30E.resfile, N34E-D77R.resfile, N34D-D77R.resfile, K30E-D77R.resfile, K30D-D77R.resfile, N35D-D77R.resfile, N35E-D77R.resfile, N34E-N35D.resfile, N34D-N35D.resfile.

Following codes were given to PyRosetta Software to apply mutations:

```
“from rosetta import*”
```

```

“from toolbox import*”
“from rosetta.protocols.rigid import*”
“from rosetta.protocols.ligand_docking import*”
“init()”
“import os” (Kestevur Doğru, 2019).

```

CYP119 (PDB ID: 1IO7) was used for mutant creation. PyRosetta downloads pdb.file and clean.pdb.file, which is PDB, all water molecules and cofactors are removed from.

```

“pose=pose_from_rcsb("1IO7")”
or “pose = pose_from_pdb(“pdb_name” + “.pdb”)”.

```

Giving this command, software downloaded PDB file from RCSB with 2 chains, therefore B chain must be removed manually from clean.pdb.file. Following command was given to PyRosetta to pose newly saved clean.pdb.file with A chain only.

```
pose = pose_from_pdb("1IO7.clean.pdb")
```

Desired mutations were indicated in created resfiles as PIKAA. Created mutants were downloaded in pdb format and were visualized using UCSF Chimera.

Heme cofactor was added manually, since heme is situated at the center of the active site and removing the heme while cleaning step may lead to a false result in following mutation steps. For this purpose, files hem.pdb and hem.mol2 formats are required. It is possible to convert files to pdb format and mol2 format by using UCSF Chimera.

Params file is important to make heme group identifiable, therefore molfile2params.py was downloaded from PyRosetta website (RosettaCommons). Saved files with .mol2 and .pdb formats must be in the PyRosetta/molfile2params directory.

Downloaded molfile2params.py was moved to C:/program files/PyRosetta, hem.mol2 and hem.pdb files were copied to C:/program files/PyRosetta/molfile2params. Command to create params file with IPython:

```

run molfile_to_params.py <.mol2 filename> -n <Residue name> or
run molfile_to_params.py HEM.mol2 -n HEM

```

Params file pdb z name needs to be changed to hem z and then moved to C:/programfiles/PyRosetta/Database/chemical/residue\_type\_sets/fa\_standard/residue\_types folder, and added to txt document in C:/program files/PyRosetta/Database/chemical/residue\_type\_sets/ fa\_standard/residue\_types.txt

open the file and type `##hem group residue_types/hem.params`. The cleaned protein file must to include the heme group's original coordinates.

```
“scorefxn = create_score_function("ref2015.wts")”
“outfile = open(r"C:\Users\Desktop\results.txt","a")”
“from rosetta.protocols.relax import*”
“relax = FastRelax()”
“relax.set_scorefxn(scorefxn)”
“generate_resfile_from_pose(pose,      "N34E.resfile",      "N34D.resfile",
"N35E.resfile", "N35D.resfile", "K30D.resfile", "K30E.resfile", "N34E-D77R.resfile",
"N34D-D77R.resfile",      "N35E-D77R.resfile",      "N35D-D77R.resfile",      "K30D-
D77R.resfile", "K30E-D77R.resfile", "N34E-N35D.resfile", "N34D-N35D.resfile")”
```

Desired mutations were indicated in created resfiles. Instead of “NATRO”, “PIKAA” was entered to change single residue to desired residue.

```
“kT = 1”
“outfile.write("Native energy of wild type protein = %f\r\n" % scorefxn(pose))”
“from rosetta.core.pack.task import TaskFactory”
“pose_list = ["N34E”, “N34D”, “N35E”, “N35D”, "K30D", "K30E”, “N34E-
D77R”, “N34D-D77R”, “N35E-D77R”, “N35D-D77R", "K30D-D77R", "K30E-D77R",
"N34E-N35D", "N34D-N35D"]”
“for i in pose_list:”
“v = i”
“i = Pose()”
“i.assign(pose)”
“print I”
“task_design = standard_task_factory()”
“task_design.push_back(ReadResfile(str(v) + ".resfile"))”
“pack_mover = PackRotamersMover(scorefxn)”
“pack_mover.task_factory(task_design)”
“pack_mover.apply(i)”
“relax.apply(i)”
“i.dump_pdb(str(v) + ".pdb")”
“outfile.write("Total energy of " + str(v) + " mutant = %f\r\n" % scorefxn(i))”
“outfile.write(" * 12 + "\n")”
“outfile.close()”
```

The final stage of the process of creating mutants is to minimize the energy of the entire structure. FastRelax function was used for this purpose because it applies energy minimization only to backbone structure. Code for FastRelax protocol:

```
“from rosetta.protocols.relax import *”
```

```
“relax = FastRelax()”
```

```
“relax.set_scorefxn(scorefunction)”
```

```
“relax.apply(pose)”
```

Final energy score calculation was performed using command

```
“pose.dump_pdb(“mutant name” + “.pdb”)”
```

```
“print scorefxn(pose)”;
```

 (Kestevur Doğru, 2019).

Created mutants were downloaded in pdb format and were visualized using UCSF Chimera.

### **2.1.3 Protein-Protein Docking**

Docking methods, a widely recognized field of science, are employed to predict the structure and interaction of protein complexes (Wass et al., 2011). Numerous fundamental biological processes are dependent on the interactions between proteins, such as mechanism of binding, signaling, regulation, recognition and effects of mutations on protein function (Baspinar et al., 2014).

Docking is the method for prediction of the 3D arrangement of a complex structure from each structure, when two proteins are bound together, according to the basis for recognition, affinity and specificity (Weng et al., 2019). According to Weng et al., (2019), docking modeling without utilizing any template and based on template are the two categories into which protein-protein docking algorithms fall. The idea behind modeling where template is used is the finding that most proteins make complexes with other protein species in a similar manner. However number of available templates are limited, therefore generally more popular is when docking modeling is performed without applying any basis template (Weng et al., 2019).

Various protein-protein docking servers are available nowadays. For instance, ClusPro server: equipped with capabilities to consider small angle X-ray scattering

(SAXS) data, discover heparin binding sites, account for pairwise distance constraints, apply attraction or repulsion, remove unstructured protein sections, and generate homo-multimers (Kozakov et al., 2018); PatchDock is built on symmetry constraints, form affinity concepts, and The SymmDock technique uses geometry-based docking to predict compounds with C<sub>n</sub> symmetries (Schneidman-Duhovny et al., 2005);

ZDock scores a global docking approach on a 3D grid employing an ensemble of structure affinity, the field of electrostatic and statistical potential terms, utilizing the Fast Fourier Transform approach (Pierce et al., 2014);

HawkDock for the structural modeling (Weng et al., 2019); Prism, template-based protein–protein interaction prediction tool (Baspinar et al., 2014); FireDock aims to address the issue of solution scoring and flexibility brought forth by quick rigid-body docking methods. The outputs include a list of refined complexes arranged according to the energy of binding function and a three-dimensional representation for comparing and analyzing the refined complexes (Mashiach et al., 2008); and many more servers.

Docking programs usually consist of two standard steps: first generate thousands of variants with all possible interactions, then score these variants using an energy function (Wass et al., 2011).

These docking servers are quick and provide global docking approaches, but the coarse-grained representation of the proteins limits the models' atomic-level precision (Lyskov & Gray, 2008). And therefore, these servers can be used as starting position for the following docking studies using RosettaDock Server to obtain better results (Davis & Baker, 2009; Lyskov et al., 2011; Lyskov & Gray, 2008).

PatchDock, ZDock and HawkDock servers were used in current research, however these servers delete heme from the structure and moreover atomic level accuracy of protein structures was defected.

RosettaDock server Rosie is a Monte Carlo-based algorithm, that has been utilized for a various of purposes, including multi-body, symmetric, antibody-antigen, peptide, and specificity docking (Lyskov & Gray, 2008). Docking process consists of several phases according to Chaudhury et al., (2011):

1. low-resolution phase: consists of cycles of randomized rigid-body perturbation. During these cycles side chains are substituted by just one unifying pseudo-atom, or centroid. It can be either a course-grained representation of residues as separate pseudo-atoms or a random starting positioning of the two members (global docking).



2. high-resolution phase, cycles of smaller rigid-body perturbations, the centroid pseudo-atoms are substituted with the side-chain atoms as in their starting separated conformations; the rigid-body orientation is energy-minimized and side-chain improvement via rotamer packing is performed; and the rigid-body displacement is specifically minimized through a gradient approach (Chaudhury et al., 2011);

3. Calculations are made for the residue-residue pair tendencies, the residue-residue interactions and bumps, and the knowledge-based terms for the residue environment (Chaudhury et al., 2010; Lyskov & Gray, 2008).

RosettaDock server Rosie was used in the current research. Docking2 protocol (Local\_Docking\_Refine) of RosettaDock server Rosie1 necessitates two different protein structures as an input in a standard pdb format with starting configuration and coordinates.

UCSF Chimera was used for sample preparation. Single mutants N34D, N34E, N35D, N35E, K30D, K30E, double mutants N34D-D77R, N34E-D77R, N35D-D77R, N35E-D77R, K30D-D77R, K30E-D77R and Pdx (PDBID: 1XLN) were complexed with the help of alignment with P450cam-Pdx crystal structure complex (PDBID: 4JWS). Mutants and Pdx with predicted coordinates were saved in separate pdb files and were submitted to dock using RosettaDock server Rosie in two separate files. Coordinates of two proteins were not overlapping and docking partners C $\alpha$  atoms were distanced from each other for higher than 5 Å to avoid collision.

According to given inputs, by improving side-chain forms and rigid-body position, the server established low energy conformations for both interacting docking partners. Server generated thousand independent structures as an output and detailed scoring information of ten variants with lowest energy scores with pictures and rank order by energy were obtained. Ten lowest-interface-energy structures were created in each docking run and they were downloaded for further analysis and visualization.

Utilizing UCSF Chimera, all variants of docked mutant-Pdx complexes were visualized and prediction accuracy of binding site between mutant CYP119 and Pdx with binding site of predicted WT CYP119-Pdx complex was assessed.

Obtained complexes were aligned with P450cam-Pdx crystal structure (with PDB id: 4JWS) and WT CYP119-Pdx complex to assess prediction accuracy of binding site of CYP119 mutant-Pdx complexes, and its correlation with these complexes. Variants superimposed with predicted WT CYP119-Pdx complex and with the lowest energy scores models of each mutant samples were selected for further detailed analysis, while

variants where Pdx was bound to sides of CYP119 other than the predicted side were eliminated.

Acceptable quality of generated variants according to CAPRI-defined criteria were as follows: with I\_rmsd value less than 1.0 Å is considered high quality, I\_rmsd value between 1.0 Å and 2.0 Å is considered medium quality, and I\_rmsd value between 2.0 Å and 4.0 Å is considered acceptable quality.

## 2.2 Experimental Methods

Materials used in the current research are listed below:

The pET11a with Wild Type (WT) CYP119, the pET28b with putidaredoxin (pPdx) and putidaredoxin reductase (pPdR) were gifts from Teruyuki Nagamune (Addgene plasmid #66131, #85084, #85083 respectively) (Suzuki, 2016; Suzuki et al., 2014).

The designed primers for N34E, D77R mutants were purchased from Sentebiolab Biyoteknoloji.

*Escherichia coli* (*E. coli*) DH5a competent cells were utilized for transformation purposes. *E. coli* BL21 (DE3) competent cells were utilized for expression purposes.

Q5 Site-Directed Mutagenesis Kit, Presto Mini Plasmid Kit (Geneaid, PDH100) DNA purification kit were used.

Used media: Luria Bertani Broth (LB) medium (10 g/L tryptone, 5 g/L yeast extract, 10 g/L NaCl) was utilized for small scale expression. Luria Bertani (LB) Agar medium (10 g/L peptone, 5 g/L yeast extract, 5 g/L NaCl, 12 g/L agar) was utilized for bacterial transformation. 2x Yeast Extract Tryptone (2xYT) medium (16 g/L tryptone, 10 g/L yeast extract, 5 g/L NaCl at pH 6.8) was utilized for large scale CYP119 expression. Terrific Broth (TB) medium (12 g/L tryptone, 24 g/L yeast extract, 5 g/L glycerol) was utilized for large scale Pdx and PdR expression. SOC medium (20 g of tryptone, 5 g of yeast extract, 0.5 g of NaCl, 10 mL of a 250 mM solution of KCl, 5 mL of a sterile solution of 2 M MgCl<sub>2</sub>, 20 mL of a sterile 1 M glucose solution; per liter at pH 7.0) was utilized for bacterial transformation experiment for all samples (Appendix A).

Used chemicals: ampicillin, kanamycin, sodium dodecyl sulfate (SDS), ammonium persulfate (APS), dithiothreitol (DTT), N,N,N',N' - tetraacetythylenediamine (TEMED), SYBR-green, purple gel loading dye (B7025S BioLabs), Pierce<sup>TM</sup> Unstained Protein MW Marker (26610 Thermofisher), benzamidine HCl, phenylmethylsulfonyl fluoride (PMSF), imidazole, sodium chloride (NaCl), potassium chloride (KCl), lauric acid, AmplexRed, horseradish peroxidase, dimethyl sulfoxide (DMSO), Nicotinamide adenine dinucleotide hydrogen (NADH), isopropyl  $\beta$ -D-1-thiogalactopyranoside (IPTG), iron (III) chloride (FeCl<sub>3</sub>), sodium dithionite, CO gas.

Used buffers: TAE buffer (40mM Tris-acetate, 1mM EDTA), 1 M Tris (pH 8.8 and pH 6.8), potassium phosphate buffer (pH 7.0, 7.4, 7.5), SDS Running Buffer (72 g glycine, 15 g Tris-base, 5 g SDS).

Equipment such as centrifuge, water bath, dry bath, incubator, evaporator, shaker, UV-Visible spectrophotometer, pH meter, sonicator, PCR-amplificatory and vortex were used during this study.

### **2.2.1 Site-Directed Mutagenesis Method for Construction of CYP119 Mutants**

Site-directed mutagenesis method is one of the effective way to create specific desired alterations in DNA with various purposes (Hogrefe et al., 2002). Q5 Site-Directed Mutagenesis Kit (BioLabs) was utilized in current research to produce N34E, D77R single mutations, and N34E-D77R double mutation on WT CYP119 enzyme. DNA and amino acid sequences of CYP119 are shown in Appendix B.

Site-specific mutation can be accomplished with the Q5 Site-Directed Mutagenesis Kit (Koo et al., 2002). It eliminates the necessity for ssDNA rescue and subcloning (Nair et al., 2016). Furthermore, using this kit eliminates the requirement for additional procedures for in vitro methylation treatment, or any requirements for unique restriction sites, multiple transformations, or special vectors (Park et al., 2002). In a single reaction, the quick three-step process produces mutants with an efficiency of more than 80% (Koo et al., 2002; Nair et al., 2016; Park et al., 2002). Using this kit, point mutations,

substitute amino acids, and delete or insert single or multiple amino acids is enabled to perform (Hogrefe et al., 2002).

Both primers must contain desired mutations, and a supercoiled double-stranded DNA vector containing the desired insert are required for the standard process (Hogrefe et al., 2002). PfuUltra HF DNA polymerase used in the method provides highest fidelity (Baugh et al., 2011). To decompose the paternal DNA sample, Dpn I endonuclease was applied (Hogrefe et al., 2002; Baugh et al., 2011). Experimental procedure consisted of following steps. The first step is primer design. Primers containing desired mutations were designed using <https://nebasechanger.neb.com> website. For N34E mutant AAC codon was substituted to GAG and for D77R mutant GAT codon was substituted to CGT.

Primers (mutated region is labeled in boldface, forward 5'-GGAGGTTTTAG**GAG**AACTTTTCGAAATTC-3' and reverse 3'-TTTGTGTACCTATAGGAAAAC-5') for N34E and primers (mutated region is labeled in boldface forward 5'-CCCTCTCCAT**CGT**GAGTTAAGATCAATG-3' and reverse 3'-GGATCTGAGGTCAGCATG-5' for D77R were purchased from Sentebiolab. Primers' properties are shown in Table 2.1.

Table 2.1. Primers' melting temperatures, molecular weights, total nmols.

Planned mutation	Primer	Tm (°C)	MW (g/mol)	Total (nmol)	100µM stock - µl TE
N34E forward	5'-GGAGGTTTTAG <b>GAG</b> AACTTTTCGAAATTC-3'	55.53	8657.7	33.1	331.2
N34E reverse	3'-TTTGTGTACCTATAGGAAAAC - 5'	46.55	6444.3	33.8	338.4
D77R forward	5'-CCCTCTCCAT <b>CGT</b> GAGTTAAGATCAATG - 3'	59.92	8523.6	39.9	398.5
D77R reverse	3'- GGATCTGAGGTCAGCATG - 5'	50.32	5579.7	35.5	355

The second step of site-directed mutagenesis is PCR-amplification of mutant DNA. Reaction mixture contained of Q5 Hot start High-Fidelity 2X master mix, 10  $\mu$ M forward and reverse primers, 25 ng/ $\mu$ L WT CYP119 and nuclease-free water. Table 2.2. shows reaction mixture concentration and volumes of reactants.

Table 2.2. PCR reaction mixture used: concentration and volumes of reactants (<https://www.neb.com/en/protocols>).

Ingredients	25 $\mu$ L Reaction	Final Concentration
Q5 Hot Start High-Fidelity 2X Master Mix	12.5 $\mu$ L	1X
10 $\mu$ M F Primer	1.25 $\mu$ L	0.5 $\mu$ M
10 $\mu$ M R Primer	1.25 $\mu$ L	0.5 $\mu$ M
Template DNA (1–25 ng/ $\mu$ L)	1 $\mu$ L	1–25 ng/ $\mu$ L
Nuclease-free Water	9.0 $\mu$ L	

Cycling Conditions are shown in Table 2.3.

Table 2.3. PCR cycling conditions (<https://www.neb.com/en/protocols>).

Step	Temperature	Time
Initial Denaturation	98°C	30 seconds
25 Cycles	98°C	10 seconds
	58°C for N34E, 59°C for D77R	10–30 seconds
	72°C	20–30 seconds/kb
Final Extension	72°C	2 minutes

PCR amplicons were checked in 1% agarose gel using TAE buffer (containing 40 mM Tris-acetate, 1 mM EDTA) and 0.5  $\mu$ g/mL SYBR-green. Samples were loaded

using 6X purple gel loading dye (B7025S BioLabs), 500 µg/mL 1 kb DNA ladder was used. Gel was run at 90 V for 1 h. The gel was checked under UV light to observe corresponded to CYP119 band (6748 bp). After observation of correct CYP119 band on agarose gel with PCR amplification reaction mixture, then amplicons were introduced immediately to a Kinase, Ligase, and Dpn I (KLD) mixture of enzymes and incubated for 30 mins at room temperature conditions for purposes of parental samples removal. KLD reaction mixture concentration and volumes of reactants can be seen in Table 2.4.

Table 2.4. KLD reaction mixture: concentration and volumes of reactants (<https://www.neb.com/en/protocols>).

	PCR Product	2X KLD Reaction Buffer	10X KLD Enzyme Mix	Nuclease-free Water
Volume	1 µL	5 µL	1 µL	3 µL
Final Concentration		1X	1X	

The third step of site-directed mutagenesis process is the transformation of mutant DNA to *E. coli* competent cells. After mixing 10 µL of KLD mixture to 100 µL of chemically competent *E. coli* cells, the mixture had been incubating on ice for a half hour. The next step was a 30-second of heat shock at 42°C, followed by a 5-minute ice incubation period. Cells were grown in 950 µL SOC media (per 100 mL: 2.0 g tryptone, 0.5 g yeast extract, 1 mL of 1 M NaCl, 0.25 mL of 1 M KCl, 1 mL of filter-sterilized 2 M Mg<sup>+2</sup> (1 M MgCl<sub>2</sub> + 1 M MgSO<sub>4</sub>), 1 mL of filter-sterilized 2 M glucose, pH 7.0), gently shaken at 37°C for an hour. After applying 100 µL of cells per agar plate with 100 µg/mL ampicillin, the plates were incubated at 37°C for the entire night. Four different colonies from transformation plates were grown at 37°C in shaker in LB Broth medium. Medium contained 100 µg/mL ampicillin.

Plasmid DNA was purified from overnight cell culture using Presto Mini Plasmid Kit (Geneaid, PDH100). First, the overnight cell culture was centrifuged for 15 minutes at 3900 rpm. Subsequently, the pellet was mixed in 200 microliters of RNase-containing resuspension buffer. After applying 200 µL of lysis buffer for cell lysis and flipping the tubes ten times, the samples were incubated for two mins at room

temperature. Samples were filled with 300  $\mu$ L of neutralizing buffer, mixed by flipping the tubes ten times, and then were centrifuged for five minutes at 15,000 rpm. Followed by introduction of supernatant onto filter columns, and addition of 600  $\mu$ L of wash buffer. 30  $\mu$ L of elution buffer was used to elute the plasmid DNA. The concentrations of plasmids were diluted to the necessary levels for sequencing, and BIYOMER at IZTECH carried out the sequence analysis.

### **2.2.2 Expression and Purification of WT and Mutant CYP119 Enzymes**

BL21 (DE3) competent *E. coli* cells were utilized for transformation of DNA of each mutant CYP119. DNA samples (5  $\mu$ L) contained around 100 ng of mutant DNA and BL21 (DE3) competent *E. coli* (50  $\mu$ L) cells were mixed gently in a transformation tube by carefully flicking 4–5 times. Cells were put on ice and incubated for half hour. Then heat shock was applied at 42°C for 45 s. Incubation on ice was performed for 2 mins. Then 950  $\mu$ L of room temperature SOC media (per 100 mL: 2.0 g tryptone, 0.5 g yeast extract, 1 mL of 1 M NaCl, 0.25 mL of 1 M KCl, 1 mL of filter-sterilized 2 M  $Mg^{+2}$  (1 M  $MgCl_2$  + 1 M  $MgSO_4$ ), 1 mL of filter-sterilized 2 M glucose, pH 7.0) was added into the mixture and gently shaken at temperature of 37°C for one hour in shaker. Centrifugation of cells at 3000 rpm for 10 mins at 25°C was carried out. A warmed selection plate was covered with 100  $\mu$ L of every dilution, which was then incubated at 37°C for overnight. As an alternative, it can be incubated for 24–36 hours at 30°C or for 48 hours at 25°C. Cells were kept at +4°C until use.

Single colony was grown overnight at 37°C 220 rpm with 100  $\mu$ g/mL ampicillin and stocked in 500  $\mu$ L of 50% glycerol in a 2 mL cryovial tube and frozen at -80°C. The final concentration of glycerol was around 25%.

WT and mutant CYP119 proteins were expressed according to following procedure: single colony was grown overnight at 37°C, 220 rpm in 100 mL of LB Broth medium with 100  $\mu$ g/mL ampicillin. The overnight cells (5 mL) were placed into 500 mL 2xYT medium (16 g tryptone, 10 g yeast extract, 5 g sodium chloride per L) with 100  $\mu$ g/mL ampicillin, pH 6.8 and incubated at 37°C, 220 rpm, up until CYP119 had an  $OD_{600}$  (optical density at 600 nm) of about 0.8. When  $OD_{600}$  reached 0.8, 1 mM of IPTG was

added and cells were grown at temperature of 30°C for 32 h in shaker. Centrifugation was used for 30 mins at a speed of 3900 g to extract bacterial cells. Pellets of cells were stored at -80°C until the following purification.

Expressions of WT and mutant CYP119s were monitored using SDS-PAGE (sodium dodecyl sulfate-polyacrylamide gel electrophoresis) analysis. After 32 h of incubation OD<sub>600</sub> was measured and corresponding volume of cells were collected for further analysis. 15% resolving gel, containing 30% acrylamide, 1 M Tris (pH 8.8), 10% SDS, 10% ammonium persulfate, TEMED, and 5% stacking gel, containing 30% acrylamide, 1 M Tris (pH 6.8), 10% SDS, 10% ammonium persulfate and TEMED were used. Before being loaded into the gel, protein samples were combined with loading dye (100 mM Tris-HCl, 4% SDS, 0.2% bromophenol blue, and 20% glycerol) and 1 mM DTT, and heated for 10 mins at 95°C. The gel was run at 30 V for 1 h, then at 120 V for 2 h. Coomassie Brilliant Blue dye was utilized to stain the gel, then ethanol and acetic acid were employed to destain it. The molecular weight of WT CYP119 is 43 kDa. Pierce™ Unstained Protein MW Marker (26610) from Thermofisher was used as ladder.

Buffers were prepared according to Table 2.5.

Table 2.5. Buffers used in CYP119 protein purification.

<b>Ingredients</b>	<b>Lysis Buffer pH 7.5</b>	<b>Desalting buffer</b>
Kpi buffer	50 mM	50 mM
NaCl	150 mM	20 mM
PMSF	0.2 mM	-
Benzamidine HCL	1 mM	-
Imidazole	10 mM	-
Glycerol	-	5%

Proteins were purified by following steps: frozen cell pellets were dissolved in Lysis buffer (50 mM potassium phosphate buffer (Kpi), 150 mM NaCl, 0.2 mM phenylmethylsulfonyl fluoride (PMSF), 1 mM benzamidine HCl, 10 mM imidazole (pH 7.5)). For each 1 g of pellet, 5 mL of lysis buffer was used. After each 30 seconds of



sonication, the cells were kept on ice for a minute. Sonication was performed until the cells were totally lysed. Lysate was incubated for 1 h at 60°C in water bath and centrifuged at 3900 rpm for 1.5 h to separate supernatant and pellet. Supernatant was purified by ammonium sulphate precipitation method. Ammonium sulphate (30%) was added and simultaneously supernatant was stirred on ice. Lysate on ice was mixed for 1 h.

Sample was centrifuged at 3900 rpm for 45 mins at 8°C. A further step was the addition of 60% of ammonium sulphate to lysate on ice and mixing in stirrer. The sample was then centrifuged at 3900 rpm for 90 mins at 8°C. Dialysis buffer (50 mM Kpi, 20 mM NaCl, 5% glycerol) was utilized to dissolve CYP119 pellets after ammonium sulphate precipitation and samples were dialyzed against the same buffer (Sakalli, 2020).

### **2.2.3 Expression and Purification of Redox Partner Proteins – Putidaredoxin (Pdx) and Putidaredoxin Reductase (PdR)**

PPdx and pPdR plasmids were gifts from Teruyuki Nagamune (catalog numbers #85084 and #85083, respectively) (Suzuki, 2016; Suzuki et al., 2014). Plasmid maps and sequences of proteins can be observed in Appendix C.

Kanamycin-containing (50 µg/mL) LB agar plates were used to grow plasmid containing cells in conditions: overnight at 37°C, 220 rpm. Liquid culture was grown likewise in 8 mL of LB broth with 50 mg/mL kanamycin overnight at 37°C 220 rpm. Overnight cells (500 µL) were stocked with 25% final volume of glycerol. Set up reaction can be observed in Table 2.6.

Table 2.6. Single digestion reaction components.

Components	Reaction sample (30 µL)
DNA	20 µL
10X NEBuffer r3.1	3 µL (10X)
BamHI	1.0 µL
Nuclease-free Water	to 30 µL

Plasmid isolation performed according to the protocol of Geneaid plasmid isolation kit according to a standard protocol. Single digestion of a plasmid was performed, reaction sample in a 1.5 mL tube containing DNA sample, restriction enzyme, buffer, dH<sub>2</sub>O up to total volume was incubated at 37°C for 60 minutes.

Agarose gel electrophoresis performed with 1% agarose gel to observe the corresponding band. pPdR plasmid is 6602 bp long. The pPdx plasmid is 5657 bp long. After observation of corresponding bands in agarose gel, transformation of pPdx and pPdR to BL21(DE3) competent *E. coli* cells were performed.

Competent *E. coli* BL21 (DE3) cells (50 µL) were thawed on ice and transferred to a transformation tube on ice. pPdx and pPdR samples (5 µL of 100 ng) were added to the cell mixture and carefully mixed without vortex. For 30 mins, the mixture was incubated on ice before a 45-s immediate heat shock at 42°C. Samples were cooled for 2 mins on ice. Then incubated in 950 µL of room temperature SOC medium at 37°C for 60 mins in 220 rpm shaker. After incubation, centrifugation was performed at 3000 rpm for 10 mins at 25°C and 100 µL of each dilution was transferred onto a warm selection plate with 50 µg/mL kanamycin and incubated overnight at 37°C. Samples were kept at +4°C until use. Colonies were observed on the next day. *E. coli* BL21 (DE3) cells containing pPdx and pPdR plasmids from the transformation plate were grown overnight in 5 mL of LB Broth with 50 mg/mL kanamycin. 500 µL of overnight cells of both redox partners were stocked with 25% final volume of glycerol and frozen at -80°C.

A single colony of bacterial cells containing pPdx and pPdR plasmids were grown in 5 mL of LB medium containing 1% glucose, 50 mg/mL kanamycin. The cells were grown at 37°C until OD<sub>600</sub> attained 0.5, around 4-5 h. Being cultivated in 500 mL of TB media with 50 mg/mL kanamycin, the cell culture was shaker-grown at 37°C and 220 rpm. When the OD<sub>600</sub> reached about 0.8, 0.5 mM of FeCl<sub>3</sub> was added to pPdx plasmid containing cells, while 0.1 mM IPTG was added to pPdR plasmid containing cells and cell cultures were grown at 27°C, 220 rpm shaker overnight. The cells were extracted by centrifugation at 3200 g for 40 min. The supernatant was discarded and pelleted cells were transferred into 50 mL tube. Cells were maintained at -80°C until purification (Suzuki, 2016).

Expressions of Pdx and PdR were monitored using SDS-PAGE analysis method. 15% resolving gel, containing 30% acrylamide, 1 M Tris (pH 8.8), 10% SDS, 10% ammonium persulfate, TEMED, and 5% stacking gel, containing 30% acrylamide, 1 M Tris (pH 6.8), 10% SDS, 10% ammonium persulfate and TEMED were used. Before

being loaded into the gel, protein samples were combined with loading dye (100 mM Tris-HCl, 4% SDS, 0.2% bromophenol blue, and 20% glycerol) and 1 mM DTT, and heated for 10 mins at 95°C. The gel was run at 30 V for 1 h, then at 120 V for 2 h. Coomassie Brilliant Blue dye was used to stain the gel, then ethanol and acetic acid were used to destain it.

Pierce™ Unstained Protein MW Marker (26610) from Thermofisher was used as ladder. MW of PdR is 45.6 kDa and MW of Pdx is 11.7 kDa. Proteins Pdx and PdR were expressed and purified according to methods by Suzuki et al., (2014) (Suzuki, 2014): pET28+Pdx and pET28+PdR plasmids were used. pET28 for Pdx/PdR is bacterial expression plasmid with kanamycin resistance gene, and has promotor T7. Buffers used in purification of PdR and Pdx proteins are summarized in Table 2.7.

Table 2.7. Buffers used in PdR and Pdx proteins purification.

<b>Lysis buffer pH 7.4</b>	<b>Wash buffer pH 7.4</b>	<b>Elution buffer pH 7.4</b>	<b>Desalting buffer pH 7.4</b>
20 mM Kpi	20 mM Kpi	20 mM Kpi	20mM Kpi
150 mM KCl	-	150 mM KCl	-
10 mM imidazole	20 mM imidazole	300 mM imidazole	-
0.2 mM PMSF	-	-	-
1 mM benzamidine HCL	-	-	-
-	-	-	5% glycerol

Pdx was purified according to method by Suzuki et al., (2016) (Suzuki, 2016). Pdx expressing cells were dissolved using lysis buffer (150 mM KCl, 10 mM imidazole, 1 mM benzamidine HCl, 0.2 mM PMSF, 20 mM Kpi pH 7.4) and sonicated for 30 s. Cell debris was removed at 3200 rpm for 40 mins centrifugation and resin (1 mL to each 8 mL) was added to the supernatant and incubated for 1 h at 4°C using rotator. Lysate was then applied to a column. Flowthrough was applied to a column two times. Ten column volumes of wash buffer (20 mM Kpi, 20 mM imidazole pH 7.4) was used to wash proteins, then protein elution was carried out with 4-5 ml of elution buffer (150 mM KCl,

300 mM imidazole, 20 mM Kpi pH 7.4). The dialysis was performed against 20 mM potassium phosphate buffer pH 7.4 containing 5% glycerol. The purified Pdx was stored at -80°C until use.

PdR was purified according to protocol by Koo et al., (2002) and Suzuki et al., (2016) (Koo et al., 2002; Suzuki, 2016). Harvested cells were lysed with lysis buffer (150 mM KCl, 10 mM imidazole, 1 mM benzamidine HCl, 0.2 mM PMSF, 20 mM Kpi) and sonicated 30 seconds and put on ice for 1 min. Sonication performed until cells are totally lysed and centrifuged at 3200 rpm for 40 min. The supernatant was subjected to 30% and 70% ammonium sulfate cuts. PdR pellets were dissolved in lysis buffer and 1 mL resin was added to each 8 mL supernatant and rotated 1 h in refrigerator. Lysate was then applied to a column. Flowthrough was applied to a column one more time. Ten column volumes of wash buffer (20 mM Kpi, 20 mM imidazole) were used to wash proteins, then proteins were eluted with 4-5 mL of elution buffer (150 mM KCl, 300 mM imidazole, 20 mM Kpi). The dialysis was performed against 20 mM potassium phosphate buffer pH 7.4 containing 5% glycerol. The purified PdR was stored at -80°C until use (Suzuki, 2014).

#### **2.2.4 UV-Visible Spectral Analysis of WT and Mutant CYP119 Enzymes**

Proteins containing the appropriate amino acids absorb the light on the UV-spectrum wavelengths of 260 – 280 nanometers (Colyer & Walker, 1996). Every chemical that contains heme exhibits the Soret peak, or absorbance peak, at about 420 nm. Denisov et al., (2005) and Unno et al., (1997) reported that the protein moiety has an impact on the Soret peak's intensity. Cytochrome P450 undergoes a spectrum shift and shifts the location of the absorbance of the Soret peak from 420 nm to 450 nm towards the red region when it is reduced and binds to carbon monoxide (CO).

This alteration gives these proteins their name, P450, where P is Pigment 450. This shift can be easily observed by comparing the absorbance of reduced P450–CO and oxidized P450. It is caused by the thiolate coupling of the heme to cysteine. The ring of the heme porphyrin has so many conjugated double bonds, which allows the molecule to absorb light in the visible portion of the spectrum (Denisov et al., 2005; Unno et al., 1997).

UV-visible spectrophotometer measures light in the visible (400–700 nm) and ultraviolet (185–400 nm) regions of the electromagnetic radiation spectrum. The concentration of a sample can be ascertained using the Beer-Lambert law, which connects the sample's concentration to the amount of light it absorbs during its passage through the sample (Colyer & Walker, 1996).

Protein concentration can be estimated using the Beer-Lambert law as shown in equation 2.1.

$$A = \epsilon cl$$

Equation 2.1. **A** is the absorbance (for instance  $A_{280}$ );  $\epsilon$  is extinction coefficient, unit  $M^{-1}cm^{-1}$ ; **c** is concentration of protein in M; **l** is the length of the cuvette / microplate in cm.

Every chemical has a unique molar extinction coefficient, which is a crucial factor in the Beer-Lambert law. A substance's molar extinction coefficient, which is wavelength-specific, indicates how much light it absorbs. CYP119 concentration can be calculated using the extinction coefficient ( $\epsilon_{415nm} = 104 \text{ mM}^{-1}\text{cm}^{-1}$ ) (Başlar et al., 2020).

WT and mutant CYP119s in 50 mM potassium phosphate at pH 7.5 were examined under the UV-Visible spectra between range of 200-800 nm with 5 nm interval. Scanning Spectrophotometer 1600PC was utilized for the purposes of analysis. Optical spectra of each sample were recorded.

### **2.2.5 UV-Visible Spectral Analysis of Putidaredoxin and Putidaredoxin Reductase**

Putidaredoxin (Pdx), the [2Fe–2S] ferredoxin from *Pseudomonas putida*, is an essential one-electron transporter that connects the terminal oxygenase enzyme P450cam and putidaredoxin reductase (PdR), containing FAD cofactor and utilizes NADH as

reported by Sevrioukova et al., (2003). Cys73Ser/Cys85Ser mutant Pdx generated and the crystal structure solved by Sevrioukova et al., (2003) was used in the current project (Sevrioukova et al., 2003). Figure 2.1 represents absorbances of putidaredoxin (Pdx).

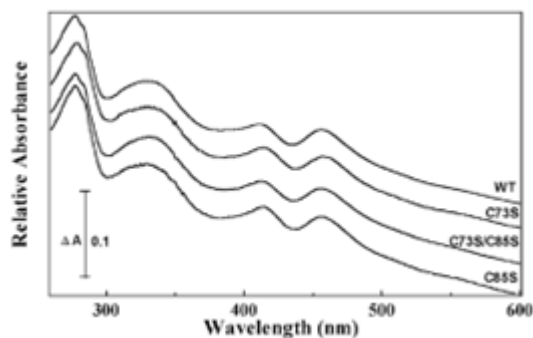


Figure 2.1. Absorbance of WT Pdx and cysteine mutants of putidaredoxin (10  $\mu\text{M}$ ) in 50 mM sodium phosphate buffer at a pH 7.5. Source of Figure: (Sevrioukova et al., 2003).

Absorbance spectra of Pdx Cys73Ser/Cys85Ser mutant resembled the wild type protein. This suggests that there was no disturbance to the metal cluster's surroundings.

*Pseudomonas putida*-derived putidaredoxin reductase (PdR) contains FAD cofactor. One of the three components of the soluble cytochrome P450cam monooxygenase system. In this study, six-histidine tag-fused (His6) PdR was utilized. With absorption peaks at 379 nm and 455 nm, a prominent shoulder at 480 nm, the absorbance spectra of the WT and His6 PdR were matched (Sevrioukova & Poulos, 2002).

Isolated Pdx and PdR (1  $\mu\text{M}$ ) were examined under the UV-Visible spectra in 50 mM potassium phosphate at pH 7.4, between range of 200-800 nm with 2 nm and 5 nm interval, respectively. UV-visible spectroscopy was carried out using a 1600PC Scanning Spectrophotometer. Concentration of Pdx was calculated using its known extinction coefficient ( $\epsilon_{412\text{nm}} = 11.0 \text{ mM}^{-1}\text{cm}^{-1}$ ) at 412 nm (Sevrioukova et al., 2003).

Figure 2.2 shows an absorbance spectrum of putidaredoxin reductase (PdR).

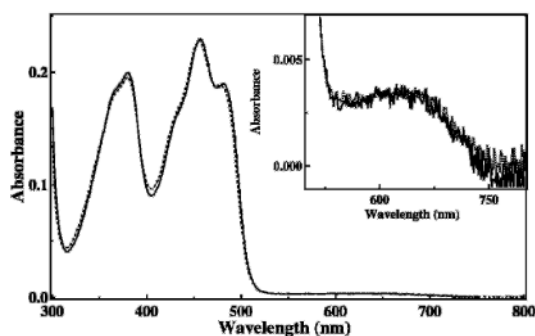


Figure 2.2. Absorbance of WT (solid) and His6 (dashed) PdR, 20  $\mu\text{M}$  enzyme dissolved in 100 mM potassium phosphate buffer at a pH 8.0. Source of Figure: (Sevrioukova & Poulos, 2002).

The concentration of PdR was calculated from its extinction coefficient at 455 nm ( $\epsilon_{455} = 10.9 \text{ mM}^{-1} \text{ cm}^{-1}$ ) (Sevrioukova et al., 2010). Optical spectra of each sample were recorded and concentration of proteins were calculated (alternatively,  $\epsilon_{378} = 9,700 \text{ M}^{-1} \text{ cm}^{-1}$  and  $\epsilon_{454} = 10,000 \text{ M}^{-1} \text{ cm}^{-1}$  for PdR) (Sevrioukova et al., 2003).

## 2.2.6 Lauric Acid Binding to WT and Mutant CYP119s: N34E, D77R and N34E-D77R

Different degrees of affinity can be observed in the binding of saturated fatty acids by CYP119, estimating the magnitudes of the spin state change and absorbance shift. Degree of affinity is characterized by dissociation constant or  $K_d$  value, which represents the ligand concentration occupied by half of receptor enzyme concentration. The smaller the  $K_d$  value means the tighter binding and thus the higher the affinity proteins.

According to literature, lauric acid binds to CYP119 more tightly ( $K_d = 16 \mu\text{M}$ ) (Sakalli, 2020) than, for instance, styrene ( $K_d = 530 \mu\text{M}$ ) (Koo et al., 2002). Therefore, using lauric acid is advantageous due to the characteristics that lauric acid is highly soluble, standards for its metabolites are available, and the plenty literature relevant to determination of its metabolites (Nguyen et al., 2021). Binding constants of WT CYP119

and mutants: N34E, D77R and N34E-D77R with substrate, lauric acid, has been identified using difference spectroscopy.

The experiment was performed at room temperature. First, solutions containing enzyme were prepared. Samples contain 1.5  $\mu\text{M}$  enzyme in 50 mM potassium phosphate buffer pH 7.4. Overall volume 7 mL was divided into two glass cuvettes each 3.5 mL after incubating samples for 10 minutes at room temperature conditions. Lauric acid stock in dimethyl sulfoxide (DMSO) was added stepwise with final concentrations (0, 10  $\mu\text{M}$ , 20  $\mu\text{M}$ , 30  $\mu\text{M}$ , 40  $\mu\text{M}$ , 50  $\mu\text{M}$ , 80  $\mu\text{M}$ , 110  $\mu\text{M}$ , 140  $\mu\text{M}$ , 170  $\mu\text{M}$ , 200  $\mu\text{M}$ ) into the enzyme's solutions and incubated for 5 minutes at room temperature before UV-spectra were taken. Reference cuvettes contained the same with substrate volume of dimethyl sulfoxide (DMSO) was added. The cuvette's DMSO concentration was less than 1% of the total volume of the solution.

UV-spectra of all samples were measured between 350 nm and 650 nm with 2nm interval, the absorbance shift was followed between 386 nm and 418 nm. Next, by fitting plots of  $\Delta 386\text{--}418$  against substrate concentration to the quadratic equation 2.2, the dissociation constant ( $K_d$ ) was calculated.

$$\Delta A = A_{max} \left( \frac{K_d + [E] + [L] - \sqrt{(K_d + [E] + [L])^2 - 4[E][L]}}{2[E]} \right)$$

Equation 2.2. Calculation of  $K_d$  and  $A_{max}$  values.

### 2.2.7 Putidaredoxin Binding to WT and Mutant CYP119s

Similar spectrum changes to those obtained with P450cam and Pdx are observed when Pdx is added to CYP119 (Koo et al., 2002). A peak at 440 nm and a trough at 414 nm can be observed by difference spectroscopy experiment (Aoki et al., 1998; Koga et al., 1993; Koo et al., 2002). The methods of Sligar et al., (1989), Aoki et al., (1998), and Koga et al., (1993) were used in the current research (Aoki et al., 1998; Koga et al., 1993; Sligar, 1989).



UV-spectrum of overall volume of 700  $\mu\text{L}$  solution containing 10 mM potassium phosphate (pH 7.4), 1 mM lauric acid, and 1.5  $\mu\text{M}$  WT and mutant CYP119 was measured. With the exception of CYP119, the reference cuvette contained the same solution.

Pdx with concentration of 0.5 mM was added stepwise to both cuvettes from 70  $\mu\text{M}$  up to 500  $\mu\text{M}$  final concentration. Difference spectra was measured between 200 nm and 750 nm with 2 nm interval, the absorbance shift was followed between 440 nm and 414 nm. Dissociation constant ( $K_d$ ) was calculated by plotting the shift of  $\Delta 440 - \Delta 414$  against concentration of substrate to the quadratic equation shown in Equation 2.2.

### **2.2.8 Assessment of Electron Transfer from Pdx to WT and Mutant CYP119s and Coupling Efficiency**

Coupling efficiency of the reaction and electron transfer from Pdx to WT and mutant CYP119s were examined according to method by Morlock et al., (2018). Uncoupling can happen with or without a substrate and is very dependent on the circumstances of the reaction (Morlock et al., 2018).

The ability of the electron transfer partners, putidaredoxin and putidaredoxin reductase, in the three-protein system to WT and mutant CYP119s was identified by following the peak of consumed NADH, the electron donor. The rate at which putidaredoxin and WT and mutant CYP119s undergo their initial electron transfer was measured at room temperature with an optimized enzyme ratio of 1:20:1 CYP119:Pdx:PdR (Morlock et al., 2018).

The final assay system of coupling efficiency experiment included followings in main sample: 0.5  $\mu\text{M}$  CYP119, 10  $\mu\text{M}$  Pdx, 0.5  $\mu\text{M}$  PdR, 100  $\mu\text{M}$  lauric acid, as well as 100  $\mu\text{M}$  AmplexRed and 0.2 U horseradish peroxidase (HRP) in 50 mM Kpi buffer pH 7.4, and controls included the same mixture: 1. except for CYP119; 2. except for substrate (lauric acid); 3. except for Pdx. Then 0.2 mM NADH was added to all samples before measuring (Koo et al., 2002; Nguyen, 2021).

UV-spectrum between 200-700 nm of solution was measured with interval of 5 nm. Both the formation of hydrogen peroxide and the consumption of NADH were

monitored for around 90 mins at room temperature simultaneously by time (1, 2, 3, 6, 9, 12, 17, 22, 27, 37, 47, 57, 87 mins) (Morlock et al., 2018).

NADH consumption was followed at 340 nm, consumed NADH was calculated with its extinction coefficient at 340 nm that is  $6220 \text{ M}^{-1}\text{cm}^{-1}$  (MW is 709.4 g/mol). The hydrogen peroxide production was followed by resorufin (MW is 375.33 g/mol) formation in the mixture at 570 nm.

Concentration of formed resorufin was calculated using its extinction coefficient at 570 nm that is  $65000 \text{ M}^{-1}\text{cm}^{-1}$ .

### **2.2.9 CO-binding to WT CYP119 and N34E, D77R Single Mutants and N34E-D77R Double Mutant**

When assessing the carbon monoxide (CO) difference spectra of the dithionite reduced state samples, P450 enzymes have a the maximum absorbance peak at 450 nm (Stresser, 2021). The term “reduced” describes the reduction of ferric ( $\text{Fe}^{+3}$ ) heme iron from to the ferrous ( $\text{Fe}^{+2}$ ) form in cytochrome P450 enzymes. The extinction coefficient determined by (Sato, 1964) as  $91 \text{ cm}^{-1}\text{mM}^{-1}$ , concentrations of the enzyme was calculated using this extinction coefficient.

The capacity of the electron transfer partners between Pdx and CYP119 (WT or mutants) was followed by comparing the peaks at 450 nm of the CO-complex CYP119 reduced with the Pdx-PdR redox system and the peaks at 450 nm of the CO-complex CYP119 reduced with sodium dithionite.

Analysis was performed by 1600PC Scanning Spectrophotometer. UV-spectra of samples were measured between 350 nm and 650 nm at room temperature.

Reference cuvette contained CYP119 ( $2 \mu\text{M}$ ) in 700  $\mu\text{L}$  potassium phosphate buffer (pH 7.4), while control cuvette contained CYP119 ( $2 \mu\text{M}$ ) in CO-bubbled 700  $\mu\text{L}$  potassium phosphate buffer (pH 7.4). Solid sodium dithionite (around 0.5–1 mg solid per milliliter of the microsomal mixture) were added to the solution to convert the ferric form of CYP119 into the ferrous form and gently mixed by pipetting. The CO treatment of potassium phosphate buffer was conducted at 1 bubble/s speed for 30 minutes prior to reduction with sodium dithionite.

Sample cuvette contained CYP119, mixed with redox partners Pdx and PdR at an optimized ratio of 1:10:2 – CYP119:Pdx:PdR (2  $\mu$ M CYP119, 20  $\mu$ M Pdx and 4  $\mu$ M PdR) in phosphate buffer (pH 7.4). NADH was added to achieve a final concentration of 0.5 mM (Nguyen et al., 2021). The CO treatment of potassium phosphate buffer was conducted at 1 bubble/s speed for 30 minutes prior to reduction with NADH.

CYP119 enzyme in the sample was determined using equation 2.3, rearranged from Beer's Law ( $A = \epsilon cl$ ).

$$\frac{\Delta(A_{450} - A_{490})_{\text{reduced, CO}}}{91 \frac{\mu\text{mol}}{\text{ml}} \times 1\text{cm}} \times 1000 \frac{\text{nmol}}{\mu\text{mol}} = \frac{\text{nmolP450}}{\text{ml}}$$

Equation 2.3. Formula for calculation of reduced and CO-complexed CYP119 concentration. Where  $(\Delta A_{450} - A_{490})_{\text{reduced, CO}}$  – absorbance at (450 – 490 nm) when reduced using dithionite reduced, CO sample (Stresser, 2021).

## CHAPTER 3

### RESULTS

#### 3.1 Structural Alignment of Proteins: CYP119 and P450cam

While the native partners for CYP119 are not known, previous studies have shown that CYP119 can accept electrons from putidaredoxin (Pdx) and putidaredoxin reductase (PdR) with low efficiency (Shimada et al., 2000). The native redox partners for Pdx and PdR is the bacterial P450 enzyme – P450cam (CYP101) (Ortiz De Montellano, 2004; Sevrioukova, 2006; Shimada et al., 2000).

Tripathi et al., (2013) have solved the crystal structure of complex of P450cam bound to putidaredoxin (Pdx) (PDB id: 4JWS) (Tripathi, 2013). To engineer three-protein-system with CYP119-putidaredoxin (Pdx)-putidaredoxin reductase (PdR), structural alignment of P450cam (PDB ID: 4JWS), Pdx (PDB ID:1XLN) and CYP119 (PDB ID: 1IO7) proteins were performed.

Effects of protein charges and electrostatic interactions in the binding site convey important properties to the protein-protein binding. By facilitating a charge attraction between proteins, it was expected to increase the binding affinity. As a result of structural alignment, the critical Arg112 residue of P450cam was superimposed with Arg80 residue of CYP119. Arg112 residue is a key residue of P450cam, which enables binding to the redox partner and is essential to the transport of electrons in the Pdx–P450cam complex (Sevrioukova & Poulos, 2011). Glu76 residue of P450cam forms a salt bridge with Arg66 of Pdx and is important to maintain connection with the electropositive side of putidaredoxin in P450cam-Pdx complex (Sevrioukova et al., 2010).

Alignment results revealed that the negatively charged Glu76 residue of P450cam corresponds to Asn34 residue of CYP119. Negatively charged Asp77 residue of P450cam, which may also make an interaction with positively charged Arg66 of Pdx

(Sevrioukova, 2006), corresponds to the residue Asn35 of CYP119. Arg109 of P450cam forms a nonbonded interaction with Trp109 of Pdx (Tripathi et al., 2013), and corresponds to Asp77 of CYP119. Figure 3.1 represents CYP119, Putidaredoxin and P450cam-Pdx complex structural alignment.

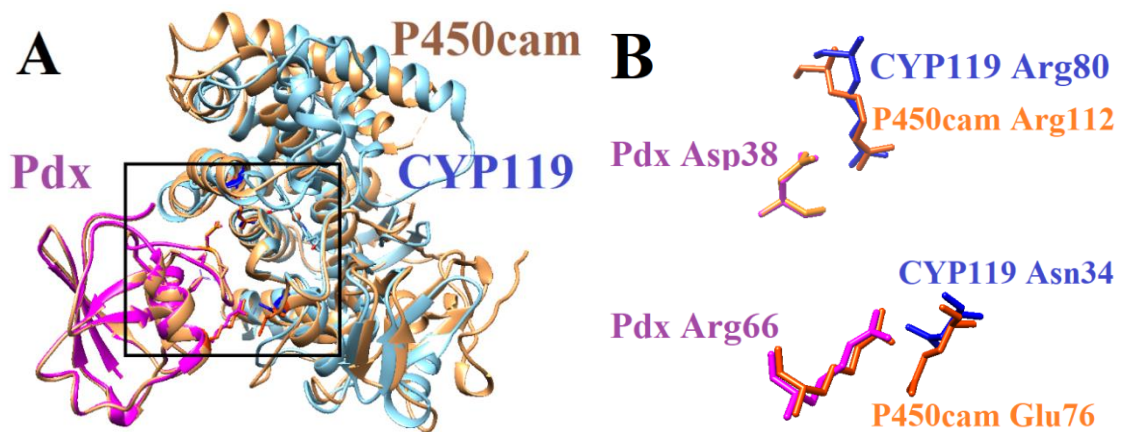


Figure 3.1. A. Structural alignment of proteins: CYP119 (PDB ID:1IO7) in blue, Pdx (PDB ID:1XLN) in purple and P450cam-Pdx (PDB ID: 4JWS) in brown. Proteins were aligned to see the interactions between P450cam-Pdx and CYP119-Pdx complexes. B. Key residues in the binding site. Asp38 of Pdx binds with Arg80 of CYP119 and Arg112 of P450cam. Asn34 residue of CYP119 (PDBID: 1IO7) corresponds to the negatively charged amino acid Glu76 of P450cam, that is necessary to preserve the positively charged side of putidaredoxin (residue Arg66) coupled. Possible residues to increase the affinity between putidaredoxin and CYP119 were identified. Images were created using UCSF Chimera.

For the following mutagenesis studies, non-conserved residues on the surface of binding sites of proteins were selected. All known conserved residues of proteins are available in literature, and according to obtained and analyzed alignment results, possible residues to increase the affinity between putidaredoxin and CYP119 were identified. Several single mutations were selected, along with double mutations containing the D77R mutant were selected for further mutant design, since according to Koo et al., (2002),

D77R mutation showed 5-fold enhancement in the rate of electron transfer between Pdx and CYP119 without impacting the thermostability of the enzyme (Koo et al., 2002). All residues are expected to be non-conserved and located in the surface area of binding site of CYP119 to putidaredoxin.

The list of mutations selected for further mutant design studies were summarized and are illustrated in Table 3.1.

Table 3.1 The list of mutations selected for mutant design process.

№	Single mutations	№	Double mutations
1	N34D	7	N34D-D77R
2	N34E	8	N34E-D77R
3	N35D	9	N35D-D77R
4	N35E	10	N35E-D77R
5	K30D	11	K30D-D77R
6	K30E	12	K30E-D77R
		13	N34E-N35D
		14	N34D-N35D


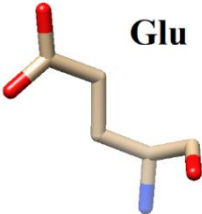
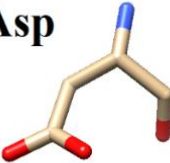
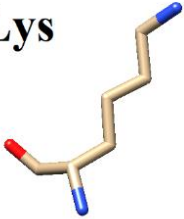
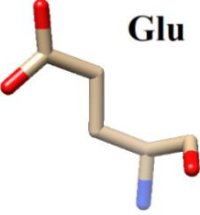
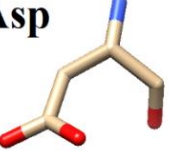
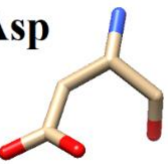
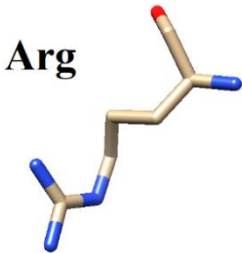
According to the structural alignment results, four residues were selected for mutation experiment, and 14 different mutations were planned to create the following changes in the interaction between CYP119 and Pdx:

1. Asn34 that corresponded to Glu76 of P450cam was changed to aspartic acid (negatively charged) and glutamic acid (negatively charged) residue.
2. Asn35 that corresponded to Asp77 of P450cam was changed to aspartic acid (negatively charged) and glutamic acid (negatively charged) residue.
3. Lys30 was replaced with aspartic acid (negatively charged) and glutamic acid (negatively charged) residue in order to make the surface more electronegative to maintain connection with the electropositive side of putidaredoxin.
4. Asp77 was replaced with arginine (positively charged), since according to Koo et al., (2002), D77R mutation resulted 5-fold enhancement in the rate of electron transfer

between putidaredoxin to CYP119 enzyme without impact on the thermostability of the enzyme (Koo et al., 2002).

Amino acids that were used for creating mutations are shown in Table 3.2.

Table 3.2 Amino acids that were used for creating mutations.

WT residues	Mutation1	Mutation2
<b>Asn</b> 	<b>Glu</b> 	<b>Asp</b> 
<b>Lys</b> 	<b>Glu</b> 	<b>Asp</b> 
<b>Asp</b> 	<b>Arg</b> 	

### 3.2 Design of CYP119 Mutant Enzymes Using PyRosetta Software

The PyRosetta Software was used to design all mutant enzymes. A “pose” containing the structure and sequence data, relative position and orientation was downloaded from RCSB website. Mutations were performed on the WT CYP119 enzyme (PDB ID: 1IO7). N34D, N34E, N35D, N35E, K30D, K30E single mutations, and N34D-

D77R, N34E-D77R, N35D-D77R, N35E-D77R, K30D-D77R, K30E-D77R, N34E-N35D, N34D-N35D double mutations were created using specific files resfiles.

Using the “ScoreFunction” the energy of structure was calculated. The heme cofactor was added manually using mol2 file format and param files. Energy minimization of the whole structure was completed using FastRelax function. Total energies in Rosetta Energy Unit (REU) of WT CYP119 and created CYP119 mutants were obtained and are illustrated in Table 3.3.

Table 3.3 Total energies (REU) of WT CYP119 and created CYP119 mutants.

№	Protein	Total energy (REU)
0	Native energy of WT CYP119	-675.3
1	N34D mutant	-686.9
2	N34E mutant	-688.7
3	N35D mutant	-687.2
4	N35E mutant	-676.1
5	K30D mutant	-680.3
6	K30E mutant	-675.6
7	N34D-D77R mutant	-687.1
8	N34E-D77R mutant	-679.7
9	N35D-D77R mutant	-685.5
10	N35E-D77R mutant	-691.6
11	K30D-D77R mutant	-684.9
12	K30E-D77R mutant	-693.5
13	N34E-N35D mutant	-691.6
14	N34D-N35D mutant	-706.5

Total energy of WT CYP119 was -675.3 REU (Rosetta Energy Unit), while mutant CYP119s total energies were ranged between -675.6 REU (K30E) and -706.5 REU (N34D-N35D), showing all mutants were stable when compared to WT CYP119. While all mutants showed increased stability, since increasing stability of CYP119 was



not main goal of the project, all mutants were subjected to docking experiments with Pdx protein partner.

### 3.3 Protein-Protein Docking Using RosettaDock Server Rosie

Protein-protein docking of WT CYP119 and 14 mutants with partner protein, putidaredoxin/putidaredoxin reductase were performed using PatchDock, ClusPro, HawkDock, Prism, and ZDock servers. However, the coarse-grained description of the proteins limits the models' accuracy at the atomic level (Lyskov & Gray, 2008). Therefore, RosettaDock server Rosie was used in the current research.

Table 3.4. Docking results of Pdx and WT/mutants CYP119 using Rosie Docking Server.

Variants that were chosen for further experimental studies are shown in bold.

№	Mutant name	Total score (REU)	Interface score (REU)	RMSD (Å)
0	WT CYP119	-502.7	-3.5	1.5
1	K30D	-500.2	-2.7	1.7
2	K30D-D77R	-502.0	-3.4	0.5
3	K30E	-500.7	-3.3	1.0
4	K30E-D77R	-498.2	-3.4	0.5
5	N35D	-503.3	-3.7	0.7
6	N35D-D77R	-502.6	-3.7	1.6
7	N35E	-503.8	-3.6	1.0
8	N35E-D77R	-501.5	-3.7	4.2
9	N34D	-503.4	-3.5	0.5
10	N34D-D77R	-500.9	-3.2	0.9
<b>11</b>	<b>N34E</b>	<b>-502.6</b>	<b>-3.0</b>	<b>1.1</b>
<b>12</b>	<b>N34E-D77R</b>	<b>-501.1</b>	<b>-3.2</b>	<b>1.6</b>
13	N34E-N35D	-503.7	-3.2	0.9
14	N34D-N35D	-504.3	-2.9	1.5

Obtained results of total scores, interface scores and RMSD values are summarized in Table 3.4. After sample preparation using UCSF Chimera, mutants and Pdx structures in a single pdb file were uploaded to the RosettaDock server as an input with starting configuration and coordinates. Server generated 1000 independent structures as an output and detailed scoring information of ten variants with lowest energy scores with pictures and rank order by energy were obtained.

Ten lowest-interface-energy structures were created in each docking run and they were downloaded for further analysis and visualization. Utilizing UCSF Chimera, all variants of docked mutant-Pdx complexes were visualized and prediction accuracy of the binding site between mutant CYP119 and Pdx with binding site of predicted WT CYP119-Pdx complex were assessed.

Figure 3.2 presents interface score and RMSD values of wild type CYP119 and 14 mutants.

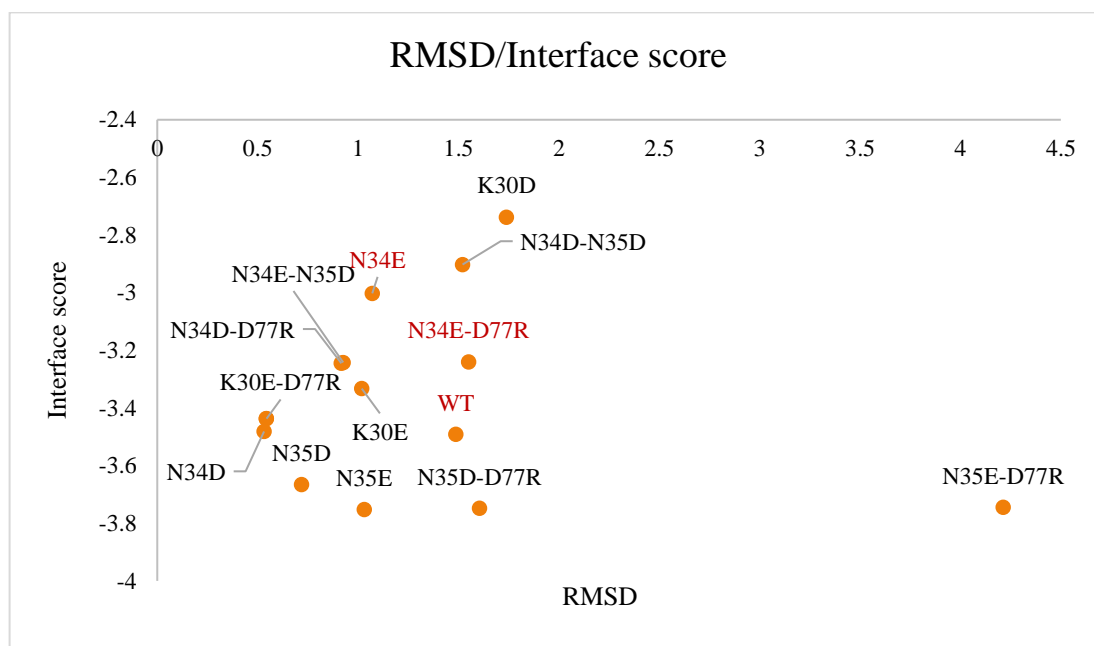


Figure 3.2. Interface score and RMSD values of WT and 14 mutant CYP119s. Variants that were chosen for further experimental studies and WT CYP119 are highlighted in red.

The linear combination of non-bonded atom-pair interaction energies makes up the Rosetta interface score (ISC). The total energy of the two monomeric structures is subtracted from the total energy of the complex structure to calculate this score. Stated differently, separable energy is subtracted from complex energy to determine the interface score for each scoring term.

The average distance between the backbone atoms of superimposed proteins, RMSD and total score of models were calculated. Total score of models renders protein-protein interaction and internal energy of the protein. The average distance between the atoms of superimposed proteins—typically the backbone atoms—is measured by the root-mean-square deviation of atomic locations, or RMSD.

Total score of models renders protein-protein interaction and internal energy of the protein. Figure 3.3 presents total score and RMSD values of wild type CYP119 and 14 mutants.

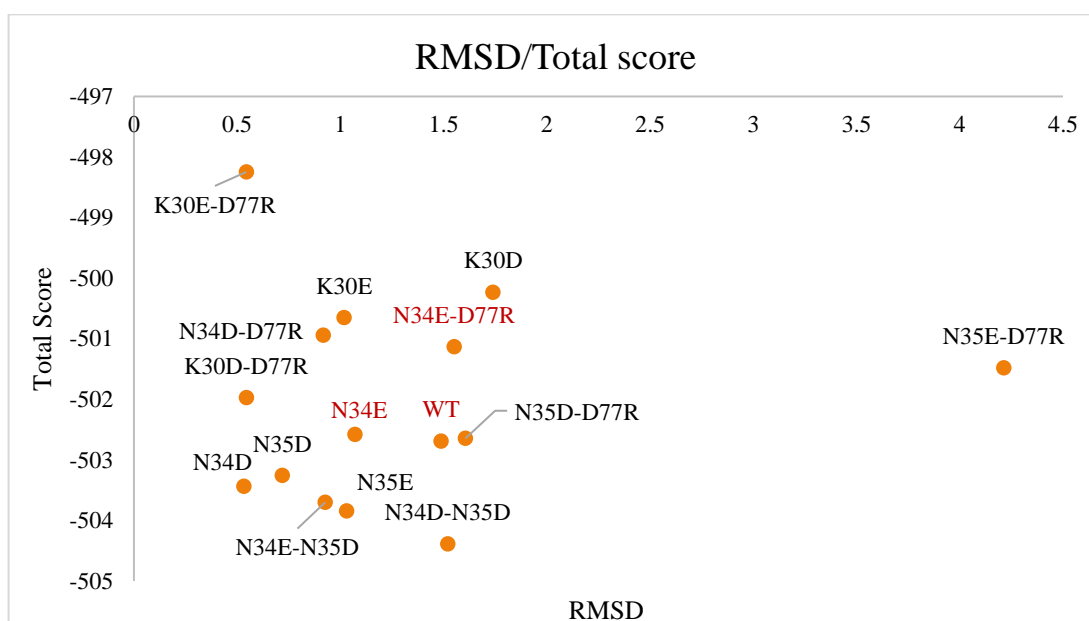


Figure 3.3. Total energy and RMSD values of WT and 14 mutant CYP119s. Variants that were chosen for further experimental studies and WT CYP119 are highlighted in red.

Selection of mutation for further experimental studies was performed according to following steps. Firstly, based on the docking results, variants with high root mean square deviation (RMSD) values were eliminated. Variants that were superimposed with predicted WT CYP119-Pdx complex, and that have the lowest root mean square deviation (RMSD) values and the lowest energy scores were selected for further detailed analysis. The data given by Rosie docking server, proteins with the lowest-interface-energy were visualized and analyzed using USCF Chimera. As Arg112 of P450cam is a key residue in the electron transfer, that binds to the electronegative residue of Pdx, Asp38, distances between these key residues were analyzed.

Arg112 of P450cam was superimposed with Arg80 in CYP119 in the alignment experiment, therefore distance between Arg80 of CYP119 and Asp38 of Pdx was measured. Arg80 of CYP119 forms a salt bridge with Asp38 of Pdx, with distance 2.862 Å and it's expected that in CYP119-Pdx complex, Arg80 residue would play a vital role in electron transfer system, forming a salt bridge with Asp38 residue of Pdx, as in P450cam-Pdx complex. Therefore, these residues and distances between them were one of the main factors in selecting mutants for further experimental studies. In WT CYP119-Pdx complex, the distance between these residues (Arg80 of CYP119 and Asp38 of Pdx) is 2.862 Å, most of the mutants bound tighter than WT, except for N35E-D77R, N34D-D77R, N34D-N35D (8.716 Å, 3.049 Å and 2.908 Å respectively). This led to elimination of these mutants from further experimental studies.

In the current project one single mutation and since the D77R mutation created by Koo and coworkers (2002) improves the binding between two proteins up to 5-fold (Koo et al., 2002), one double mutation containing D77R mutation were planned to be created. In the second round of elimination, as double mutants N35E-D77R, N34D-D77R were already eliminated, hence, single N35E and N34D mutants, as well as N34D-N35D double mutation, which does not contain D77R mutation, were also eliminated. In the third round of elimination, distances between mutated residues and residues in the binding surface of Pdx were measured. The distance between key residues of P450cam-Pdx complex, Arg109-Asp38 respectively is 6.766 Å was another factor to eliminate mutants. Arg109 is key residue in the second electron tranfer process.

All mutations with the distance between key residues Arg109-Asp38 more than 6.766 Å were eliminated. Mutants with the distance between mutated residues of CYP119 and Arg66 of Pdx more than 5.0 Å were eliminated. Thus K30E, K30D, K30E-D77R, K30D-D77R, N35D mutants were eliminated. Asn34 replaced with Glu34 helps to form

electronegative region of CYP119 and expected to alleviate the charge repulsion with Arg66 of Pdx surface.

Schematic representation of some of the mutant CYP119 enzymes docked with Pdx are shown in Figure 3.4.

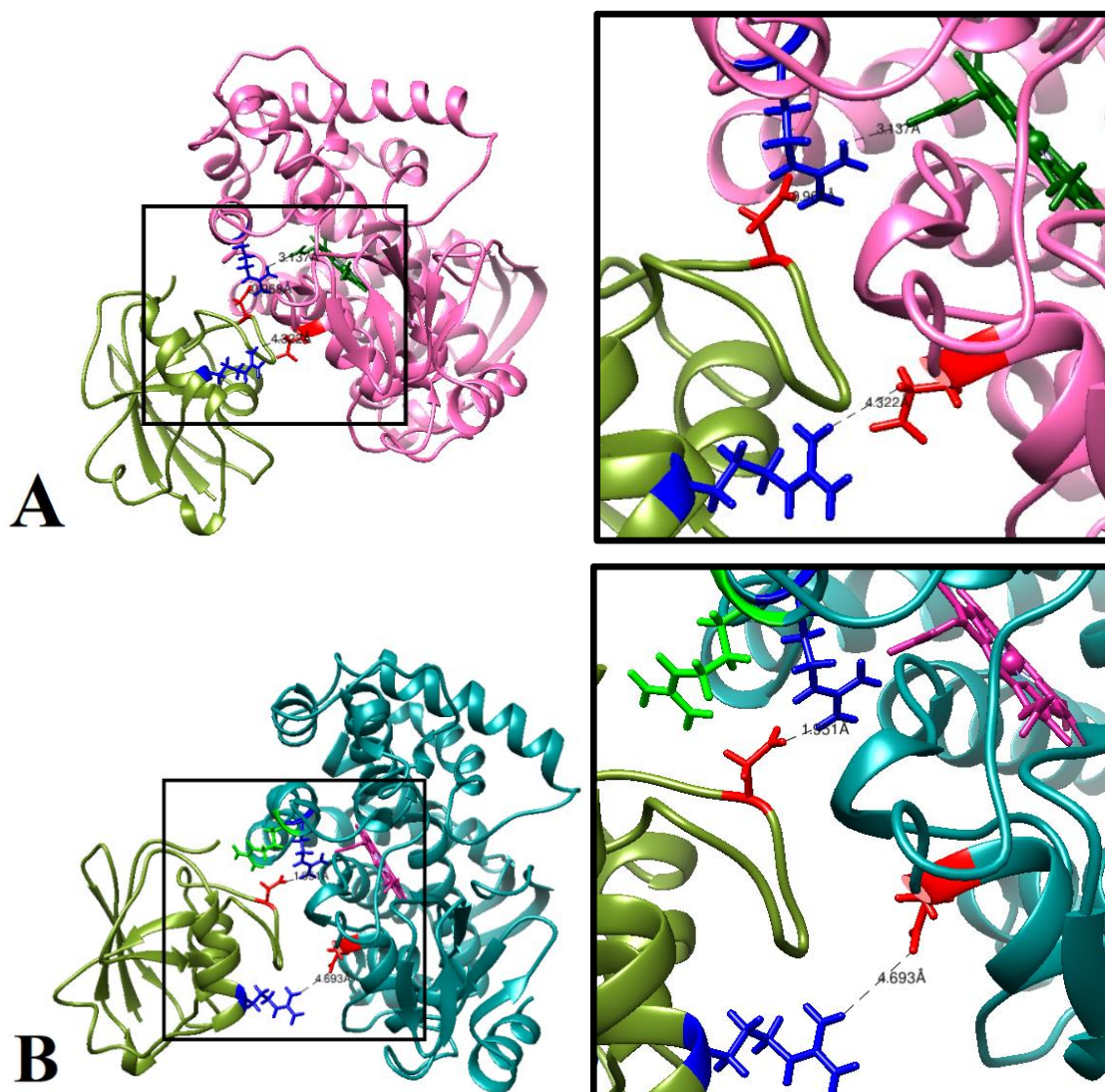


Figure 3.4. Distances between important residues of mutant CYP119s and Pdx complex. A. N34E CYP119 (in magenta) - Pdx (in green) complex; Arg80-Asp38, Glu34-Arg66 of CYP119-Pdx; B. N34E-D77R CYP119 (in cyan) - Pdx (in green) complex; Arg80-Asp38, Glu34-Arg66, Arg77-Asp38 of CYP119-Pdx.

Table 3.5. Distances between key residues of docked Pdx with mutants of CYP119, compared to docked Pdx with wild type CYP119, as well as compared to crystal structure of P450cam-Pdx complex (PDB ID: 4JWS).

Interacting Residues	Distance between residues (Å)															
	P450cam	WT CYP119	K30D	K30E	K30E-D77R	K30E-D77R	N35D	N35D-D77R	N35E	N35E-D77R	N34D	N34D-D77R	N34E	N34E-D77R	N34E-N34E-D77R	N34E-N34E-N35D
P450cam-Pdx complex crystal structure	3.02	2.86	1.01	2.82	0.44	2.6	2.17	2.37	8.72	2.78	3.05	0.97	1.95	2.34	2.91	
Arg112-Asp38																
Glu76-Arg66	4.02	3.98								4.81*	5.41*	4.32*	4.69*	6.49*	5.03*	
Asp77-Arg66	6.30	6.06				6.17*	4.13*	5.82*	9.23*					6.45*	6.61*	
Arg109-Trp106	4.13	7.81					2.61*		10.9*		3.81*		3.16*			
Arg109-Asp38	6.77	7.03					6.33*		9.67*		6.49*		6.27*			
Arg72-Arg66	9.49	8.67	12.05*	8.01*	8.1*											

\*Denotes the distance between corresponding mutated residues

Distances between key residues of Pdx and mutant CYP119s are summarized in Table 3.5. Mutations chosen for further experimental studies are labeled in bold. According to results summarized in Table 3.5, the best mutants were identified to be N34E, N34E-D77R, N35D-D77R.

N35D-D77R double mutation showed the 6.329 Å distance for Arg77-Asp38, however N35D single mutation was already eliminated. Therefore N34E, N34E-D77R mutations were selected for further experimental studies.

In addition to this mutant, the D77R single mutation by Koo et al., (2002) was selected to be introduced into the WT CYP119, in order to compare with N34E and N34E-D77R mutants, that are believed to bind better and therefore, enhance the electron transfer.

### **3.4 Construction of CYP119 Mutants Using Site-Directed Mutagenesis**

#### **Method**

As described above, computational studies have predicted that an increased affinity to Pdx can be obtained with N34E and N34E-D77R mutants. The DNA CYP119 in pET11a was a gift from Teruyuki Nagamune (Addgene library #66131) (Suzuki et al., 2014).

Mutants were obtained by using Q5® Site-Directed Mutagenesis Kit (New England Biolabs) which uses PCR to obtain mutated DNA. PCR products were confirmed in 1% agarose gel in TAE buffer (40 mM Tris-acetate, 1 mM EDTA).

Mutated plasmids were transformed to BL21 (DE3) *E. coli* competent cells followed by sequence analysis performed by BIYOMER at IZTECH confirmed desired mutations (Appendix B). DNA of each mutant CYP119 were transformed into BL21 (DE3) competent *E. coli* cells according to protocol by Baslar et al., (2020) and single colony of each mutation was stocked in 25% glycerol at -80°C (Başlar et al., 2020).

Figure 3.5 depicts 1% agarose gel with PCR products of mutants, N34E mutant, N34E-D77R mutant, D77R mutant. Bands between 6 kb and 8 kb were observed. Transformation plates for each mutant samples can be observed in Figure 3.6.

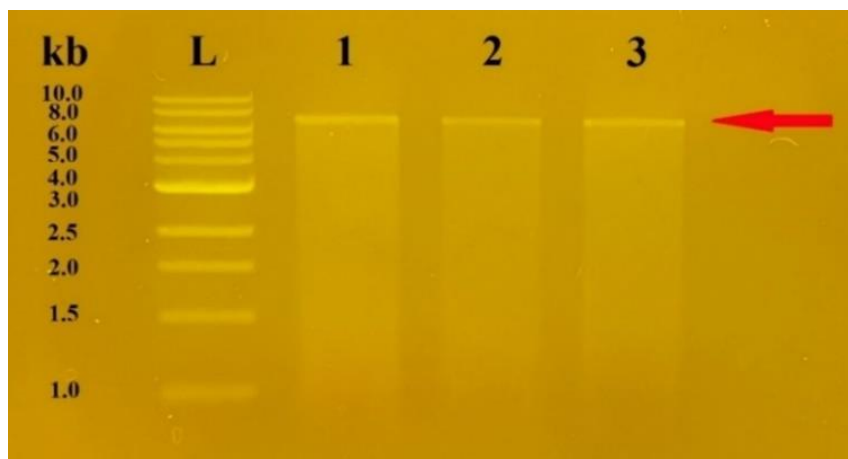


Figure 3.5. PCR products with mutated primers in 1% agarose gel. L – 1 kb Ladder; 1. N34E mutant; 2. N34E-D77R mutant; 3. D77R mutant. WT CYP119 gene is 6748 bp long.

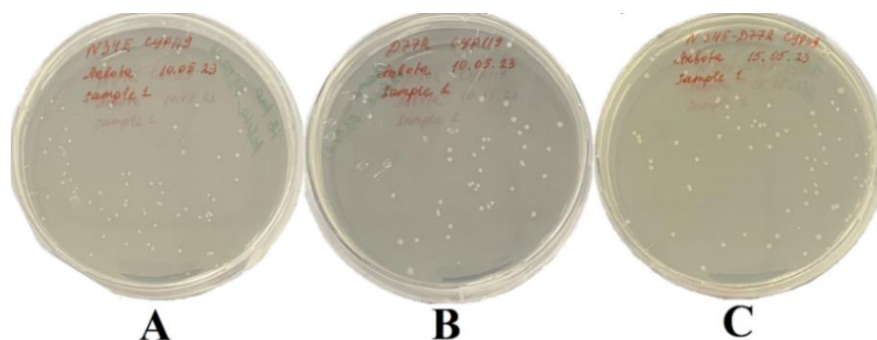


Figure 3.6. A. N34E single mutation; B. D77R single mutation; C. N34E-D77R double mutation.

### 3.5 Expression and Purification of WT and Mutant CYP119 Enzymes

WT and mutant CYP119 proteins were expressed according to protocol by Başlar et al., (2020). Protein expression was induced using 1 mM of IPTG, cells were grown at temperature of 30°C for 32 h (Başlar et al., 2020).



Expressions of WT and mutant CYP119s were monitored using SDS-PAGE analysis and results are illustrated in Figure 3.7.

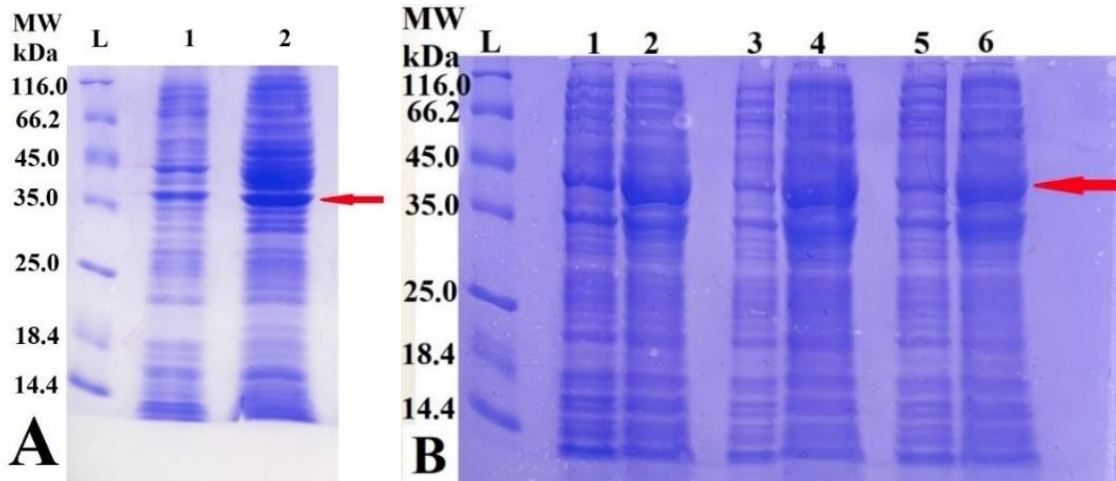


Figure 3.7. A. Expression of WT CYP119 observed by SDS-PAGE: L – Protein Marker; 1. WT CYP119 before IPTG; 2. WT CYP119 after addition of IPTG and incubating for 32 h; B. Expression of mutants observed by SDS-PAGE: L – Protein Marker; 1. N34E CYP119 before IPTG; 2. N34E CYP119 after addition of IPTG and incubating for 32 h, 3. D77R CYP119 before IPTG; 4. D77R CYP119 after addition of IPTG and incubating for 32 h, 5. N34E-D77R CYP119 before IPTG; 6. N34E-D77R CYP119 after addition of IPTG and incubating for 32 h. Pierce™ Unstained Protein MW Marker (26610) from ThermoFisher was used as ladder.

Purifications of WT and mutant CYP119s were monitored using SDS-PAGE analysis and results are illustrated in Figure 3.8.

WT and mutant CYP119s were purified according to protocol by Sakalli (2020) (Sakalli, 2020). Shortly, lysed cell pellets were precipitated by 30% and 60% ammonium sulphate.

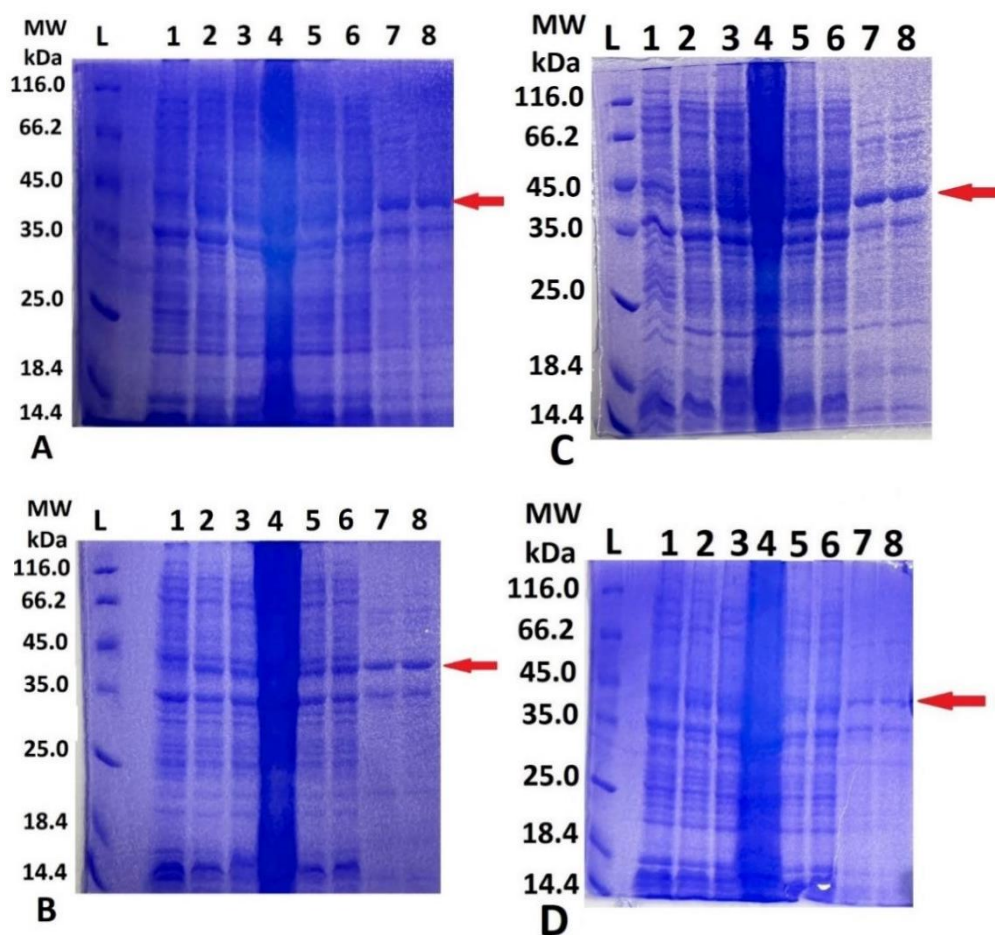


Figure 3.8. A. Isolation of WT CYP119 was monitored by SDS-PAGE; B. N34E; C. N34E-D77R; D. D77R. L – Protein Marker; 1. Before adding IPTG; 2. After adding IPTG and incubating for 32h; 3. Lysed in lysis buffer; 4. Sonicated and centrifugation after sonication pellet sample; 5. Ammonium sulphate precipitation 30%; 6. Ammonium sulphate precipitation 60%; 7. After dialysis.

### 3.6 Cloning, Expression and Purification of Redox Partner Proteins – Putidaredoxin (Pdx) and Putidaredoxin Reductase (PdR)

Plasmids pPdx and pPdR were gifts from Teruyuki Nagamune (catalog numbers #85084 and #85083, respectively) (Suzuki, 2016; Suzuki et al., 2014). Single digestion of a plasmid was performed to confirm the plasmid.

1% agarose gel results can be observed in Figure 3.9.

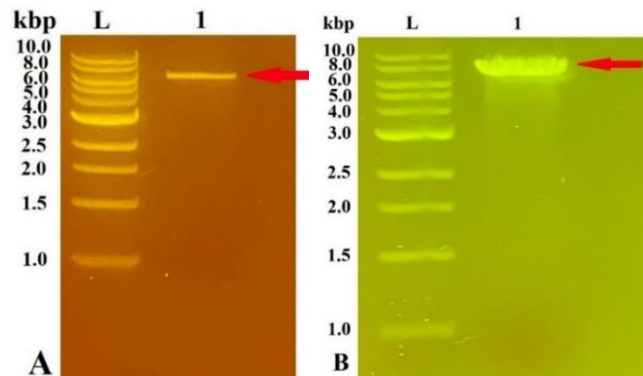


Figure 3.9. Confirmation of obtained plasmids by digestion and agarose gel. A. L – ladder. 1. Pdx (expected 5657 bp); B. L – ladder. 1. PdR (expected 6602 bp).

Total vector size of pPdx plasmid is 5657 bp, pPdR plasmid is 6602 bp long. As a result, bands were observed between 6 kbp and 8 kbp, therefore obtained results were considered as confirmation of correct plasmid. Transformation of pPdx and pPdR to BL21 (DE3) competent *E. coli* cells were performed. Colonies were observed on the next day. Figure 3.10 illustrates transformation plates with colonies containing pPdx and pPdR plasmids.

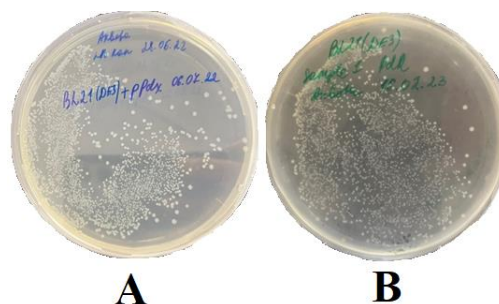


Figure 3.10. Colonies obtained after transformation of plasmids containing genes coding for Pdx (A) and PdR (B). A. pPdx transformed to BL21 (DE3) *E.coli*; B. pPdR transformed to BL21 (DE3) *E.coli*.

Expressions of Pdx and PdR were monitored using SDS-PAGE analysis. MW of PdR is 45.6 kDa and MW of Pdx is 11.7 kDa. Pdx protein expression was induced with 0.5 mM of FeCl<sub>3</sub>, while PdR protein expression was induced with 0.1 M IPTG (Suzuki, 2016). Pdx expression results are shown in Figure 3.11. A single colony of bacterial cells containing pPdx and pPdR plasmids were expressed according to protocol by Suzuki (2016).

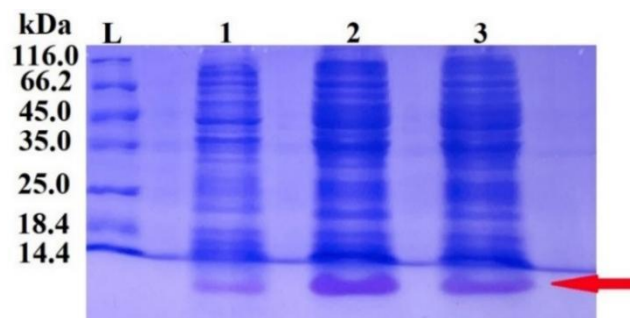


Figure 3.11. Expression of Pdx followed by SDS-PAGE. (MW of Pdx is 11.7 kDa). L – Protein Marker; 1. Pdx before adding FeCl<sub>3</sub>; 2. Pdx after addition of FeCl<sub>3</sub> and incubating overnight at 27°C; 3. Pdx after addition of FeCl<sub>3</sub> and IPTG, incubating overnight at 27°C.

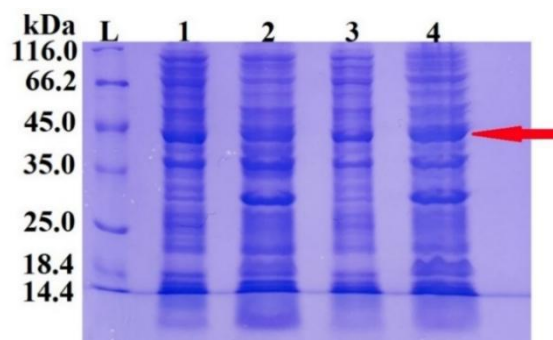


Figure 3.12. Expression of PdR followed by SDS-PAGE. (MW of PdR is 45.6 kDa). L – Protein Marker; 1. PdR OD<sub>600</sub>=0.8; 2. PdR after incubating overnight at 27°C; 3. PdR before IPTG; 4. PdR after incubating with IPTG overnight at 27°C.

More protein expression was observed in the absence of IPTG, therefore Pdx expression was performed only with addition of FeCl<sub>3</sub>. PdR expression results are shown in Figure 3.12. For PdR expression more protein was observed in the presence of IPTG therefore expressions were performed with IPTG addition. Pdx purification was monitored by SDS-page and results are illustrated in Figure 3.13. Pdx protein was purified with Ni-NTA column according to method by Suzuki (2016) using lysis buffer (150 mM KCl, 10 mM imidazole, 20 mM potassium phosphate buffer (Kpi) at pH 7.5), wash buffer (20 mM Kpi at pH 7.5, 20 mM imidazole), elution buffer (300 mM KCl, 300 mM imidazole, 20 mM Kpi at pH 7.5) (Suzuki, 2016).

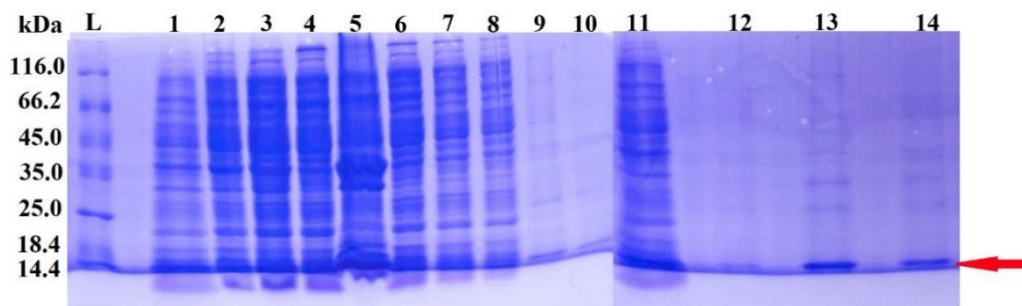


Figure 3.13. Purification of Pdx followed by SDS-PAGE. L – Protein Marker; 1. Pdx before FeCl<sub>3</sub>; 2. Pdx after addition of FeCl<sub>3</sub> and incubating overnight at 27°C; 3. After addition of lysis buffer; 4. After sonication; 5. After centrifugation (pellet); 6. After centrifugation (supernatant); 7. Flowthrough; 8-10. Column wash; 11. Pdx after addition of FeCl<sub>3</sub> and incubating overnight at 27°C; 12. Column wash; 13-14. Elution of Pdx.

PdR was purified according to previous studies carried out by Koo et al., (2002) and Suzuki (2016). First, cells were lysed with lysis buffer (150 mM KCl, 10 mM imidazole, 20 mM Kpi, 1 mM benzamidine HCl, 0.2 mM PMSF at pH 7.4) and centrifuged at 22000 rpm for 30 min, the supernatant was subjected to 30% and 70% ammonium sulfate cuts. PdR pellets were dissolved in lysis buffer and applied to Ni-NTA column, washed (20 mM Kpi, 20 mM imidazole at pH 7.4), then eluted (300 mM KCl, 300 mM imidazole, 20 mM Kpi at pH 7.4) (Koo et al., 2002; Suzuki, 2016).

SDS-page results for PdR purification are illustrated in Figure 3.14. In Figure 3.14A cell lysate was applied directly to the column without ammonium sulfate precipitation and PdR was expressed without adding IPTG. In Figure 3.14B cell lysate was applied to the column after ammonium precipitation steps and IPTG was used for induction of expression.

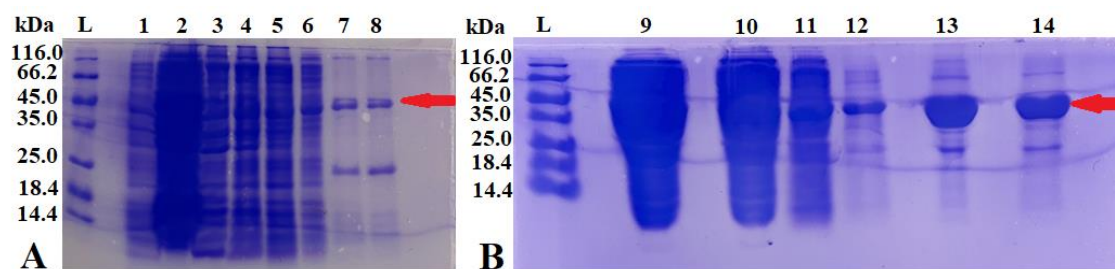


Figure 3.14. Purification of PdR followed by SDS-Page. A. PdR expression without IPTG and isolation without ammonium sulfate precipitation. L – Protein Marker; 1. Without IPTG; 2. Lysis Buffer; 3. Sonicated, centrifuged (pellet); 4. Sonicated, centrifuged (supernatant); 5. Flowthrough; 6. Wash Buffer; 7. and 8. Elution of PdR; B. PdR expression with IPTG and isolation with ammonium sulfate precipitation 9. 70% ammonium sulfate precipitation; 10. Flowthrough; 11 and 12. Column wash; 13 and 14. Elution of PdR.

### 3.7 UV-Visible Spectral Analysis of WT and Mutant CYP119s

UV-Visible spectra of WT and mutant CYP119 enzymes: N34E, D77R and N34E-D77R mutants were investigated. WT and mutant CYP119s (1.5  $\mu$ M) in 50 mM potassium phosphate at pH 7.4 were examined under the UV-Visible spectra. Optical spectra of WT and mutant CYP119s can be seen in Figure 3.15. Similar to previously published spectra, WT CYP119 had maximum absorbance at 415 nm and split  $\alpha/\beta$  bands at 531 and 565 nm. Mutations did not cause a significant Soret shift and mutant CYP119s showed maximum absorbance at 415 nm too. However, broadening in  $\alpha/\beta$  bands was observed. N34E-D77R and D77R mutants showed split  $\alpha/\beta$  bands at 531 and 565 nm,

while N34E mutant showed split  $\alpha/\beta$  bands at 525nm and 565 nm. Heme incorporation of N34E, N34E-D77R and D77R mutant CYP119s were examined from the 415 nm (Soret) and 280 nm ratio. This ratio was 0.32, 0.52, 0.53 and 0.59 for N34E, N34E-D77R and D77R mutant CYP119s and WT CYP119 respectively. For each protein, they exhibit the proper heme incorporation levels.

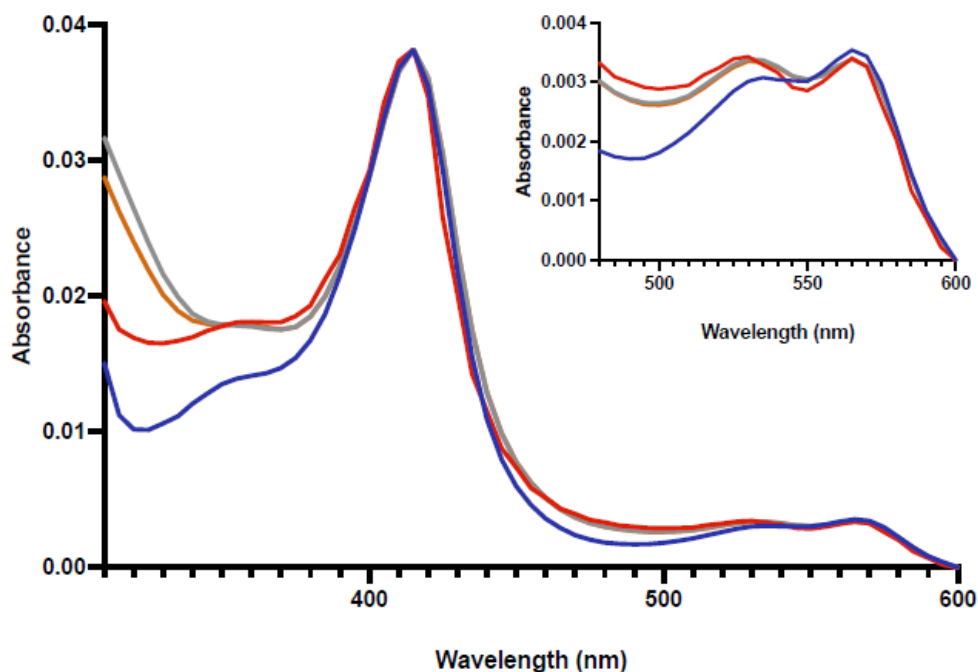


Figure 3.15. UV-Visible Spectra of WT and mutant CYP119s. Blue: WT CYP119; Red: N34E mutant; Grey: N34E-D77R mutant; Orange: D77R mutant.

### 3.8 UV-Visible Spectral Analysis of Putidaredoxin and Putidaredoxin Reductase

UV-spectra of redox partner proteins – putidaredoxin and putidaredoxin reductase were investigated. Isolated Pdx (1.5  $\mu\text{M}$ ) in 50 mM potassium phosphate at pH 7.5 was analyzed under the UV-Visible spectra. Absorbance spectra of obtained Pdx was similar to the spectra recorded in literature and shown in Figure 3.16 (Sevrioukova et al., 2003).

Absorbance maximum was observed at 280 nm, as well as peaks at 340 nm, 415 nm and 460 nm were observed.

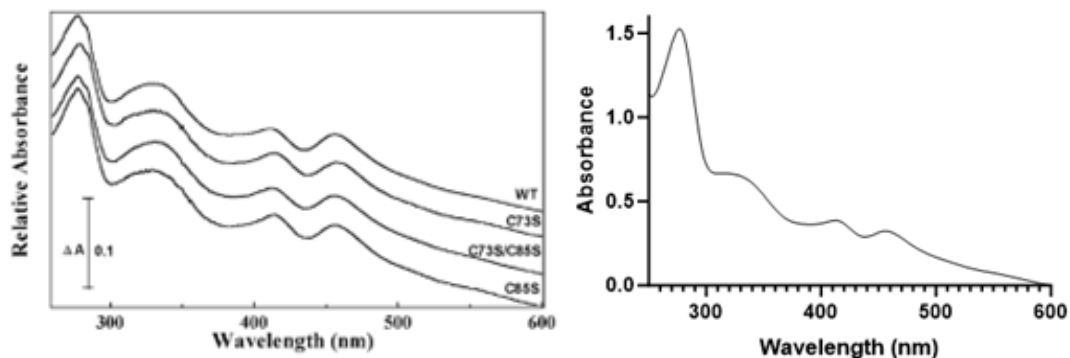


Figure 3.16. A. UV-Visible spectra of Pdx from Sevrioukova et al., (2003) (Sevrioukova et al., 2003). B. UV-Visible spectra of Pdx obtained, maximum absorbance is observed at around 280 nm.

Isolated PdR (1.5  $\mu$ M) in 50 mM potassium phosphate at pH 7.5 was analyzed under the UV-Visible spectra. Optical spectra of PdR can be seen in Figure 3.17.

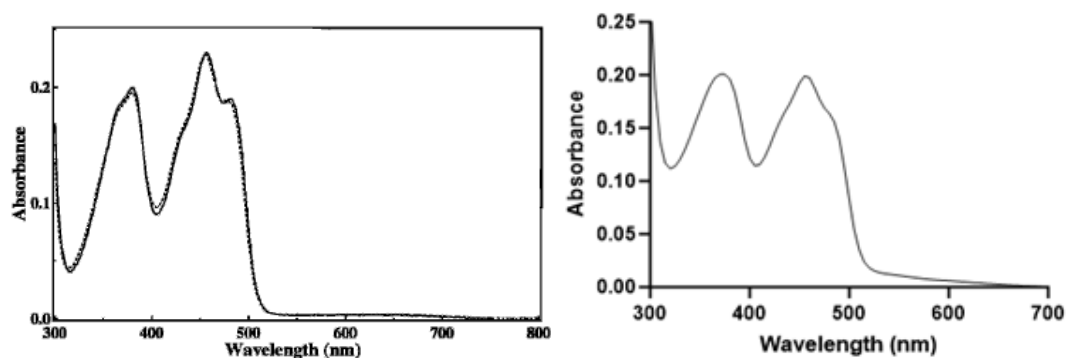


Figure 3.17. A. Absorption spectra of WT (solid) and His6 (dashed) PdR, 20  $\mu$ M enzyme dissolved in 100 mM potassium phosphate buffer pH 8.0. Source of figure A: (Sevrioukova & Poulos, 2002). B. UV-Visible spectra of PdR obtained in the current study.



The absorbance spectra of obtained PdR is similar to the spectra reported in literature and included a distinct shoulder at 480 nm, absorption maxima at 379 and 455 nm, and a small broad absorption peak in the long wavelength region as published by Sevrioukova et al., (2002) (Sevrioukova & Poulos, 2002).

### 3.9 Lauric Acid Binding to WT and Mutant CYP119s

To understand if the mutations had any effect on substrate binding to CYP119, UV-Visible spectra of samples were measured in the presence of lauric acid. Lauric acid concentration was increased stepwise up to 200  $\mu\text{M}$ . Lauric acid binding to WT, N34E, D77R and N34E-D77R CYP119 were compared using difference spectroscopy; shifts in the Soret peaks of each sample were followed with increasing lauric acid concentrations.

Obtained results revealed no significant difference in Soret peaks, comparing WT CYP119 and mutants.

Table 3.6.  $K_d$  values of substrate (lauric acid) binding to WT and mutant CYP119s.

Enzyme	Lauric Acid Binding $K_d$ ( $\mu\text{M}$ )
WT CYP119	$19 \pm 6$
N34E CYP119	$35 \pm 19$
N34E-D77R CYP119	$23 \pm 11$
D77R CYP119	$87 \pm 53$

Dissociation constant ( $K_d$ ) for lauric acid was estimated by plotting the absorbance difference against substrate concentration. The  $K_d$  of each mutant for the binding of lauric acid was similar within error relative to WT CYP119, taking into account that mutations were created on surface amino acids of proximal side of CYP119. D77R mutant binds lauric acid with similar  $K_d$  with WT CYP119 according to Koo et al., (2002) (Koo et al., 2002).

Difference spectroscopy observed a trough at 418 nm and a peak at 386 nm in all samples as shown in Figure 3.18.

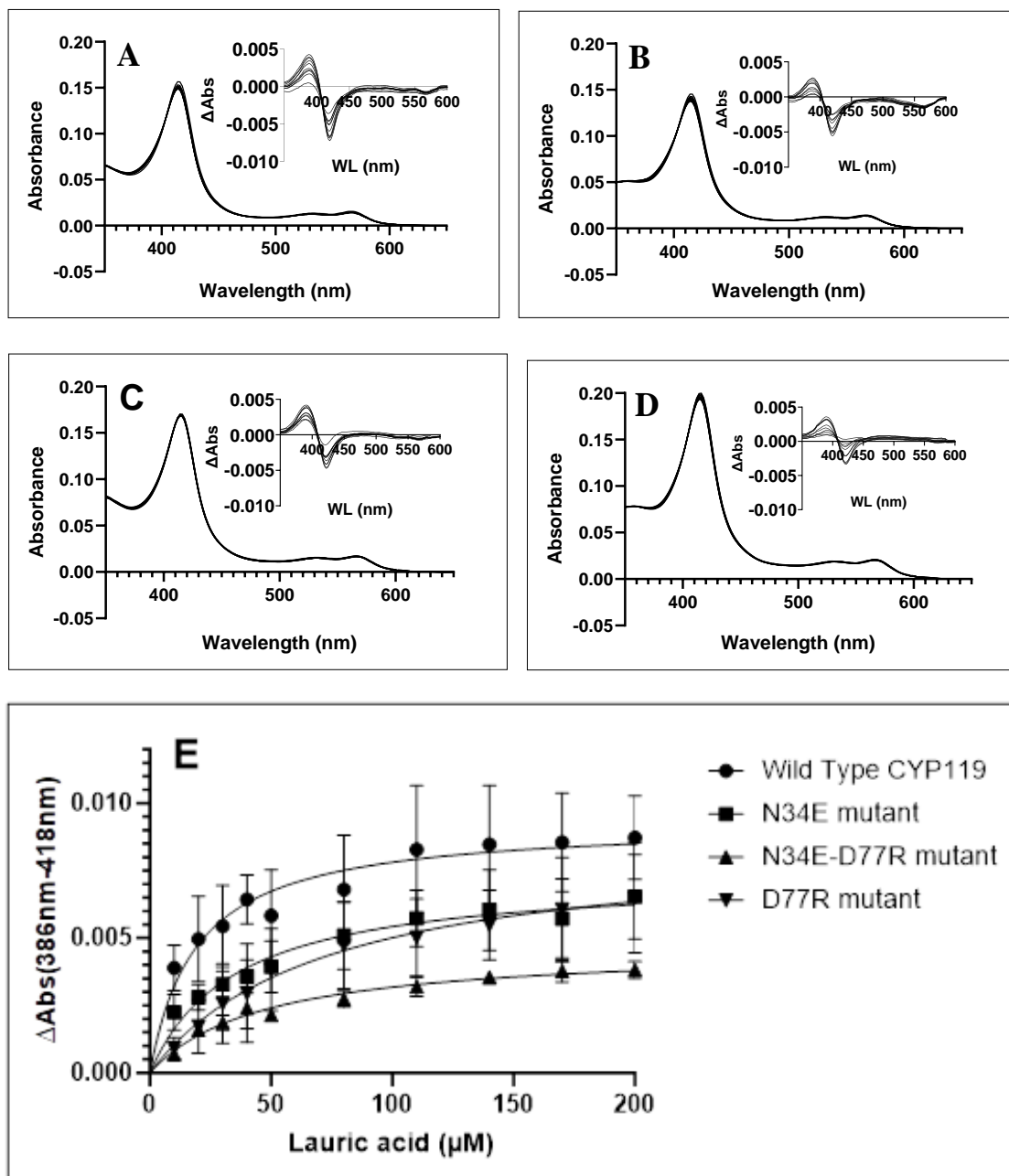


Figure 3.18. Lauric acid binding to WT and mutant CYP119s. Soret peaks of enzymes and difference spectra are shown. A. WT CYP119, B. N34E mutant, C. N34E-D77R mutant, D. D77R mutant. E. Absorbance shift (386-418) against substrate (lauric acid) concentrations were fitted to equation to calculate  $K_d$  numbers.

Obtained number for D77R mutant in the current research is  $87 \pm 53 \mu\text{M}$ , while WT CYP119 showed  $19 \pm 6 \mu\text{M}$  dissociation constant. The dissociation constants of new mutants, N34E and N34E-D77R, were  $35 \pm 19 \mu\text{M}$  and  $23 \pm 11 \mu\text{M}$ , respectively, as shown in Table 3.6. The dissociation constant obtained for WT CYP119 was consistent with the value obtained in previous studies by Sakalli (2020) ( $16.8 \mu\text{M}$ ) (Sakalli, 2020).

### 3.10 Putidaredoxin Binding to WT and Mutant CYP119s

To understand if the designed mutations resulted in increased affinity of CYP119 to Pdx, Pdx binding to WT and mutant CYP119s was investigated with UV-Visible spectroscopy. A similar spectral shift to that seen with P450cam and Pdx is obtained when Pdx is added to CYP119.

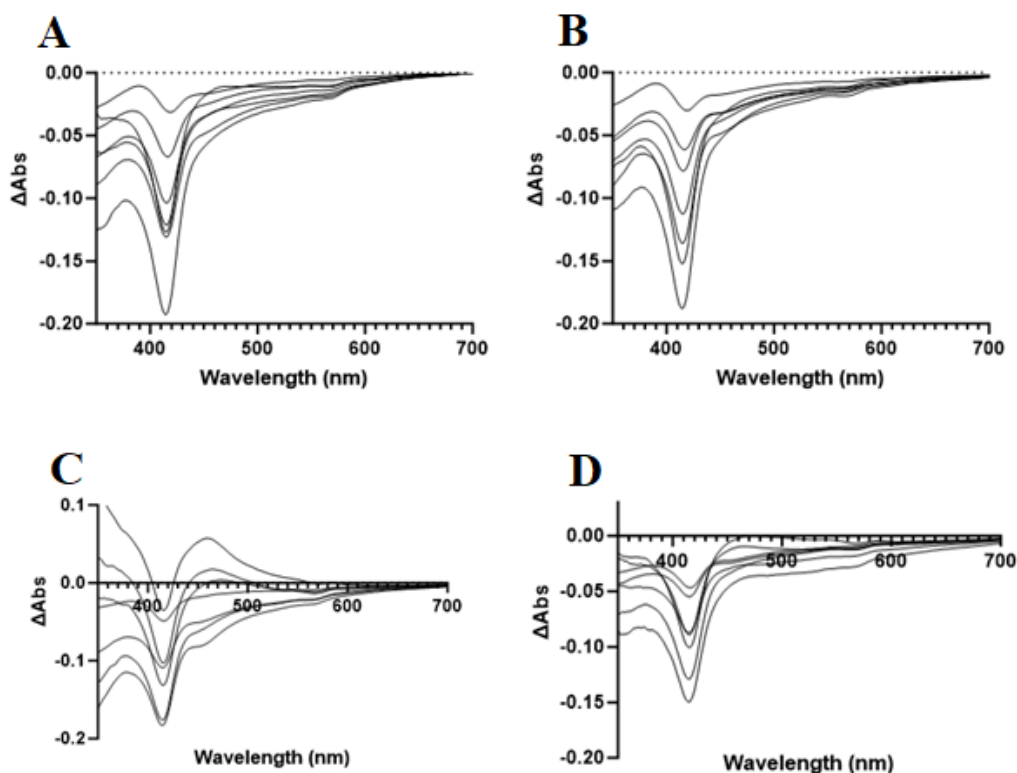


Figure 3.19. Difference spectra of Pdx binding to WT CYP119 (A); N34E CYP119 (B); N34E-D77R CYP119 (C); D77R CYP119 (D)

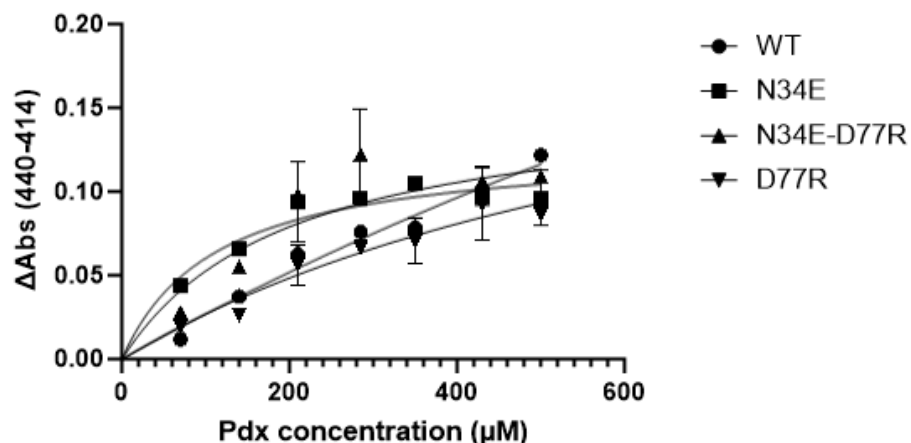


Figure 3.20. The binding of Pdx to WT, N34E, N34E-D77R and D77R CYP119 enzymes observed by difference spectra. Non-linear fitting of  $\Delta\text{Abs}$  and Pdx concentration.

In the difference spectra of Pdx bound WT CYP119 and N34E, D77R single mutants and N34E-D77R double mutants revealed a trough at 414 nm and a peak at 440 nm in all samples, as shown in Figure 3.19 and Figure 3.20 represents non-linear fitting of  $\Delta\text{Abs}$  and Pdx concentration.

Table 3.7 illustrates Pdx binding  $K_d$  in presence of lauric acid ( $\mu\text{M}$ ).

Table 3.7. Effect of Mutations on binding of Pdx to CYP119.

Enzyme	Pdx binding $K_d$ in presence of lauric acid ( $\mu\text{M}$ )
WT CYP119	$2390 \pm 224$
N34E CYP119	$112 \pm 48$
D77R CYP119	$797 \pm 184$
N34E-D77R CYP119	$200 \pm 31$

The reported  $K_d$  for Pdx binding for WT and D77R CYP119 in the presence of lauric acid are  $2100 \mu\text{M}$  and  $500 \mu\text{M}$ , respectively (Koo et al., 2002); which is consistent

with our observations. The  $K_d$  for Pdx binding for WT showed  $2390 \pm 224 \mu\text{M}$ , while  $112 \pm 48 \mu\text{M}$  for N34E,  $797 \pm 184 \mu\text{M}$  for D77R and  $200 \pm 31 \mu\text{M}$  for N34E-D77R.

### 3.11 Assessment of Electron Transfer from Pdx to WT and Mutant CYP119s and Coupling Efficiency

The first electron transfer from NADH to heme center of CYP119 by putidaredoxin through putidaredoxin reductase acceptor was tested according to methods by Koo et al., (2002), Morlock et al., (2018) and Nguyen et al., (2021). Optimized enzyme ratio of 1:20:1 of CYP119:Pdx:PdR was used in reaction mixtures. Experimental procedure was as illustrated in Table 3.8.

Table 3.8. Reaction mixture for NADH consumption and hydrogen peroxide formation reaction.

Reaction mixture	Sample	Control 1	Control 2	Control 3
0.5 $\mu\text{M}$ CYP119	+	-	+	+
10 $\mu\text{M}$ Pdx	+	+	+	-
0.5 $\mu\text{M}$ PdR	+	+	+	+
100 $\mu\text{M}$ lauric acid	+	+	-	+
100 $\mu\text{M}$ AmplexRed	+	+	+	+
0.2 U HRP	+	+	+	+
50 mM Kpi (pH 7.4)	+	+	+	+
0.2 mM NADH	+	+	+	+

Experiment was performed at room temperature. Final concentration 0.2 mM of NADH consumption was measured under the UV-spectrum between 200-700 nm with 5 nm interval. NADH consumption was followed at absorbance 340 nm (Koo et al., 2002; Morlock, 2018; Nguyen, 2021).

NADH consumption results can be observed in Figure 3.21.

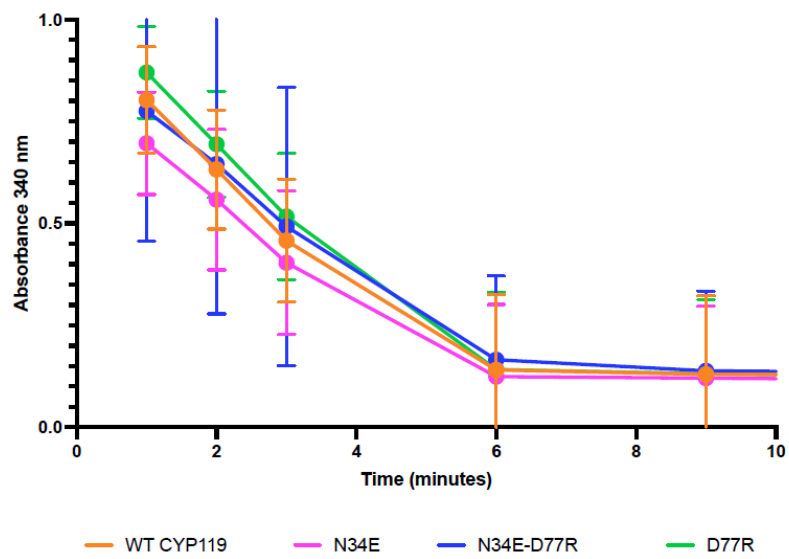


Figure 3.21. NADH consumption by WT CYP119 (orange), N34E (pink), N34E-D77R (blue), D77R (green) mutations over time.

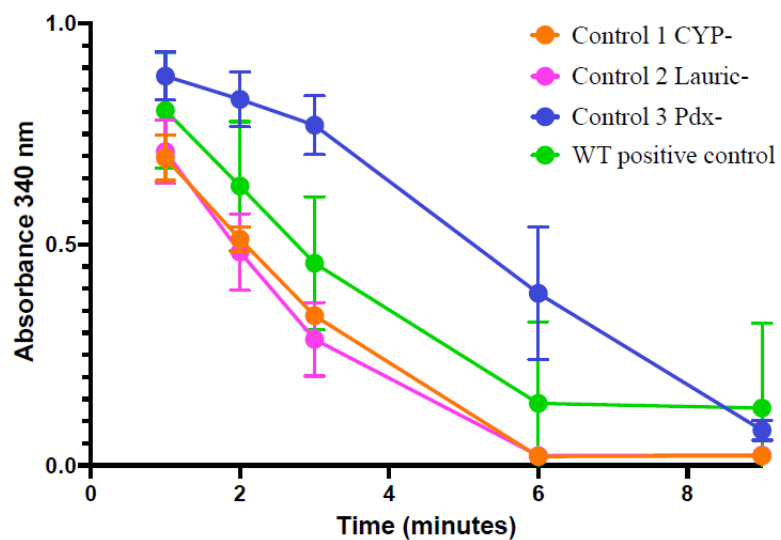


Figure 3.22. NADH consumption by Control 1 – in the absence of CYP119 (orange), Control 2 – in the absence of lauric acid (pink), Control 3 – in the absence of Pdx (blue), WT positive control (green) over time.

NADH consumption results of controls can be observed in Figure 3.22.

Simultaneously hydrogen peroxide formation was followed at absorbance 570 nm of resorufin formation (Koo et al., 2002; Morlock, 2018; Nguyen, 2021). The N-acetyl-3,7-dihydroxyphenoxazin known as AmplexRed and horseradish peroxidase (HRP) method is commonly applied to detect hydrogen peroxide (Morlock, 2018). According to Morlock et al., (2018), HRP catalyzes the reduction of hydrogen peroxide to water. As well as HRP oxidizes two AmplexRed molecules to the AmplexRed red radical by transferring a single electron. As a result, one fluorescent resorufin molecule and one AmplexRed molecule are formed. The overall stoichiometry of the reaction of resorufin to hydrogen peroxide is 1:1.

Figure 3.23 represents  $H_2O_2$  formation in a reaction.

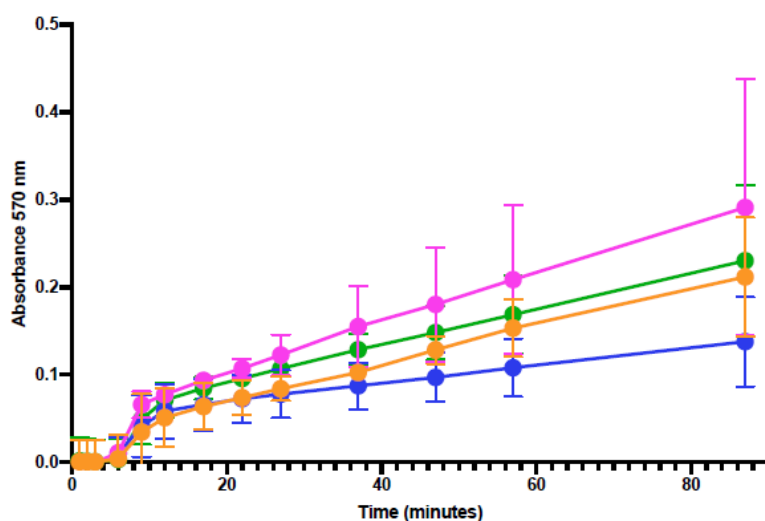


Figure 3.23.  $H_2O_2$  formation in a reaction with WT CYP119 (orange), N34E (pink), N34E-D77R (blue), D77R (green) mutations over time, 570 nm was followed for resorufin production.

In P450 reactions when the electrons are transferred to oxygen instead of substrate, superoxide anion, or hydrogen peroxide can be formed instead of product. These reactive oxygen species can then be further reduced to water. This process is called uncoupling. Despite the consumption of NADH, reaction does not lead to the desired

product, furthermore the reactive oxygen species can react with amino acids and inactivate the enzyme.

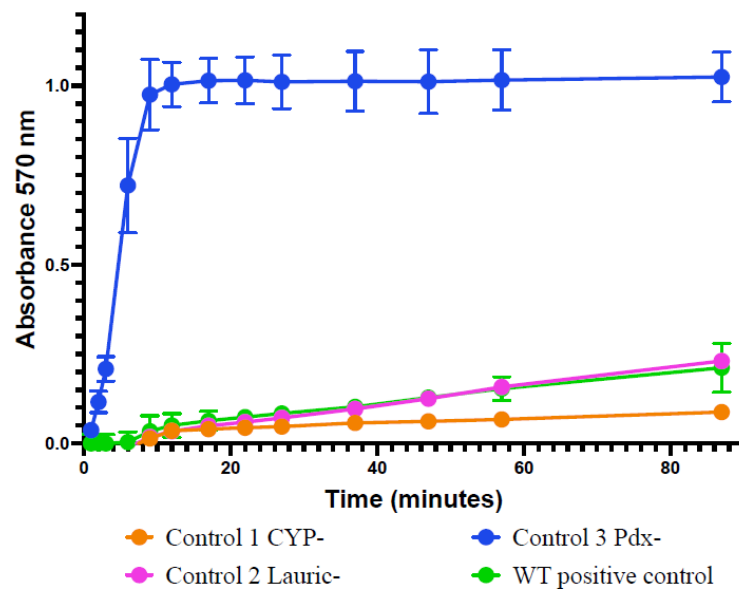


Figure 3.24.  $H_2O_2$  formation in a reaction with Control 1 – in the absence of CYP119 (orange), Control 2 – in the absence of lauric acid (pink), Control 3 – in the absence of Pdx (blue), over time, 570 nm was followed for resorufin production, WT positive control (green).

Coupling efficiency of the CYP119 reaction was examined according to method by Morlock et al., (2018). The formation of hydrogen peroxide was observed by following resorufin formation at 570 nm and the consumption of NADH at 340 nm were monitored for about 90 mins at room temperature (Morlock et al., 2018).

As a result, resorufin production was observed in all samples, respectively hydrogen peroxide production is observed, as can be seen in Figure 3.23. Hydrogen peroxide concentrations formed after 90 mins are determined as  $3.26 \pm 0.07 \mu M$ ,  $4.49 \pm 0.15 \mu M$ ,  $2.14 \pm 0.05 \mu M$ ,  $3.54 \pm 0.09 \mu M$  in WT, N34E, N34E-D77R and D77R samples, respectively. This shows that N34E-D77R mutation resulted in lower  $H_2O_2$  formation by significantly increasing coupling efficiency.

Concentrations of consumed NADH in reaction and formed  $H_2O_2$  were calculated and can be compared in Table 3.9.



Table 3.9. Concentrations of NADH consumed and formed H<sub>2</sub>O<sub>2</sub> in reaction. Values are reported as the mean of triplicate determinations  $\pm$  SD.

Time (min)	Consumed NADH ( $\mu$ M)			
	WT	N34E	N34E-D77R	D77R
6	177.4 $\pm$ 0.18	180.0 $\pm$ 0.18	173.3 $\pm$ 0.21	177.2 $\pm$ 0.19
9	179.0 $\pm$ 0.19	180.6 $\pm$ 0.18	177.7 $\pm$ 0.19	178.9 $\pm$ 0.18
17	179.6 $\pm$ 0.19	181.7 $\pm$ 0.18	178.6 $\pm$ 0.19	180.8 $\pm$ 0.18
37	180.3 $\pm$ 0.19	182.6 $\pm$ 0.18	178.9 $\pm$ 0.19	181.3 $\pm$ 0.18
47	180.8 $\pm$ 0.19	182.6 $\pm$ 0.18	179.0 $\pm$ 0.19	181.6 $\pm$ 0.18
57	180.9 $\pm$ 0.19	182.7 $\pm$ 0.18	179.1 $\pm$ 0.19	181.7 $\pm$ 0.18
87	181.2 $\pm$ 0.19	183.4 $\pm$ 0.18	179.9 $\pm$ 0.19	182.5 $\pm$ 0.19
	Formed H <sub>2</sub> O <sub>2</sub> ( $\mu$ M)			
	WT	N34E	N34E-D77R	D77R
6	0.06 $\pm$ 0.03	0.18 $\pm$ 0.02	0.16 $\pm$ 0.02	0.04 $\pm$ 0.02
9	0.53 $\pm$ 0.04	1.02 $\pm$ 0.02	0.66 $\pm$ 0.04	0.75 $\pm$ 0.03
17	0.98 $\pm$ 0.03	1.45 $\pm$ 0.002	1.03 $\pm$ 0.03	1.3 $\pm$ 0.01
37	1.58 $\pm$ 0.004	2.4 $\pm$ 0.05	1.36 $\pm$ 0.03	1.98 $\pm$ 0.02
47	1.98 $\pm$ 0.02	2.79 $\pm$ 0.07	1.51 $\pm$ 0.03	2.28 $\pm$ 0.03
57	2.35 $\pm$ 0.03	3.22 $\pm$ 0.09	1.68 $\pm$ 0.03	2.59 $\pm$ 0.04
87	3.26 $\pm$ 0.07	4.49 $\pm$ 0.15	2.14 $\pm$ 0.05	3.54 $\pm$ 0.09

### 3.12 First Reduction of WT CYP119 and to N34E, D77R Single Mutants and N34E-D77R Double Mutant

Electron transfer capacity was determined by comparing the peak at 450 nm of the carbon monoxide (CO)-complex of ferrous CYP119 reduced with Pdx-PdR redox system and the control peak at 450 nm of the CO-complex CYP119 reduced with sodium dithionite using the UV-Visible spectrum. Obtained results can be observed in Table 3.10.

Table 3.10. Concentrations of CO-complexed reduced CYP119 proteins. Concentration (%) is calculated by taking the ratio of the observed CO-bound CYP119 concentration reduced with redox partners, Pdx and PdR, to the observed CO-bound CYP119 concentration obtained by samples reduced with sodium dithionite. Values are reported as the mean of duplicate determinations  $\pm$  SD.

Enzyme	Concentration ( $\mu$ M)	Concentration (%)
WT CYP119	$0.09 \pm 0.007$	6.2
N34E CYP119	0.22	11.4
D77R CYP119	$0.31 \pm 0.08$	20.4
N34E-D77R CYP119	$0.63 \pm 0.1$	45.7

Difference spectra of reduced CYP119 bound with CO can be observed in Figure 3.25.

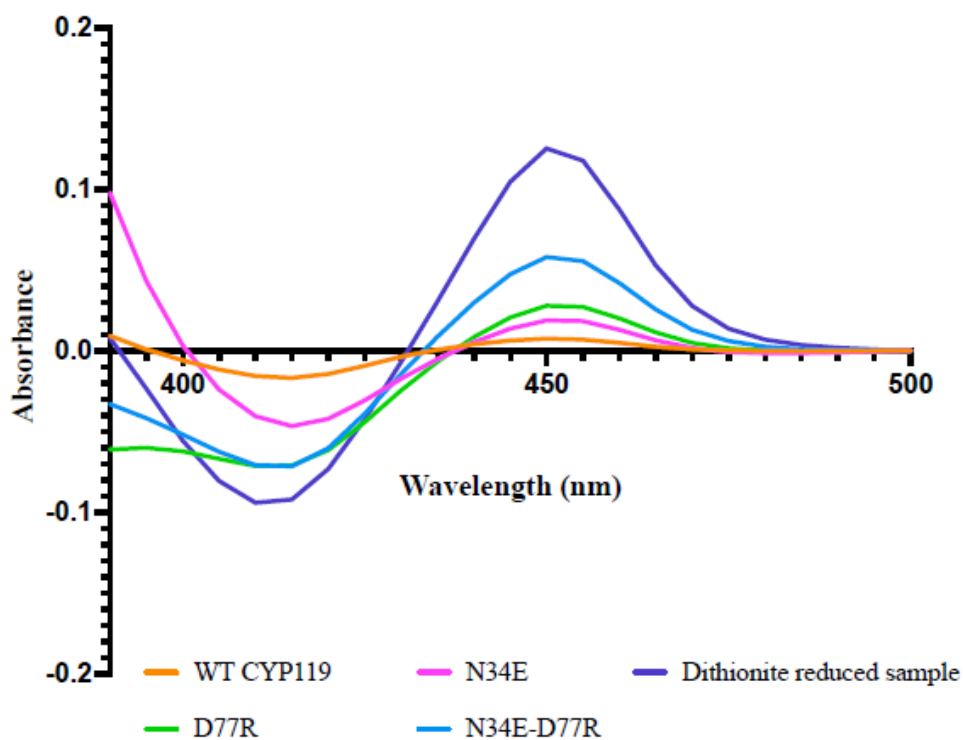


Figure 3.25. Reduced CO-bound WT and mutant CYP119s. WT (orange); N34E (pink); N34E-D77R (blue); D77R (green); Dithionite reduced sample (purple).

Carbon monoxide (CO) and the ferrous form of the heme protein bond together to form a complex that, in particular, produces a spectrum with a wavelength maximum at 450 nm. This complex is caused by the distinctive cysteine thiolate axial ligand to the heme iron in these proteins. Only the reduced (ferrous) form of P450 binds CO gas.

When WT CYP119 was reduced by Pdx-PdR redox system 6.2% of the total possible CYP119 was reduced. While in N34E CYP119 showed 11.4% recovery, whereas in D77R CYP119 20.4% and in N34E-D77R CYP119 45.7%.

## CHAPTER 4

### DISCUSSION

Cytochrome P450 enzymes are exceptional catalysts with incredible versatility. There is no other enzyme group known with such a large number of accepted substrates and catalyzed reaction types as P450s. These characteristics make P450s exclusively attractive as catalysts. Especially, thermophilic members of this superfamily, that are preferred for industrial applications, such as CYP119.

Several limitations of P450s are 1. uncoupling of an oxidation reaction without producing of desired product but consuming costly NAD(P)H; 2. The need for electron donor (NAD(P)H) in their enzymatic reactions, as well as redox partner proteins to transfer the electron from donor to the heme iron. To overcome some of these limitations, various methods are currently used according to Bernhardt and Urlacher (2014). For example, a notable enhancement in product production can be achieved by enhancing the affinity of the redox partner. As literature says (Bernhardt & Urlacher, 2014), truncation of adrenodoxin (Adx) showed 20-fold increased efficiency in formation of bovine CYP11B1-dependent hydrocortisone, enhanced activity for 3-fold in formation of CYP11B1-dependent corticosterone and furthermore conversion of CYP11A1-dependent cholesterol was improved for a 75-fold (Bernhardt & Urlacher, 2014). These impressive examples clearly demonstrate that by optimizing the redox partner affinities, it is possible to substantially increase the production of products (Bernhardt & Urlacher, 2014).

CYP119, enzyme of interest in the current research, can utilize putidaredoxin (Pdx) and putidaredoxin reductase (PdR), which are originally native redox partners for P450cam, another member of P450 family. Improved electron transfer to CYP119 from Pdx can be obtained by creating a more favorable protein-protein interaction. Similarly, the electron transfer rate can be increased by improving protein-protein relationships in a three-protein system that comprises the redox partner proteins Pdx and PdR. Such an example is D77R mutation on CYP119 made by Koo et al., (2002) that increased electron transfer rate for 5-fold compared to WT CYP119 (Koo et al., 2002). Using alignment

method of P450cam and CYP119 proteins, to increase the affinity between the enzyme and the redox partner protein Pdx. As a result, D77R mutation not only 5-fold improved the electron transfer from Pdx to CYP119 enzyme, furthermore D77R mutation did not show any impacts on the thermostability of the enzyme and  $K_s$  values of several substrates stayed the same (for example, lauric acid and styrene) (Koo et al., 2002).

On the basis of the hypothesis that Pdx binds to CYP119 at the proximal side and since CYP119 and P450cam have the high structural identity, structural alignment of these two proteins, CYP119 and P450cam, was analyzed in deep detail, especially Pdx binding regions of enzymes. Results showed that key residue in the electron transfer of P450cam-Pdx complex, Arg112 corresponds to Arg80 residue in CYP119. It's expected, that in CYP119-Pdx complex Arg80 also would play a vital role in electron transfer system, forming a salt bridge with Asp38 residue of Pdx. Alignment of two proteins CYP119 and P450cam shows that Asp77 of CYP119 corresponds to Arg109 of P450cam, which is considered as an important residue for P450cam-Pdx association. Therefore, these residues and distances between them were one of the main factors in selecting mutants for further experimental studies.

Amino acid residues of P450cam, Glu76 and Asp77 maintain connection with electropositive side of Pdx, with the Arg66 residue. These residues are important residues in P450cam-Pdx binding. Glu76 and Asp77 corresponds to Asn34 and Asn35 residues in CYP119 respectively, giving the idea to create mutations of Asn34 or Asn35 residues changing them to negatively charged residues either Glu or Asp, so they can also form salt bridge with Arg66 residue of Pdx. Surmeli Lab member, Ekin Kestevur Dogru suggested that mutation of Lys30 of CYP119 to Glu or Asp residue may interact with Arg66 of Pdx and maintain contact of two proteins.

Depending on alignment results 14 mutations in total were selected for further computational studies: N34D, N34E, N35D, N35E, K30D, K30E single mutations. As well as double mutations N34E-N35D, N34D-N35D, together with N34D-D77R, N34E-D77R, N35D-D77R, N35E-D77R, K30D-D77R, K30E-D77R, since D77R mutation already showed 5-fold increase in electron transfer rate according to Koo et al., (2002).

The two double mutants N34E-N35D and N34D-N35D were created because amino acid residues of P450cam, Glu76 and Asp77 maintain connection with electropositive side of Pdx, with Arg66 residue. These residues are important residues in P450cam-Pdx binding.

Rather than on the distal side, where substrate-binding occurs, Asn34 and Asp77 are found on the proximal surface region of the protein. Therefore, the mutations of current residues also are not anticipated to affect the lauric acid affinity of the enzyme. All residues are expected to be non-conserved and located in the surface area of binding site of CYP119 to putidaredoxin (Pdx).

PyRosetta Software was used for computational prediction and design of proteins. Prediction and design rely on the thermodynamic principle. A scoring function that employs mathematical representations of the main biophysical forces—such as Van der Waals energies, hydrogen bonds, electrostatics, etc.—as a function of configuration is used to approximate the free energy of a given structure or sequence. Created mutants were downloaded in pdb format and were visualized using UCSF Chimera. Total energy of WT CYP119 was -675.3, while total energies of mutant CYP119 ranged between -675.6 (K30E) and -706.5 (N34D-N35D), showing all mutants were, relatively to WT CYP119, more stable. Yet all mutants showed increased stability, all mutants were subjected to docking experiments with Pdx protein partner, because increasing stability of CYP119 was not main goal of the project.

Protein-protein docking of WT and mutant CYP119s with partner protein Pdx were performed using PatchDock, ClusPro, HawkDock, Prism, and ZDock servers. Servers listed above are fast and let global docking searches; however, models are not accurate at the atomic-level (Lyskov & Gray, 2008). Also, all of them don't recognize the heme group of CYP119. Therefore, RosettaDock Server was used to obtain better results. The docking findings support earlier research by demonstrating the critical role of the electrostatic forces play in protein-protein recognition and binding. The methods described here is apparent to be a promising tool to study the electron transport pathways using available computer resources.

## CHAPTER 5

### CONCLUSION

P450s are exclusively attractive as catalysts. Especially, thermophilic members of this superfamily are preferred for industrial applications, such as CYP119. Main purpose of the current project was to overcome one of several limitations that P450s have, uncoupling of an oxidation reaction without producing of desired product but consuming costly NAD(P)H.

P450 enzymes need electron donor (NAD(P)H) in their enzymatic reactions, as well as redox partner proteins to transfer the electron from the donor to heme iron. Enzyme of interest of the current project, CYP119 can utilize putidaredoxin (Pdx) and putidaredoxin reductase (PdR), which are originally native redox partner for P450cam, another member of P450 family. D77R mutation on CYP119 made by Koo et al., (2002), obtained an increased electron transfer rate of 5-fold compared to WT CYP119 by creating a more favorable protein-protein interaction in a three-protein system including putidaredoxin (Pdx) and putidaredoxin reductase (PdR) (Koo et al., 2002).

Using rational design N34E, N34E-D77R CYP119 variants were selected for increasing the affinity of CYP119 with Pdx. PyRosetta Software was used to create mutations and Rosie Docking Server was used for protein-protein docking. Site-directed mutagenesis method was applied to create N34E, N34E-D77R and D77R mutations, sequences were confirmed by BIYOMER at IZTECH. WT and mutant CYP119s were expressed and purified. Electron transfer partners Pdx and PdR were expressed and purified. Results were confirmed with SDS-PAGE analysis.

To understand if the mutations had any effect on substrate binding to CYP119, UV-spectra of samples were measured in the presence of CYP119 substrate lauric acid. Obtained results of substrate binding experiments revealed no significant difference in Soret peaks, comparing WT CYP119 and mutants. The dissociation constant ( $K_d$ ) of lauric acid for D77R mutant in current research is  $87 \pm 53 \mu\text{M}$ , while WT CYP119 showed

$19 \pm 6 \mu\text{M}$ . The dissociation constants of lauric acid to the new mutants, N34E and N34E-D77R, were  $35 \pm 19 \mu\text{M}$  and  $23 \pm 11 \mu\text{M}$  respectively.

To understand if the designed mutations resulted in increased affinity of CYP119 to Pdx, Pdx binding to WT and mutant CYP119 was investigated. The reported  $K_d$  for Pdx binding for WT and D77R CYP119 in the presence of lauric acid are  $2100 \mu\text{M}$  and  $500 \mu\text{M}$ , respectively (Koo et al., 2002); which is consistent with our observations. The  $K_d$  for Pdx binding for WT showed  $2390 \pm 224 \mu\text{M}$ , while  $112 \pm 48 \mu\text{M}$  for N34E,  $797 \pm 184 \mu\text{M}$  for D77R and  $200 \pm 31 \mu\text{M}$  for N34E-D77R. These results provide direct evidence that the N34E, N34E-D77R mutants bind to Pdx with higher affinity. Thus, the increasing binding affinity of Pdx to CYP119 was increased for 21-fold in N34E mutation and 12-fold N34E-D77R mutation, which correlates well with the 21-fold and 12-fold increase in the electron-transfer rate observed for N34E and N34E-D77R proteins, respectively, over WT CYP119. D77R mutation confirmed around 4-fold increase in binding as suggested by Koo et al., (2002).

The first electron transfer from NADH to heme center of CYP119 by Pdx through PdR acceptor was tested according to Koo et al., (2002), Morlock et al., (2018) and Nguyen et al., (2021) method (Koo et al., 2002; Morlock et al., 2018; Nguyen, 2021). In addition to being very dependent on the circumstances of the reaction, uncoupling can happen with or without a substrate. Three major ways are: 1. instead of products, a superoxide anion is formed instead of product and the enzyme returns to its resting state; 2. hydrogen peroxide is formed from dissociation of coordinated peroxide or hydroperoxide anion from the iron, thus completing the unproductive two electron reduction of oxygen; 3. uncoupling, in which the substrate is not oxygenated but rather the ferryl-oxo intermediate is oxidized to water, resulting with formation of two water molecules.

According to method of Morlock et al., (2018) simultaneously NADH consumption and hydrogen peroxide formation were followed. Hydrogen peroxide produced in the reaction was calculated in all samples and results showed that  $3.26 \pm 0.07 \mu\text{M}$ ,  $4.49 \pm 0.15 \mu\text{M}$ ,  $2.14 \pm 0.05 \mu\text{M}$ ,  $3.54 \pm 0.09 \mu\text{M}$  of hydrogen peroxide was formed in WT, N34E, N34E-D77R and D77R samples, respectively. This shows that N34E-D77R mutation almost doubled coupling efficiency.

Electron transfer capacity of enzymes was determined by comparing the peak at 450 nm of the carbon monoxide (CO)-bound CYP119 reduced with Pdx-PdR redox system and reduced with sodium dithionite. Only the reduced (ferrous) form of P450



binds CO. When WT CYP119 was reduced by the Pdx-PdR redox system 6.2% of the total possible CYP119 was reduced. While in N34E CYP119 showed 11.4% recovery, whereas in D77R CYP119 20.4% and in N34E-D77R CYP119 45.7%.

We conclude that obtained results after alignment method of the crystal structure of Pdx and the generated docked structures are feasible docking arrangements as compatible with all the currently existing data in literature. P450s recognize and bind small molecule substrates considerably differently than they bind proteins. It is anticipated that the electron transfer proteins will be attached to the P450s on flat surface from proximal face of the heme. On the other hand, the substrates bind in the protein cavity on the distal side of the heme. On the distal side of the heme, in the protein cavity, the substrates bind. Consequently, these results imply that the alignment of proteins utilized to identify the interacting surface residues and the assumption of a conserved docking region for Pdx on CYP119 were both completely appropriate. These findings are confirmed by the dissociation constants for Pdx's binding to CYP119, which additionally demonstrate that the N34E and N34E-D77R mutants bind to Pdx with greater affinity.

This project provides an engineered novel cytochrome P450 enzyme, CYP119, to be employed in three-protein system, including redox partner proteins, putidaredoxin (Pdx) and putidaredoxin reductase (PdR). P450s are promising biocatalyst that catalyze the oxidation of vast range of substrates in a stereoselective and regioselective manner. CYP119 is a thermophilic member of the superfamily, its N34E and N34E-D77R mutants provide higher affinity to Pdx, thus increasing the electron transfer rate from electron donor, NADH, to the heme cofactor of CYP119. This is an important development for industrial applications, because P450s are vastly used in synthesis of drugs, such as progesterone, cortisone, pravastatin, artemisinic acid, synthesis of steroids, synthesis of agrochemicals, as well as the antibiotics manufacture, such as erythromycin and tetracenomycin.

## REFERENCES

- Aoki Masaaki, Ishimori Koichiro, & Morishima Isao. 1998. "Roles of negatively charged surface residues of putidaredoxin in interactions with redox partners in P450cam monooxygenase system." *Biochimica et Biophysica Acta - Protein Structure and Molecular Enzymology* 1386(1): 157–167. [https://doi.org/10.1016/S0167-4838\(98\)00094-6](https://doi.org/10.1016/S0167-4838(98)00094-6)
- Aoki Masaaki, Ishimori Koichiro, Morishima Isao & Yoshinao Wada. 1998. "Roles of valine-98 and glutamic acid-72 of putidaredoxin in the electron transfer complexes with NADH-putidaredoxin reductase and P450cam." *Inorganica Chimica Acta* 272(1): 80-88. [https://doi.org/10.1016/s0020-1693\(97\)05946-x](https://doi.org/10.1016/s0020-1693(97)05946-x)
- Başlar M. Semih. 2019. "Directed evolution of a Cytochrome P450 enzyme to increase peroxidation activity." [Master Degree Thesis, Izmir Institute of Technology]. <https://grcris.iyte.edu.tr/handle/11147/10929>
- Başlar M. Semih, Sakallı Tuğçe, Güralp Gülce, Kestevur Doğru Ekin, Haklı Emre, & Surmeli Nur Başak. 2020. "Development of an improved Amplex Red peroxidation activity assay for screening cytochrome P450 variants and identification of a novel mutant of the thermophilic CYP119." *Journal of Biological Inorganic Chemistry* 25(7): 949–962. <https://doi.org/10.1007/s00775-020-01816-w>
- Baspınar Alper, Cukuroglu Engin, Nussinov Ruth, Keskin Ozlem, & Gursoy Attila. 2014. "PRISM: a web server and repository for prediction of protein – protein interactions and modeling their 3D complexes." *Nucleic acids Research* 42(5): 285–289. <https://doi.org/10.1093/nar/gku397>
- Bernhardt Rita. 2006. "Cytochromes P450 as versatile biocatalysts." *Journal of Biotechnology* 124(1): 128–145. <https://doi.org/10.1016/j.jbiotec.2006.01.026>
- Bernhardt Rita, & Urlacher B. Vlada. 2014. "Cytochromes P450 as promising catalysts for biotechnological application: Chances and limitations." *Applied Microbiology and Biotechnology* 98(14): 6185–6203. <https://doi.org/10.1007/s00253-014-5767-7>
- Blair Emek, Greaves John, & Farmer J. Patrick. 2004. "High-temperature electrocatalysis using thermophilic P450 CYP119: Dehalogenation of CCl<sub>4</sub> to CH<sub>4</sub>." *Journal of*

*the American Chemical Society*, 126(28): 8632–8633.  
<https://doi.org/10.1021/ja0488333>

- Bornscheuer T. Uwe, & Pohl Martina. 2001. "Improved biocatalysts by directed evolution and rational protein design." *Current Opinion in Chemical Biology* 2001(5): 137–143. [https://doi.org/10.1016/s1367-5931\(00\)00182-4](https://doi.org/10.1016/s1367-5931(00)00182-4)
- Chang Yang-Tyng, & Loew Gilda. 2000. "Homology modeling, molecular dynamics simulations, and analysis of CYP119, a P450 enzyme from extreme acidothermophilic archaeon *Sulfolobus solfataricus*." *Biochemistry* 39(10): 2484–2498. <https://doi.org/10.1021/bi991966u>
- Chaudhury Sidhartha, Berrondo Monica, Weitzner D. Brian, Muthu Pravin, Bergman Hannah, & Gray, J. Jeffrey. 2011. Benchmarking and analysis of protein docking performance in Rosetta v3.2. *PLoS ONE* 6(8): 1-13  
<https://doi.org/10.1371/journal.pone.0022477>
- Chaudhury Sidhartha, Lyskov Sergey, & Gray, J. Jeffrey. 2010. "PyRosetta : a script-based interface for implementing molecular modeling algorithms using Rosetta." *Bioinformatics* 26(5): 689–691. <https://doi.org/10.1093/bioinformatics/btq007>
- Chen Hui, Lin Yao, Long, Yi Tao, Minter D. Shelley, & Ying, Yi-Lun. 2021. "Nanopore-based measurement of the interaction of P450cam monooxygenase and putidaredoxin at the single-molecule level." *Faraday Discussions* 233(1): 295–302. <https://doi.org/10.1039/d1fd00042j>
- Colyer John, & Walker M. John 1996. "Protein Handbook Second Edition." <https://link.springer.com/book/10.1385/1592591698?page=5#about-this-book>
- Dalby A. Paul 2011. "Strategy and success for the directed evolution of enzymes." *Current Opinion in Structural Biology* 21(4): 473–480. <https://doi.org/10.1016/j.sbi.2011.05.003>
- Davis W. Ian, & Baker David 2009. "Rosetta Ligand Docking with Full Ligand and Receptor Flexibility." *Journal of Molecular Biology* 385(2): 381–392. <https://doi.org/10.1016/j.jmb.2008.11.010>
- Denisov G. Ilia, Hung Shao-Ching, Weiss E. Kara, McLean A. Mark, Shiro Yoshitsugu, Park Sam-Yong, Champion M. Paul, & Sligar G. Stephen. 2001. "Characterization of the oxygenated intermediate of the thermophilic cytochrome P450 CYP119." *Journal of Inorganic Biochemistry* 87(4): 215–226.

[https://doi.org/10.1016/S0162-0134\(01\)00328-2](https://doi.org/10.1016/S0162-0134(01)00328-2)

- Denisov G. Ilya, Makris M. Thomas, Sligar G. Stephen, & Schlichting Ilme. 2005. "Structure and chemistry of cytochrome P450." *Chemical Reviews* 105(6): 2253–2277. <https://doi.org/10.1021/cr0307143>
- Donova V. Marina, Nikolayeva M. Vera, Dovbnaya V. Dmitry, Gulevskaya A. Seraphima, & Suzina E. Natalia. 2007. "Methyl- $\beta$ -cyclodextrin alters growth, activity and cell envelop features of sterol-transforming mycobacteria." *Microbiology* 153(6): 1981–1992. <https://doi.org/10.1099/mic.0.2006/001636-0>
- Goddard D. Thomas, Huang C. Conrad & Ferrin E. Thomas. 2005. "Software Extensions to UCSF Chimera for Interactive Visualization of Large Molecular Assemblies." *Structure* 13(1): 473–482. <https://doi.org/10.1016/j.str.2005.01.006>
- Goldstone V. Jared, McArthur G. Andrew, Kubota Akira, Zanette Juliano, Parente Tiago, Jönsson E. Maria, Nelson R. David, & Stegeman J. John. 2010. "Identification and developmental expression of the full complement of Cytochrome P450 genes in Zebrafish." *BMC Genomics* 11(1): 643-647. <https://doi.org/10.1186/1471-2164-11-643>
- Gromiha M. Michael. 2019. "Protein Structural Bioinformatics: An Overview." *Encyclopedia of Bioinformatics and Computational biology* 2(1): 445–459. <https://doi.org/10.1016/B978-0-12-809633-8.20278-1>
- Guengerich F. Peter. 2007. "Mechanisms of Cytochrome P450 Substrate Oxidation: MiniReview." *Biochem Molecular Toxicology* 21(4): 163-168. <https://doi.org/10.1002/jbt>
- Guengerich F. Peter. 2009. "Measurement of cytochrome P450 and NADPH-cytochrome P450 reductase." *Nature Protocols* 24(4): 1245-1251. <https://doi.org/10.1038/nprot.2009.121>.
- Guengerich F. Peter. 2018. "Mechanisms of Cytochrome P450-Catalyzed Oxidations." *ACS Catal.* 8 (12): 10964-10976. <https://doi.org/10.1021/acscatal.8b03401>
- Hannemann Frank, Bichet Andreas, Ewen M. Kerstin, & Bernhardt Rita. 2007a. "Cytochrome P450 systems-biological variations of electron transport chains." *Biochimica et Biophysica Acta - General Subjects*, 1770(3): 330–344. <https://doi.org/10.1016/j.bbagen.2006.07.017>

- Hannemann Frank, Bichet Andreas, Ewen M. Kerstin, & Bernhardt Rita. 2007b. "Cytochrome P450 systems — biological variations of electron transport chains." *Biochimica et Biophysica Acta - General Subjects* 1770(3): 330–344. <https://doi.org/10.1016/j.bbagen.2006.07.017>
- Harford-Cross F. Charles, Carmichael B. Angus, Allan K. Fiona, England A. Paul, Rouch A. Duncan, & Wong Luet-Lok. 2000. "Protein engineering of cytochrome P458(cam) (CYP101) for the oxidation of polycyclic aromatic hydrocarbons." *Protein Engineering, Design and Selection* 13(2): 121–128. <https://doi.org/10.1093/protein/13.2.121>
- Hawkes B. David, Adams W. Gregory, Burlingame L. Alma, Ortiz de Montellano R. Paul & De Voss J. James. 2002. "Cytochrome P450cin (CYP176A), Isolation, Expression and Characterization." *Journal of Biological Chemistry* 277(31): 27725–27732. <https://doi.org/10.1074/jbc.M203382200>
- Hirakawa Hidehiko, & Nagamune Teruyuki. 2010. "Molecular Assembly of P450 with Ferredoxin and Ferredoxin Reductase by Fusion to PCNA." *ChemBioChem* 11(11): 1517–1520. <https://doi.org/10.1002/cbic.201000226>
- Hiroi Toyoko, Kishimoto Wataru, Chow Toshio, Imaoka Susumi. 2001. "Progesterone Oxidation by Cytochrome P450 2D Isoforms in the Brain." *Endocrinology* 142(9): 3901–3908. <https://doi.org/10.1210/endo.142.9.8363>
- Hiruma Yoshitaka, Hass A. S. Mathias, Kikui Yuki, Liu Wei-Min, Ölmez Betül, Skinner P. Simon, Blok Anneloes, Kloosterman Alexander, Koteishi Hiroyasu, Löhr Frank, Schwalbe Harald, Nojiri Masaki, & Ubbink Marcellus. 2013. "The Structure of the Cytochrome P450cam – Putidaredoxin Complex Determined by Paramagnetic NMR Spectroscopy and Crystallography." *Journal of Molecular Biology* 425(22): 4353–4365. <https://doi.org/10.1016/j.jmb.2013.07.006>
- Hogrefe H. Holly, Cline Janice, Youngblood L. Geri, & Allen M. Ronda. 2002. "Creating randomized amino acid libraries with the Quikchange® multi site-directed mutagenesis kit." *BioTechniques* 33(5): 1158–1165. <https://doi.org/10.2144/02335pf01>
- Itoh Aya, & Howe A. Gregg. 2001. "Molecular Cloning of a Divinyl Ether Synthase." *The Journal of Biological Chemistry* 276(5): 3620–3627. <https://doi.org/10.1074/jbc.M008964200>
- Jackson J. Colin, Lamb C. David, Marczylo H. Timothy, Warrilow G. S. Andrew, Manning J. Nigel, Lowe J. David, Kelly E. Diane, & Kelly L. Steven. 2002. "A

Novel Sterol 14 $\alpha$  -Demethylase / Ferredoxin Fusion Protein ( MCCYP51FX ) from *Methylococcus capsulatus* Represents a New Class of the Cytochrome P450 Superfamily." *Journal of Biological Chemistry* 277(49): 46959–46965. <https://doi.org/10.1074/jbc.M203523200>

Jiang Hualin, Li Xueqin, Li Menglin, Niu Pingping, Wang Tao, Chen Dezhi, Chen Pinghua, & Zou Jian-Ping. 2019. "A new strategy for triggering photocatalytic activity of Cytochrome P450 by coupling of semiconductors." *Chemical Engineering Journal* 358(1): 58–66. <https://doi.org/10.1016/j.cej.2018.09.199>

Kemper Byron. 2004. "Structural basis for the role in protein folding of conserved proline-rich regions in cytochromes P450." *Toxicology and Applied Pharmacology* 199(3): 305–315. <https://doi.org/10.1016/j.taap.2003.11.030>

Kestevur Doğru Ekin 2019. "Bioinformatics Based Approach To Design a Thermophilic P450 for Industrial Biocatalysis." [Master Degree Thesis, Izmir Institute of Technology]. <https://gcris.iyte.edu.tr/handle/11147/10934>

Kim Donghak, Cha Gun-Su, Nagy D. Leslie, Yun Chul-Ho, & Guengerich F. Peter. 2014. "Kinetic analysis of lauric acid hydroxylation by human cytochrome P450 4A11." *Biochemistry* 53(39): 6161–6172. <https://doi.org/10.1021/bi500710e>

Koga Hideo, Sagaraa Yasuhiro, Yaoi Tsuyoshi, Tsujimura Mitsushi, Nakamura Kazuhide, Sekimizu Kazuhisa, Makinob Ryu, Shimada Hideo, Ishimura Yazuru., Yura Kei, Go Mitiko, Ikeguchi Masamichi, & Horiuchi Tadao. 1993. "Essential role of the Arg112 residue of cytochrome P450cam for electron transfer from reduced putidaredoxin." *FEBS letters* 331(1): 109–113. [https://doi.org/10.1016/0014-5793\(93\)80307-g](https://doi.org/10.1016/0014-5793(93)80307-g)

Koo S. Laura, Immoos E. Chad, Cohen S. Michael, Farmer J. Patrick, & Ortiz de Montellano R. Paul. 2002. "Enhanced electron transfer and lauric acid hydroxylation by site-directed mutagenesis of CYP119." *Journal of the American Chemical Society* 124(20): 5684–5691. <https://doi.org/10.1021/ja017174g>

Koo S. Laura, Tschirret-Guth A. Richard, Straub E. Wesley, Moënne-Loccoz Pierre, Loehr M. Thomas, & Ortiz De Montellano R. Paul. 2000. "The active site of the thermophilic CYP119 from *Sulfolobus solfataricus*." *Journal of Biological Chemistry* 275(19): 14112–14123. <https://doi.org/10.1074/jbc.275.19.14112>

Kozakov Dima, Hall R. David, Xia Bing, Porter A. Kathryn, Padhorny Dzmity, Yueh Cristine, Beglov Dmitri & Vajda Sandor. 2018. "The clusPro web server for protein-protein docking." *Nature protocols* 12(2): 255–278.

<https://doi.org/10.1038/nprot.2016.169>

- Krest M. Courtney, Onderko L. Elizabeth, Yosca H. Timothy, Calixto C. Julio, Karp F. Richard, Livada Jovan, Rittle Jonathan, & Green T. Michael. 2013. "Reactive intermediates in cytochrome P450 catalysis." *Journal of Biological Chemistry* 288(24): 17074–17081. <https://doi.org/10.1074/jbc.R113.473108>
- Kumar Santosh. 2010. "Engineering cytochrome P450 biocatalysts for biotechnology, medicine and bioremediation." *Expert Opinion on Drug Metabolism and Toxicology* 6(2): 115–131. <https://doi.org/10.1517/17425250903431040>
- Le H. Kathy, Adolf-bryfogle Jared, Klima C. Jason, Lyskov Sergey, Labonte Jason, Bertolani Steven, Burman Sourya Roy, Leaver-Fay Andrew, Weitzner Brian, Nance, Morgan, Das Rhiju, Dunbrack Roland, Schief William, & Kuhlman Brian. 2021. "PyRosetta Jupyter Notebooks Teach Biomolecular Structure Prediction and design." *Biophysicist* 2(1): 108–122. <https://doi.org/10.35459/tbp.2019.000147>
- Leaver-Fay Andrew, Tyka Michael, Lewis M. Steven, Lange F. Oliver, Jacak Ron, Kaufman Kristian, Renfrew P. Douglas, Smith A. Colin, Davis W. Ian, Cooper Seth, Treuille Adrian, Mandell J. Daniel, Ban Y. Andrew, Fleishman J. Sarel, Corn E. Jacob, & Kim E. David. 2011. "ROSETTA3: an object-oriented software suite for the simulation and design of macromolecules." *Methods in Enzymology* 487(1): 545–574. <https://doi.org/10.1016/B978-0-12-381270-4.00019-6>.
- Lewis F. V. David, & Pratt M. John. 1998. "The P450 catalytic cycle and oxygenation mechanism." *Drug Metabolism Reviews* 30(4): 739–786. <https://doi.org/10.3109/03602539808996329>
- Li Shengying, Du Lei, Bernhardt Rita. 2020. "Redox Partners: Function Modulators of Bacterial P450 Enzymes." *Trends in Microbiology* 28(6): 445–454. <https://doi.org/10.1016/j.tim.2020.02.012>
- Li Yougen, Drummond D. Allan, Sawayama M. Andrew, Snow D. Christopher, Bloom D. Jesse, & Arnold H. Frances. 2007. "A diverse family of thermostable cytochrome P450s created by recombination of stabilizing fragments." *Nature Biotechnology* 25(9): 1051–1056. <https://doi.org/10.1038/nbt1333>
- Liu Hong-ming, Yuan Meng, Liu Ai-min, Ren Lei, Zhu Guo-ping, & Sun Li-na. 2021. "A bifunctional enzyme belonging to cytochrome P450 family involved in the O - dealkylation and N - dealkoxymethylation toward chloroacetanilide herbicides

in *Rhodococcus* sp.B2." *Microbial Cell Factories* 20(61): 1–13.  
<https://doi.org/10.1186/s12934-021-01544-z>

Liu Zhuo, Lemmonds Sara, Huang Juan, Tyagi Madhusudan, Hong Liang, & Jain Nitin. 2018. "Entropic contribution to enhanced thermal stability in the thermostable P450 CYP119." *Proceedings of the National Academy of Sciences of the United States of America* 115(43): E10049–E10058. <https://doi.org/10.1073/pnas.1807473115>

Luthra Abhinav, Denisov G. Iliia, & Sligar G. Stephen. 2011. "Temperature Derivative Spectroscopy to monitor the autoxidation decay of Cytochromes P450." *Analytical Chemistry* 83(13): 5394–5399. <https://doi.org/10.1021/ac2009349>

Lutz Stefan. 2010. "Beyond directed evolution-semi-rational protein engineering and design." *Current Opinion in Biotechnology* 21(6): 734–743. <https://doi.org/10.1016/j.copbio.2010.08.011>

Lyskov Sergey, & Gray J. Jeffrey. 2008. "The RosettaDock server for local protein-protein docking." *Nucleic Acids Research* 36(2): W233–W238. <https://doi.org/10.1093/nar/gkn216>

Lyskov Sergey, Weitzner D. Brian & Gray J. Jeffrey. 2011. "Real-Time PyMOL Visualization for Rosetta and PyRosetta." *Plos One* 6(8): e21931. <https://doi.org/10.1371/journal.pone.0021931>.

Marshall A Shannon, Lazar A. Greg, Chirino J. Arthur, Desjarlais R. John. 2010. "Rational design and engineering of therapeutic proteins." *Drug Discovery Today* 8(5): 212–221. [https://doi.org/10.1016/s1359-6446\(03\)02610-2](https://doi.org/10.1016/s1359-6446(03)02610-2)

Mashiach Efrat, Schneidman-Duhovny Dina, Andrusier Nelly, Nussinov Ruth & Wolfson J. Haim. 2008. "FireDock : a web server for fast interaction refinement in molecular docking" *Nucleic acids Research* 36(2): 229–232. <https://doi.org/10.1093/nar/gkn186>

Maves A. Shelley, & Sligar G. Stephen. 2001. "Understanding thermostability in cytochrome P450 by combinatorial mutagenesis." *Protein Science* 10(1): 161–168. <https://doi.org/10.1110/ps.17601>

McDonnel Anne. 2013. "Basic Review of the Cytochrome P450 System." *Journal of the Advanced Practitioner in Oncology* 4(4): 263-268. <https://doi.org/10.6004/jadpro.2013.4.4.7>



- McIntosh A. John, Farwell C. Christopher, & Arnold H. Frances. 2014. "Expanding P450 catalytic reaction space through evolution and engineering." *Current Opinion in Chemical Biology* 19(1): 126–134. <https://doi.org/10.1016/j.cbpa.2014.02.001>
- McLean J. Kristy, Luciakova Dominika, Belcher James, Tee L. Kang, & Munro W. Andrew. 2015. "Biological diversity of cytochrome P450 redox partner systems." *Advances in Experimental Medicine and Biology* 851(1): 299–317. [https://doi.org/10.1007/978-3-319-16009-2\\_11](https://doi.org/10.1007/978-3-319-16009-2_11)
- Meunier Bernard, De Visser P. Samuel, & Shaik Sason. 2004. "Mechanism of oxidation reactions catalyzed by cytochrome P450 enzymes." *Chemical Reviews* 104(9): 3947–3980. <https://doi.org/10.1021/cr020443g>
- Michizoe Junji, Ichinose Hirofumi, Kamiya Noriho, Maruyama Tatsuo & Goto Masahiro. 2005. "Functionalization of the cytochrome P450cam monooxygenase system in the cell-like aqueous compartments of water-in-oil emulsions." *Journal of Bioscience and Bioengineering* 99(1): 12–17. <https://doi.org/10.1263/jbb.99.12>
- Miller C. Justin, Lee J. H. Zoel, Mclean A. Mark, Chao R. Rebecca, Stone S. J. Isabella, Pukala L. Tara, Bruning B. John, De Voss J. James, Schuler A. Mary, Sligar G. Stephen, & Bell G. Stephen. 2023. "Engineering C-C Bond Cleavage Activity into a P450 Monooxygenase Enzyme." *Journal of the American Chemical Society* 145(16): 9207–9222. <https://doi.org/10.1021/jacs.3c01456>
- Modi R. Anuja, & Dawson H. John. 2015. "Oxidizing intermediates in P450 catalysis: A case for multiple oxidants." *Advances in Experimental Medicine and Biology*, 851(1): 63–81. [https://doi.org/10.1007/978-3-319-16009-2\\_2](https://doi.org/10.1007/978-3-319-16009-2_2)
- Morlock Kristin Lisa. 2018. "Investigation on the general activity and uncoupling of the catalytic cycle of different Cytochrome P450 monooxygenases." [PhD thesis, Ernst-Moritz-Arndt-Universität Greifswald]. <https://epub.uni-greifswald.de/frontdoor/index/index/year/2018/docId/2338>
- Morlock Lisa Kristin, Böttcher Dominique, & Bornscheuer T. Uwe. 2018. "Simultaneous detection of NADPH consumption and H<sub>2</sub>O<sub>2</sub> production using the Ampliflu™ Red assay for screening of P450 activities and uncoupling." *Applied Microbiology and Biotechnology* 102(2): 985–994. <https://doi.org/10.1007/s00253-017-8636-3>
- Nagano Shingo, Shimada Hideo, Tarumi Akiko, Hishiki Takako, Kimata-Arigo Yoko, Egawa Tsuyoshi, Suematsu Makoto, Park Sam-Yong, Adachi Shin-Ichi, Shiro Yoshitsugu, & Ishimura Yuzuru. 2003. "Infrared Spectroscopic and Mutational Studies on Putidaredoxin-Induced Conformational Changes in Ferrous CO-

P450cam." *Biochemistry* 42(49): 14507–14514.  
<https://doi.org/10.1021/bi035410p>

- Nair C. Pramod, McKinnon A. Ross, & Miners O. John. 2016. "Cytochrome P450 structure–function: insights from molecular dynamics simulations." *Drug Metabolism Reviews* 48(3): 434–452. <https://doi.org/10.1080/03602532.2016.1178771>
- Nakahara Kazuhiko, Tanimoto Tatsuo, Hatano Ken-ichi, Usuda Koji, & Shoun Hirofumi. 1993. "Cytochrome P-450 55A1 (P-450dNIR) acts as nitric oxide reductase employing NADH as the direct electron donor." *Journal of Biological Chemistry* 268(11): 8350–8355. [https://doi.org/10.1016/S0021-9258\(18\)53102-1](https://doi.org/10.1016/S0021-9258(18)53102-1)
- Nelson R. David. 2009. "The cytochrome P450 homepage." *Human Genomics* 4(1): 59–65. <https://doi.org/10.1186/1479-7364-4-1-59>
- Ngcobo Phelelani Erick, Nkosi Bridget Valeria Zinhle, Chen Wanping, Nelson R. David, & Syed Khajamohiddin. 2023. "Evolution of Cytochrome P450 Enzymes and Their Redox Partners in Archaea." *International Journal of Molecular Sciences* 24(4): 4161–4167 <https://doi.org/10.3390/ijms24044161>
- Nguyen Kim-Thoa, Ngoc-Lan Nguyen, Mohammed Milhim, Van-Tung Nguyen, Thi-Hong-Nhung Lai, Huy-Hoang Nguyen, Thi-Thanh-Xuan Le, Thi-Tuyet-Minh Phan, Rita Bernhardt. 2021. "Characterization of a thermophilic cytochrome P450 of the CYP203A subfamily from Binh Chau hot spring in Vietnam" *FEBS Open Bio* 11(1): 124–132. <https://doi.org/10.1002/2211-5463.13033>
- Niemeyer M. Christof, Rabe S. Kresten. 2008. "Characterization of the Peroxidase Activity of CYP119 , a Thermostable P450 From *Sulfolobus acidocaldarius*." *ChemBioChem* 9(3): 420–425. <https://doi.org/10.1002/cbic.200700450>
- Nishida R. Clinton, & Ortiz De Montellano R. Paul. 2005. "Thermophilic cytochrome P450 enzymes." *Biochemical and Biophysical Research Communications* 338(1): 437–445. <https://doi.org/10.1016/j.bbrc.2005.08.093>
- Ortiz de Montellano R. Paul. 2003. "Aromatic stacking as a determinant of the thermal stability of CYP119 from *Sulfolobus solfataricus*." *Archives of Biochemistry and Biophysics* 409(1): 52–58. [https://doi.org/10.1016/S0003-9861\(02\)00402-2](https://doi.org/10.1016/S0003-9861(02)00402-2)
- Ortiz De Montellano R. Paul. 2004. "Cytochrome P450: Structure, Mechanism, and Biochemistry (third edition)." *Springer* New York.

<https://doi.org/10.1007/b139087>

- Paine F. Mary, Hart L. Heather, Ludington S. Shana, Haining L. Robert, Rettie E. Allan & Zeldin C. Darryl. 2006. "The human intestinal cytochrome P450 "pie"." *Drug Metabolism and Disposition* 34(5): 880–886. <https://doi.org/10.1124/dmd.105.008672>
- Park Sam-Yong, Yamane Kazuhide, Adachi Shin-Ichi, Shiro Yoshitsugu., Weiss E. Kara, Maves A. Shelley, & Sligar G. Stephen. 2002. "Thermophilic cytochrome P450 (CYP119) from *Sulfolobus solfataricus*: High resolution structure and functional properties." *Journal of Inorganic Biochemistry* 91(4): 491–501. [https://doi.org/10.1016/S0162-0134\(02\)00446-4](https://doi.org/10.1016/S0162-0134(02)00446-4)
- Peterson A. Julian, Lorence C. Matthew, & Amarneh Bilal. 1990. "Putidaredoxin reductase and putidaredoxin: Cloning, sequence determination, and heterologous expression of the proteins." *Journal of Biological Chemistry* 265(11): 6066–6073. [https://doi.org/10.1016/s0021-9258\(19\)39292-0](https://doi.org/10.1016/s0021-9258(19)39292-0)
- Pettersen F. Eric, Goddard D. Thomas, Huang C. Conrad, Couch S. Gregory, Greenblatt M. Daniel, Meng C. Elaine, & Ferrin E. Thomas. 2004. "UCSF Chimera — A Visualization System for Exploratory Research and Analysis." *Journal of Computational Chemistry* 25(13): 1605-1612. <https://doi.org/10.1002/jcc.20084>
- Pierce G. Brian, Wiehe Kevin, Hwang Howook, Kim Bong-Hyun., Vreven Thom & Weng Zhiping. 2014. "Structural bioinformatics ZDOCK server: interactive docking prediction of protein – protein complexes and symmetric multimers." *Bioinformatics* 30(12): 1771–1773. <https://doi.org/10.1093/bioinformatics/btu097>
- Pochapsky C. Thomas. 1996. "A structure-based model for cytochrome P450 am-pufidaredoxin interactions." *Biochimie* 78(9): 723–733. [https://doi.org/10.1016/s0300-9084\(97\)82530-8](https://doi.org/10.1016/s0300-9084(97)82530-8)
- Pochapsky S. Susan, Pochapsky C. Thomas, & Wei W. Julie. 2003. "A Model for Effector Activity in a Highly Specific Biological Electron Transfer Complex: The Cytochrome P450 cam - Putidaredoxin Couple" *Biochemistry* 42(19): 5649–5656. <https://doi.org/10.1021/bi034263s>
- Poulos L. Thomas, & Johnson F. Eric. 2015. "Structures of cytochrome P450 enzymes." *Cytochrome P450: Structure, Mechanism, and Biochemistry, Fourth Edition* 3–32. [https://doi.org/10.1007/978-3-319-12108-6\\_1](https://doi.org/10.1007/978-3-319-12108-6_1)

- Puchkaev V. Andrei, & Ortiz De Montellano R. Paul. 2005. "The *Sulfolobus solfataricus* electron donor partners of thermophilic CYP119: An unusual non-NAD(P)H-dependent cytochrome P450 system." *Archives of Biochemistry and Biophysics* 434(1): 169–177. <https://doi.org/10.1016/j.abb.2004.10.022>
- Ro Dae-Kyun, Eric M. Paradise, Mario Ouellet, Karl J. Fisher, Karyn L. Newman, John M. Dingu, Kimberly A. Ho, Rachel A. Eachus, Timothy S. Ham, James Kirby, Michelle C. Y. Chang, Sydnor T. Withers, Yoichiro Shiba, Richmond Sarpong & Jay D. Keasling. 2006. "Production of the antimalarial drug precursor artemisinic acid in engineered yeast." *Nature* 440(1): 940-943. <https://doi.org/10.1038/nature04640>
- Roitberg E. Adrian, Holden J. Marcia, Mayhew P. Martin, Kurnikov V. Igor, Beratan N. David, & Vilker L. Vincent. 1998. "Binding and Electron Transfer between Putidaredoxin and Cytochrome P450cam. Theory and Experiments." *Journal of American Chemical Society* 120(35): 8927–8932. <https://doi.org/10.1021/ja9739906>
- Sakaki Tosiya. 2012. "Practical application of cytochrome P450." *Biological and Pharmaceutical Bulletin* 35(6): 844–849. <https://doi.org/10.1248/bpb.35.844>
- Sakalli Tuğçe 2020. "Characterization of designed novel Cytochrome P450 for industrial biocatalysis" [Master Degree Thesis, Izmir Institute of Technology]. <https://grcris.iyte.edu.tr/handle/11147/11099>
- Sato Ryo, Omura Tsuneo. 1964. "The Carbon Monoxide Binding Pigment of Liver Microsome; Solubilization, Purification, and properties" *Journal of Biological Chemistry* 239(7): 2379–2385. [https://doi.org/10.1016/S0021-9258\(20\)82245-5](https://doi.org/10.1016/S0021-9258(20)82245-5)
- Schneidman-Duhovny Dina, Inbar Yuval, Nussinov Ruth, & Wolfson J. Haim. 2005. "PatchDock and SymmDock : servers for rigid and symmetric docking." *Nucleic Acids Research* 33(2): 363–367. <https://doi.org/10.1093/nar/gki481>
- Serizawa Nobufusa, Tatsuji Matsuoka, Shunichi Miyakoshi, Kazuhiko Tanzawa, Kaori Nakahara, Masahiko Hosobuchi. 1989. "Purification and characterization of cytochrome P450sca from *Streptomyces carbophilus*." *FEBS* 184(3): 707-713. <https://doi.org/10.1111/j.1432-1033.1989.tb15070.x>
- Sevrioukova F. Irina, Poulos L. Thomas, Kuznetsov Vadim. 2006. "Putidaredoxin-to-Cytochrome P450cam Electron Transfer: Differences Between the Two Reductive Steps Required for Catalysis." *Biochemistry* 45(39): 11934-11944. <https://doi.org/10.1021/bi0611154>

- Sevrioukova F. Irina, Garcia Carlos, Li Huiying, Bhaskar Bharatheeswaran., & Poulos L. Thomas. 2003. "Crystal structure of putidaredoxin, the [2Fe-2S] component of the P450cam monooxygenase system from *Pseudomonas putida*." *Journal of Molecular Biology* 333(2): 377–392. <https://doi.org/10.1016/j.jmb.2003.08.028>
- Sevrioukova F. Irina, Hazzard T. James, Tollin Gordon & Poulos L. Thomas. 2001. "Laser flash induced electron transfer in P450cam monooxygenase: Putidaredoxin reductase - Putidaredoxin interaction." *Biochemistry* 40(35): 10592–10600. <https://doi.org/10.1021/bi010874d>
- Sevrioukova F. Irina, Li Huiying, & Poulos L. Thomas. 2004. "Crystal Structure of Putidaredoxin Reductase from *Pseudomonas putida*, the Final Structural Component of the Cytochrome P450cam Monooxygenase." *Journal of Molecular Biology* 336(4): 889–902. <https://doi.org/10.1016/j.jmb.2003.12.067>
- Sevrioukova F. Irina, & Poulos L. Thomas. 2002. "Putidaredoxin Reductase , a New Function for an Old Protein\*." *Journal of Biological Chemistry* 277(28): 25831–25839. <https://doi.org/10.1074/jbc.M201110200>
- Sevrioukova F. Irina, & Poulos L. Thomas. 2011. "Structural biology of redox partner interactions in P450cam monooxygenase: A fresh look at an old system." *Archives of Biochemistry and Biophysics* 507(1): 66–74. <https://doi.org/10.1016/j.abb.2010.08.022>
- Sevrioukova F. Irina, Poulos L. Thomas, & Churbanova Y. Inna. 2010. "Crystal Structure of the Putidaredoxin Reductase-Putidaredoxin Electron Transfer Complex" *Protein Structure and Folding* 285(18): 13616–13620. <https://doi.org/10.1074/jbc.M110.104968>
- Shaik Sason & Dubey Dutta Kshatresh. 2021. "The catalytic cycle of cytochrome P450: a fascinating choreography." *Trends in Chemistry* 3(12): 1027–1044. <https://doi.org/10.1016/j.trechm.2021.09.004>
- Sheng Xin, John H. Horner, Martin Newcomb. 2008. "Spectra and Kinetics Studies of the Compound I derivative of Cytochrome P450 119" *Journal of American Chem Soc.* 130(40): 13310–13320. doi:10.1021/ja802652b
- Shimada Hideo, Nagano Shingo, Hori Hiroshi & Ishimura Yuzuru. 2000. "Putidaredoxin – cytochrome P450cam interaction." *Journal of Inorganic Chemistry* 83(4): 255–260. [https://doi.org/10.1016/s0162-0134\(00\)00173-2](https://doi.org/10.1016/s0162-0134(00)00173-2). PMID: 11293545

- Shoji Osami, & Watanabe Yoshihito. 2014. "Peroxygenase reactions catalyzed by cytochromes P450" *Journal of Biological Inorganic Chemistry* 19(4–5): 529–539. <https://doi.org/10.1007/s00775-014-1106-9>
- Sibbesen Ole, De Voss J. James, & Ortiz de Montellano R. Paul. 1996. "Putidaredoxin reductase-putidaredoxin-cytochrome P450(cam) triple fusion protein. Construction of a self-sufficient *Escherichia coli* catalytic system." *Journal of Biological Chemistry* 271(37): 22462–22469. <https://doi.org/10.1074/jbc.271.37.22462>
- Sligar G. Stephen. 1989. "Putidaredoxin competitively inhibits cytochrome b5-cytochrome P450cam association: A Proposed Molecular Model for a Cytochrome P450cam. electron transfer complex." *Biochemistry* 28(20): 8201–8205. <https://doi.org/10.1021/bi00446a035>
- Stresser M. David. 2021. "Spectral Quantitation of Total Cytochrome P450 in Microsomes Using a Single-Beam Spectrophotometer." *Language, Society and Power. An Introduction* 3(4): 56–74. [https://doi.org/10.1007/978-1-0716-1542-3\\_4](https://doi.org/10.1007/978-1-0716-1542-3_4)
- Surpeta Bartłomiej, Sequeiros-Borja Carlos Eduardo & Brezovsky Jan. 2020. "Dynamics, a powerful component of current and future in silico approaches for protein design and engineering." *International Journal of Molecular Sciences* 21(8): 2713 <https://doi.org/10.3390/ijms21082713>
- Sutcliffe J. Michael, Kemp A. Carol, & Mare Jean-Didier. 2005. "Progress in cytochrome P450 active site modeling" *Archives of Biochemistry and Biophysics* 433(2): 361–368. <https://doi.org/10.1016/j.abb.2004.08.026>
- Suzuki Risa, Hidehiko Hirakawa, Teruyuki Nagamune. 2014. "Electron donation to an archaeal cytochrome P450 is enhanced by PCNA-mediated selective complex formation with foreign redox proteins." *Biotechnology* 9(12): 1573-1581. <https://doi.org/10.1002/biot.201400007>
- Suzuki Risa, Hidehiko Hirakawa, Teruyuki Nagamune. 2016. "Immobilization of a Bacterial Cytochrome P450 Monooxygenase System on a Solid Support." *Journal of German Chemical Society* 55(48): 15002–15006. <https://doi.org/10.1002/anie.201608033>
- Syed Khajamohiddin, Shale Karabo, Nazir K. H. M. Nazmul Hussain, Krasevec Nada, Mashele Sitheni Samson, & Pagadala Sekhar Nataraj. 2014. "Genome-wide identification, annotation and characterization of novel thermostable cytochrome

P450 monooxygenases from the thermophilic biomass-degrading fungi *Thielavia terrestris* and *Myceliophthora thermophila*." *Genes and Genomics* 36(3): 321–333. <https://doi.org/10.1007/s13258-013-0170-9>

Szczebara M. Florence, Chandelier Cathy, Villeret Coralie, Masurel Amelie, Bourot Stephane, Duport Catherine, Blanchard Sofie, Groisillier Agnes, Testet Eric, Costaglioli Patricia, & Cauet Gilles. 2003. "Total biosynthesis of hydrocortisone from a simple carbon source in yeast." *Nature Biotechnology* 21(1): 143–149. <https://doi.org/10.1038/nbt775>

Tani Fumito, Liu Jin-Gang & Naruta, Yoshinori. 2002. "Synthetic models of the active site of cytochrome c oxidase: influence of tridentate or tetradentate copper chelates bearing a His--Tyr linkage mimic on dioxygen adduct formation by heme/Cu complexes." *Chemistry* 13(22): 6365-78. doi:10.1002/chem.200601884.

Tripathi M. Sarvind, Li Huiying, & Poulos L. Thomas. 2013. "Structural Basis for Effector Control and Redox Partner Recognition in Cytochrome P450." *Science* 340(6137): 1227–1230. <https://doi.org/10.1126/science.1235797>

Unno Masashi , Christian F. James, Benson E. David, Gerber Nancy, Sligar G. Stephen, & Champion M. Paul. 1997. "Resonance Raman Investigations of Cytochrome P450 cam Complexed with Putidaredoxin." *Journal of the American Chemical Society* 119 (28): 6614–6620. <https://doi.org/10.1021/ja963785a>

Unno Masashi, Shimada Hideo, Toba Yoko, Makino Ryu, & Ishimura Yuzuru. 1996. "Role of Arg112 of cytochrome P450(cam) in the electron transfer from reduced putidaredoxin. Analyses with site-directed mutants." *Journal of Biological Chemistry* 271(30): 17869–17874. <https://doi.org/10.1074/jbc.271.30.17869>

Van Beilen B. Jan, Duetz A. Wouter, Schmid Andreas, & Witholt Bernand. 2003. "Practical issues in the application of oxygenases." *Trends in Biotechnology* 21(4): 170–177. [https://doi.org/10.1016/S0167-7799\(03\)00032-5](https://doi.org/10.1016/S0167-7799(03)00032-5)

Wade C. Rebecca, Winn J. Peter, Schlichting Ilme, & Sudarko. 2004. "A survey of active site access channels in cytochromes P450." *Journal of Inorganic Biochemistry* 98(7): 1175–1182. <https://doi.org/10.1016/j.jinorgbio.2004.02.007>

Wallrapp Frank, Masone Diego, & Guallar Victor. 2008. "Electron transfer in the P450cam/PDX complex. The QM/MM e-pathway." *Journal of Physical Chemistry A* 112(50): 12989–12994. <https://doi.org/10.1021/jp803538u>

- Wang Yonghua. 2007. "Stochastic simulations of the cytochrome P450 catalytic cycle." *Journal of Physical Chemistry B* 111(16): 4251–4260. <https://doi.org/10.1021/jp071222n>
- Wang Li. 2018. "Enhanced Turnover for the P450 119 Peroxygenase-Catalyzed Asymmetric Epoxidation of Styrenes by Random Mutagenesis." *Chemistry European Journal* 24(11): 2741-2749. <https://doi.org/10.1002/chem.201705460>
- Wass N. Mark, Fuentes Gloria, Pons Carles, Pazos Florencio, & Valencia Alfonso. 2011. "Towards the prediction of protein interaction partners using physical docking." *Molecular Systems Biology* 7(469): 1–8. <https://doi.org/10.1038/msb.2011.3>
- Wei Xiaoyao. 2019. "Enhanced Activity and Substrate Specificity by Site-Directed Mutagenesis for the P450 119 Peroxygenase Catalyzed Sulfoxidation of Thioanisole." *ChemistryOpen* 8(8): 1076–1083. <https://doi.org/10.1002/open.201900157>
- Weng Gaoqi, Wang Ercheng, Wang Zhe, Liu Hui, Zhu Feng, Hou Tingjun, & Li Dan. 2019. "HawkDock: a web server to predict and analyze the protein – protein complex based on computational docking and MM / GBSA." *Nucleic Acids Research* 47(5): 322–330. <https://doi.org/10.1093/nar/gkz397>
- Winkler Margit, Geier Martina, Hanlon P. Steven, Nidetzky Bernd, & Glieder Anton. 2018. "Human Enzymes for Organic Synthesis." *Angewandte Chemie - International Edition*, 57(41): 13406–13423. <https://doi.org/10.1002/anie.201800678>
- Xie Zhenzhen, Liu Ziwei, Zhou Shuyu, Ma Lixin, Liu Weidong, Huang Jian-Wen, Li Xiuqin, Hu Yuechan, Min Jian, Yu Xuejing, Guo Rei-Ting, & Chen Chun-Chi. 2020. "Structural insight into the electron transfer pathway of a self-sufficient P450 monooxygenase." *Nature Communications* 11(1): 1–6. <https://doi.org/10.1038/s41467-020-16500-5>
- Zhang Chun. 2014. "Enhanced turnover rate and enantioselectivity in the asymmetric epoxidation of styrene by new T213G mutants of CYP119" *RCS Advances* 52(1): 27526–27531. <https://doi.org/10.1039/c4ra04626a>
- Zhang Wei, Pochapsky, S. Susan, Pochapsky C. Thomas, & Jain U. Nitin. 2008. "Solution NMR Structure of Putidaredoxin-Cytochrome P450cam Complex via a Combined Residual Dipolar Coupling-Spin Labeling Approach Suggests a Role for Trp106 of Putidaredoxin in Complex Formation." *Journal of Molecular Biology* 384(2): 349–363. <https://doi.org/10.1016/j.jmb.2008.09.037>



Zollner Andy, Dragan Calin-Aurel, Pistorius Dominik, Muller Rolf, Helge B. Bode, Peters T. Frank, Maurer H. Hans, & Bureik Matthias. 2009. "Human CYP4Z1 catalyzes the in-chain hydroxylation of lauric acid and myristic acid." *Biological chemistry* 390(4): 313–317. <https://doi.org/10.1515/BC.2009.030>

## APPENDIX A

Table A.1. The list of bacterial culture mediums used in current research.

№	Medium name	Recipe
1	LB Broth	(10 g tryptone, 10 g NaCl, 5 g yeast extract) LB Broth was dissolved in 1 L of dH <sub>2</sub> O and autoclaved for 15 minutes at 121°C. Appropriate antibiotics was added Stored at room temperature
2	LB Agar	Preparation Of Agar Plates 32 g/L LB Agar was dissolved in 1 L of dH <sub>2</sub> O and autoclaved for 15 minutes at 121°C. After addition of an appropriate antibiotics, medium was poured to petri plates and cooled to room temperature. Stored at +4°C
3	TB	47.6 g/L of TB was dissolved in 1 L of dH <sub>2</sub> O and autoclaved at 121°C for 15 mins. After cooling down 4 ml of glycerol was added. <i>or</i> (12 g/L tryptone, 24 g/L yeast extract, 5 g/L glycerol) Note: glycerol will be sterilized through the prepared (prewet with 5-10 ml of sterile H <sub>2</sub> O) a 0.22 µm syringe filter
4	2xYT	(16 g/L tryptone, 10 g/L yeast extract, 5 g/L sodium chloride) 2xYT at pH=6.8 autoclaved at 121°C 15 mins
5	SOC	Preparing 100 mL of SOC medium: Add to 95 mL of dH <sub>2</sub> O, and mix to dissolve: 0.5 g yeast extract and 2.0 g tryptone and 1 mL of 1 M NaCl and 1 mL of 1 M KCl • Bring the pH down to 7.0. • Autoclave and let it cool to a temperature of less than 60°C. One milliliter of filter-sterilized 2 M Mg <sup>+2</sup> (1 M MgCl <sub>2</sub> + 1 M MgSO <sub>4</sub> ) should be added. • Pour in 1 mL of the 2 M glucose solution that has been filter-sterilized. • To get a final volume of 100 mL, add sterile dH <sub>2</sub> O.

Table A.2. The list of proteins and their PDBIDs used in alignment analysis.

№	Protein name	PDBID
1	P450cam-Pdx complex	4JWS
2	CYP119	1IO7
3	Pdx	1XLN

Table A.3. The list of antibiotics used in current research.

№	Name	Recipe
1	Ampicillin	<p>Recommended concentration of ampicillin stock is 100 mg/mL. Recommended working concentration of ampicillin is 100 µg/mL</p> <p>Follow the procedure:</p> <p>0.2 g of ampicillin is dissolved in 2 mL of sterile H<sub>2</sub>O. Then filtered using 0.22 µm syringe filter for sterilization.</p> <p>Draw through 5–10 ml of sterile H<sub>2</sub>O to prewet a 0.22 µm syringe filter; discard water. Stock is stored at -20°C for 1 year</p>
2	Kanamycin	<p>Recommended concentration of kanamycin stock is 50 mg/mL. Recommended working concentration of kanamycin is 50 µg/mL</p> <p>Follow the procedure:</p> <p>0.1 g of ampicillin is dissolved in 2 mL of sterile H<sub>2</sub>O.</p> <p>Then filtered using 0.22 µm syringe filter for sterilization. Draw through 5–10 ml of sterile H<sub>2</sub>O to prewet a 0.22 µm syringe filter; discard water. Stock is stored at -20°C for 1 year</p>

Table A.4. The list of Buffers used in current research.

№	Buffer name	Recipe																																							
1	Potassium phosphate (Kpi)	<p>According to table below, in order to get 1 M stock solution with pH 7.4, dissolve in 1 liter water <math>K_2HPO_4</math> and <math>KH_2PO_4</math>. Working molarity is 0.02 M, prepare it from 1 M: 20 ml of stock+980 ml water. Control with pH-meter.</p> <table border="1" data-bbox="719 607 1252 1099"> <thead> <tr> <th>pH</th> <th><math>K_2HPO_4</math> mL</th> <th><math>KH_2PO_4</math> mL</th> </tr> </thead> <tbody> <tr><td>5.8</td><td>8.5</td><td>91.5</td></tr> <tr><td>6.0</td><td>13.2</td><td>86.8</td></tr> <tr><td>6.2</td><td>19.2</td><td>80.8</td></tr> <tr><td>6.4</td><td>27.8</td><td>72.2</td></tr> <tr><td>6.6</td><td>38.1</td><td>61.9</td></tr> <tr><td>6.8</td><td>49.7</td><td>50.3</td></tr> <tr><td>7.0</td><td>61.5</td><td>38.5</td></tr> <tr><td>7.2</td><td>71.7</td><td>28.3</td></tr> <tr><td>7.4</td><td>80.2</td><td>19.8</td></tr> <tr><td>7.6</td><td>86.6</td><td>13.4</td></tr> <tr><td>7.8</td><td>90.8</td><td>9.2</td></tr> <tr><td>8.0</td><td>94</td><td>6</td></tr> </tbody> </table> <p>In order to prepare 500 ml of 20mM of potassium phosphate buffer (pH 7.4) mix followings:</p> <p>40.1 ml <math>K_2HPO_4</math>+ 9.9 ml <math>KH_2PO_4</math>+450 ddH<sub>2</sub>O (0.1 M), 100 ml of 0.1 M KPi + 400 ddH<sub>2</sub>O (0.02 M) adjust pH</p> <p><b>Kpi 1 M pH 7.4</b> 40.1 ml <math>K_2HPO_4</math> 9.9 ml <math>KH_2PO_4</math> 450 ml ddH<sub>2</sub>O</p>	pH	$K_2HPO_4$ mL	$KH_2PO_4$ mL	5.8	8.5	91.5	6.0	13.2	86.8	6.2	19.2	80.8	6.4	27.8	72.2	6.6	38.1	61.9	6.8	49.7	50.3	7.0	61.5	38.5	7.2	71.7	28.3	7.4	80.2	19.8	7.6	86.6	13.4	7.8	90.8	9.2	8.0	94	6
pH	$K_2HPO_4$ mL	$KH_2PO_4$ mL																																							
5.8	8.5	91.5																																							
6.0	13.2	86.8																																							
6.2	19.2	80.8																																							
6.4	27.8	72.2																																							
6.6	38.1	61.9																																							
6.8	49.7	50.3																																							
7.0	61.5	38.5																																							
7.2	71.7	28.3																																							
7.4	80.2	19.8																																							
7.6	86.6	13.4																																							
7.8	90.8	9.2																																							
8.0	94	6																																							
2	1xTAE	<p>242 g Tris Base 57.1 mL glacial acetic acid 100 mL 0.5 M EDTA (pH 8.0) dH<sub>2</sub>O</p> <p>First, make a concentrated TAE buffer stock solution (50x). Dissolve Tris Base in 750 mL of deionized water to do this. After adding the EDTA and acetic acid, add water to get the level up to 1 liter. The 50x TAE buffer should have a final pH of roughly 8.5. Add 49 parts deionized water to one-part 50x TAE buffer to create the 1x TAE working buffer.</p>																																							

cont. on the next page

**Table A.4. (cont.)**

3	10X SDS Running Buffer	For 500 ml pH 8.3: 72 g Glycine, 15 g Tris Base, 5 g SDS were dissolved in 500 dH <sub>2</sub> O
4	Staining solution	Solution 1 250 ml EtOH 50 ml Acetic Acid 200 ml dH <sub>2</sub> O Solution 2 25 ml EtOH 37,5 ml Acetic Acid 437,5 ml dH <sub>2</sub> O
5	CYP119 Lysis	50 mM Kpi+150 mM NaCl+0.2 mM PMSF+1 mM benzamidine HCl + 10 mM imidazole (pH 7.5)
6	CYP119 Dialysis	50 mM Kpi, 20 mM NaCl, 5% glycerol Desalting buffer preparation KPi buffer 0.1 M with pH 7.5 was prepared.  80.2 ml K <sub>2</sub> HPO <sub>4</sub> (17.418 g in 100 ml water) +19.8 ml KH <sub>2</sub> PO <sub>4</sub> (2.7216 g in 20 ml water) +900 ml dH <sub>2</sub> O to get 1 L of 0.1 M KPi adjust pH 7.5 750 ml of KPi+1.7565 g NaCl + 75 ml glycerol+ dH <sub>2</sub> O up to 1.5 L adjust pH 7.5
7	Pdx/PdR Lysis	150 mM KCl, 10 mM imidazole, 1 mM benzamidine HCL, 0.2 mM PMSF, 20 mM Kpi pH 7.4
8	Pdx/PdR Wash	20 mM Kpi, 20 mM imidazole pH 7.4
9	Pdx/PdR Elution	150 mM KCl, 300 mM imidazole, 20 mM Kpi pH 7.4
10	Pdx/PdR dialysis	5% glycerol, 20 mM potassium phosphate buffer pH 7.4
11	EDTA 0.5M	100 mM EDTA  To prepare a 100 mL solution of 100 mM EDTA, pH 8 from a 0.5 M stock, you will need to do the following: <ol style="list-style-type: none"> <li>1. Measure out 186.1 g of EDTA and dissolve it in 1000 distilled water. This will give you a 0.5 M stock solution.</li> <li>2. Take 200 mL of the 0.5 M stock solution and add it to a container.</li> <li>3. Measure the pH of the solution and adjust it to 8 using a suitable buffer, such as NaOH or HCl.</li> <li>4. Stir the solution well to ensure that the EDTA is fully dissolved and the pH is well-adjusted.</li> <li>5. Your 100 mL solution of 100 mM EDTA, pH 8 is now ready to use.</li> </ol>

**cont. on the next page**



## APPENDIX B

CYP119 consists of 366 amino acids, 15  $\alpha$ -helices and 7  $\beta$ -sheets. Amino acid sequence corresponds to:

MYDWFSEMRKKDPVYYDGNIWQVFSYRYTKEVLNNSKFSDDLGTGYH  
ERLEDLRNGKIRFDIPTRYTMLTSDPPLHDELRSMSADIFSPQKLQTLTFFIRETT  
RSLDSDIDPREDDIVKKLAVPLPIIVISKILGLPIEDKEKFKEWSDLVAFRLGKPGGE  
IFELGKKYLELIGYVKDHLNSGTEVVSRVVNSNLSDIEKLGYYILLIAGNETTTN  
LISNSVIDFTRFNLWQRIREENLYLKAIEEALRYSPPVMRTVRKTKERVKLGDQT  
IEEGEYVRVWIASANRDEEVFHDGKFKIPDRNPNPHLSFGSGIHLCLGAPLARLE  
ARIAIEEFSKRFRHIEILDTEKVPNEVLNGYKRLVVRLKS

WT CYP119 nucleotide sequence is:

ATG TAT GAC TGG TTT AGT GAG ATG AGA AAG AAA GAC CCA GTG TAT  
TAT GAC GGA AAC ATA TGG CAG GTG TTT TCC TAT AGG TAC ACA AAG  
GAG GTT TTA AAC AAC TTT TCG AAA TTC TCC TCA GAT CTT ACA GGT TAC  
CAC GAA AGG CTT GAG GAC CTA AGG AAC GGT AAA ATA AGG TTC GAC  
ATC CCC ACT AGG TAT ACC ATG CTG ACC TCA GAT CCC CCT CTC CAT GAT  
GAG TTA AGA TCA ATG TCA GCA GAT ATA TTC TCG CCT CAA AAG CTA  
CAG ACA CTT GAG ACA TTT ATT AGG GAG ACC ACC AGA AGC CTA TTA  
GAC TCA ATT GAC CCT AGG GAA GAC GAC ATA GTG AAG AAG TTA GCT  
GTT CCA CTA CCA ATA ATA GTT ATC TCA AAA ATA TTG GGT CTC CCA ATT  
GAA GAT AAG GAG AAG TTC AAA GAG TGG TCA GAC TTA GTC GCA TTC  
AGG TTG GGT AAG CCT GGA GAA ATA TTT GAG CTA GGT AAG AAG TAC  
CTT GAG TTA ATA GGT TAT GTG AAG GAT CAT CTA AAT TCA GGG ACC  
GAA GTG GTC AGC AGA GTT GTC AAC TCA AAC CTC TCA GAC ATA GAG  
AAA CTC GGA TAC ATT ATT TTA CTT CTC ATA GCG GGT AAT GAG ACT ACA  
ACT AAC TTA ATA TCA AAC TCT GTT ATT GAC TTC ACT AGG TTT AAC CTG  
TGG CAG AGG ATA AGG GAA GAG AAC CTC TAC CTT AAG GCT ATC GAA  
GAG GCT TTA AGG TAT TCT CCT CCT GTG ATG AGG ACT GTA AGA AAG  
ACT AAG GAA AGA GTG AAA TTG GGT GAT CAG ACT ATT GAA GAG GGA  
GAG TAC GTT AGA GTA TGG ATA GCC TCA GCA AAC AGG GAC GAG GAG  
GTG TTT CAT GAC GGA GAG AAG TTC ATC CCT GAC AGG AAT CCG AAC

CCA CAC TTA AGC TTT GGG TCT GGA ATA CAT CTG TGT TTA GGT GCT CCT  
 TTG GCT AGA TTA GAG GCA AGA ATA GCA ATT GAG GAA TTT TCA AAA  
 AGG TTT AGG CAC ATT GAG ATA TTG GAT ACT GAA AAA GTT CCA AAT  
 GAA GTG CTG AAT GGT TAT AAG AGA CTA GTG GTC AGG TTG AAG AGT  
 AAT GAA, where red labeled codons are amino acids to be mutated.

## SEQUENCE RESULTS OF MUTANTS

### N34E sequence

```

1      ccttggggaa attccctcta gaaataatth tgtttaactt taagaaggag atatacatat
61     gtatgactgg tttagtgaga tgagaaagaa agaccagtg tattatgacg gaaacatttg
121    gcagggtgtt tcctataggt acacaaagga ggtttttagag aacttttcga aattctcctc
181    agatcttaca ggttaccacg aaaggcttga ggacctaaagg aacggtaaaa taaggttcga
241    catccccact aggtatacca tgctgacctc agatccccct ctccatgatg agttaagatc
301    aatgtcagca gatataattct cgcctcaaaa gctacagaca cttgagacat ttattagggg
361    gaccaccaga agcctattag actcaattga ccctagggaa gacgacatag tgaagaagtt
421    agctgttcca ctaccaataa tagttatctc aaaaatattg ggtctcccaa ttgaagataa
481    ggagaagttc aaagagtggg cagacttagt cgcattcagg ttgggtaagc ctgggaaat
541    atttgagcta ggtaagaagt accttgagtt aataggttat gtgaaggatc atctaaatc
601    agggaccgaa gtggtcagca gagttgtcaa ctcaaacctc tcagacatag agaaactcgg
661    atacattatt ttactttctca tagcgggtaa tgagactaca actaacttaa tatcaaactc
721    tgttattgac ttacttaggt ttaacctgtg gcagaggata agggaagaga acctctacct
781    taaggctatc gaagaggctt taaggatttc tctcctgtg atgaggactg taagaaagac
841    taaggaaaga gtgaaattgg gtgatcagac tattgaagag ggagagtacg ttagagtatg
901    gatagcctca gcaaacaggg acgaggaggt gtttcatgac ggagagaagt tcatccctga
961    caggaatccg aaccacact taagctttgg gtctggaata catctgtggt taggtgctcc
1021   tttggctaga ttagaggcaa gaatagcaat tgaggaatth tcaaaaaggt ttagggccat
1081   tgagatattg gaaactgaaa aagttccaat gaagtgggta aagggtataa agaataaggg
1141   tcaggttgaa aaataaagaa aaagggtcgc gtggtataaa acccgaaaga aaataaaatg
1201   gtggttgc

```

### N34E-D77R sequence

```

1      tgmgtcattt cccctctaga ataatthtgt ttaactthaa gaaggagata tacatatgta
61     tgactgggaa gkgrratgag aaagaaagac ccagtgattt atgacgyyaa acatttggca
121    ggtgttttcc tataggtaca caaaggaggt tttagagaac ttttcgaaat tctcctcaga
181    tcttacaggt taccacgaaa ggcttgagga cctaaggaac ggtaaaataa ggttcgacat
241    cccacttagg tataccatgc tgacctcaga tccccctctc catcgtgagt taagatcaat
301    gtcagcagat atattctcgc ctcaaaagct acagacactt gagacattta ttagggagac
361    caccagaagc ctattagact caattgacct tagggaagac gacatagtga agaagttagc
421    tgttccacta ccaataatag ttatctcaaa aatattgggt ctccaattg aagataagga
481    gaagttcaaa gagtggtcag acttagtcgc attcaggttg ggtaaagcctg gagaaatatt
541    tgagctaggt aagaagtacc ttgagttaat aggttatgtg aaggatcadc taaattcagg
601    gaccgaagtg gtcagcagag ttgtcaactc aaacctctca gacatagaga aactcggata

```



```

661 cattatntta cttctcatag cgggtaatga gactacaact aacttaatat caaactctgt
721 tattgacttc actaggttta acctgtggca gaggataagg gaagagaacc tctaccttaa
781 ggctatcgaa gaggctntaa ggtattctcc tctgtgatg aggactgtaa gaaagactaa
841 aggaagagt gaaattgggt gatcagacta ttgaagaggg agagtacgtt agagtatgga
901 tagccctcag caaacagga caggaggtg ttcatgacg gagagaagtt catccctgac
961 agaatccga acccacactt aagctttggg tctggcaawt acatctgtga tttaggtgct
1021 cttgctaga ttagaggcca agaat

```

### D77R sequence

```

1 tmmggtyca ttcccctcta gaataatntt gtttaacttt aagaaggaga tatacatatg
61 tatgactggg ttarwgrgrk gagaaagaaa gaccaggtgt attatgacgg aaacatttgg
121 cagggtnttt cctataggta cacaaaggag gntntaaaca actnttcgaa attctcctca
181 gatcttacag gttaccacga aaggcttgag gacntaagga acggtaaaat aaggttcgac
241 atcccacta ggtataccat gctgacctca gatcccctc tccatcgtga gntaagatca
301 atgtcagcag atatatctc gcctcaaaag ctacagacac ttgagacatt tattagggag
361 accaccagaa gcctattaga ctcaattgac ctagggaag acgacatagt gaagaagnta
421 gctgntccac taccaataat agttatctca aaaatattgg gtctcccaat tgaagataag
481 ragaagntca aagagtggtc agacttagtc gcattcaggt tgggtaagcc tggagaaata
541 tntgagctag gtaagaagta cttgagnta atagnttatg tgaagntca tctaaatntca
601 gggaccgaag tggtcagcag agttgtcaac tcaaacctct cagacataga gaaactcgga
661 tacattatnt tacttctcat agcgggtaat gagactaaa ctaactntat atcaaacctct
721 gntattgact tcactagntt taacctgtgg cagagntaa gngaagagaa cctctacctt
781 aaggctatcg aagaggctnt aagntattct cctcctgtga tgaggactgt aagaaagact
841 aaagaaaga gtgaaatntg gtgatcagac twattgaaga gngagagntac gntagagntat
901 tggataggcc tcagcaaaac aggacgagga gntgntntcat gacggaraga agntcatccc
961 ctgacaggca ttccgaacca cacttaagcc tntgggatct gngaatacag tctggakntt
1021 aagtgctycc gnttgccnt rga

```

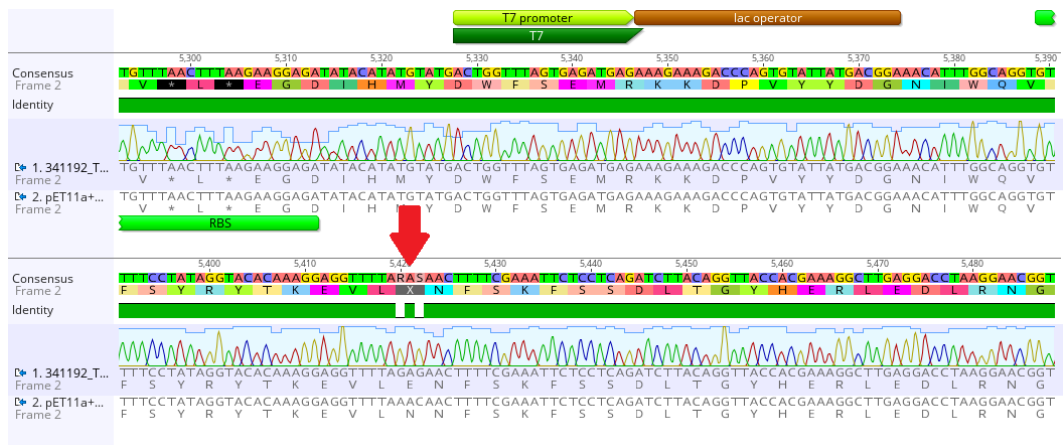
CYP119 consists of 366 amino acids, 15  $\alpha$ -helices and 7  $\beta$ -sheets. Amino acid sequence corresponds to:

MYDWFSEMRKKDPVYYDGNIWQVFSYRYTKEVLNNFSKFSSDLTGYP  
ERLEDLRNGKIRFDIPTRYTMLTSDPPLHDELRSMSADIFSPQKLQTLTFIRETT  
RSLDSDIDPREDDIVKLA VPLPIIVISKILGLPIEDKEKFKESWDLVAFRLGKPGE  
IFELGKKYLELIGYVKDHLNSGTEVVS RVVNSNLSDIEKLG YIILLIAGNETTNT  
LISNSVIDFTRFNLWQRIREENLYLKAIEEALRYSPPVMRTVRKTKERVKLG DQT  
IEEGEYVRVWIASANRDEEVFHDGEKFI PDRNPNPHLSFGSGIHLCLGAPLARLE  
ARIAIEEFKRFRHIEILDTEKVPNEVLNGYKRLVVRLKS

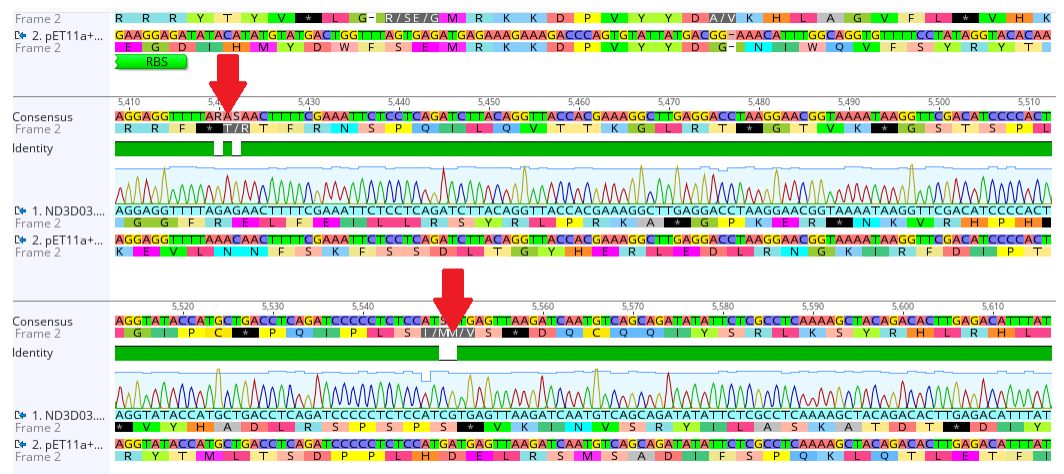
Mutated residues are shown in bold.

Sequencing analysis results showed mutated DNA region. Figure B 1 shows the WT CYP119 region and mutant CYP119 region.

A



B



C

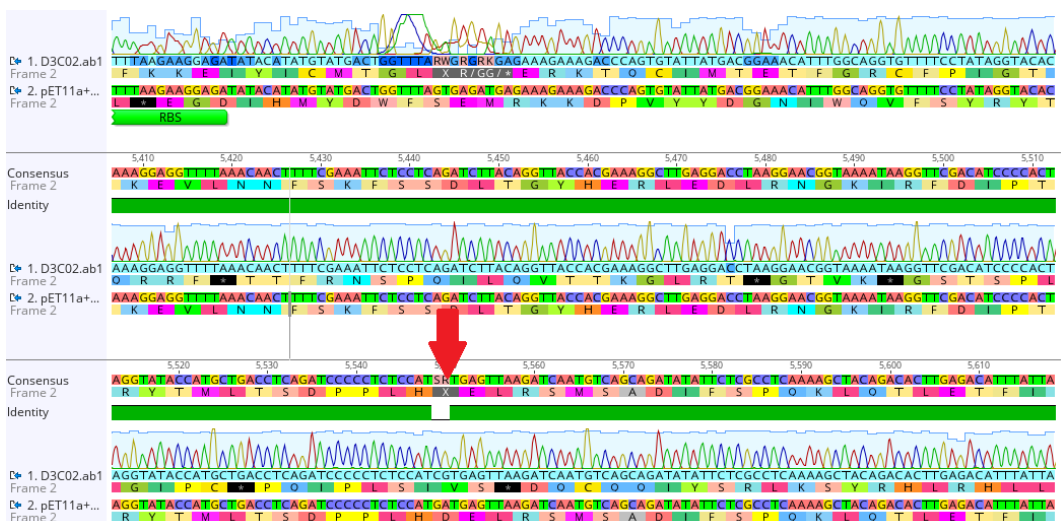


Figure B 1. Sequencing analysis results of mutated DNA A. N34E mutant B. N34E-D77R mutant C. D77R mutant.

## APPENDIX C

PPdx was a gift from Teruyuki Nagamune (catalog numbers #85084) (Suzuki, 2014). pET28b for Pdx is bacterial expression plasmid with kanamycin resistance gene, and having promoter T7. Plasmid map of pPdx can be seen in Figure C.1.

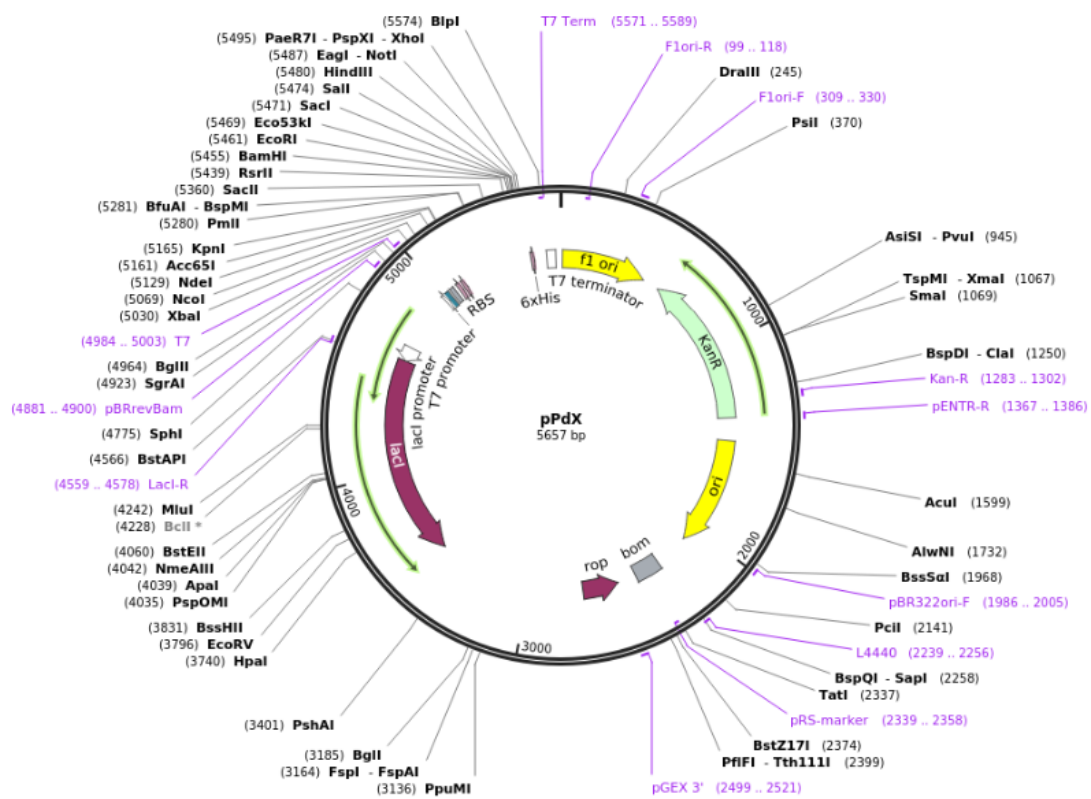


Figure C.1. Plasmid map of pPdx (catalog numbers #85084) (Suzuki, 2014).

PPdR was a gift from Teruyuki Nagamune (catalog numbers #85083) (Suzuki, 2014). pET28b for PdR is bacterial expression plasmid with kanamycin resistance gene, and having promoter T7. Plasmid map of pPdR can be seen in Figure C.2.

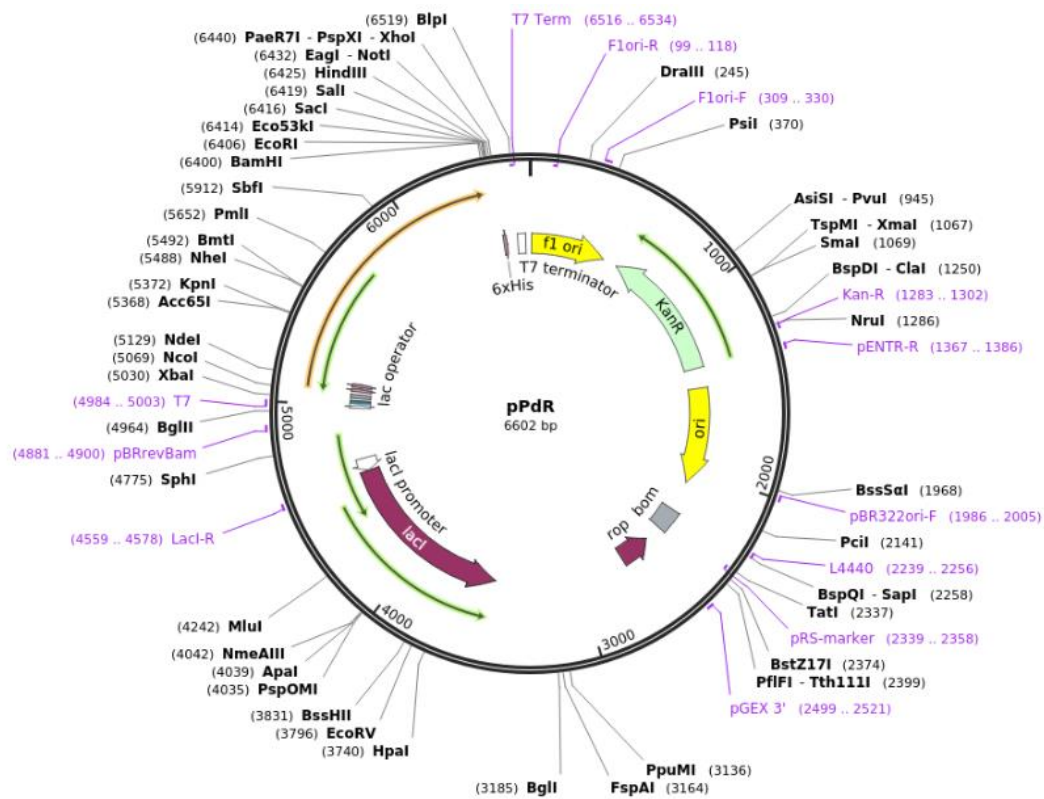


Figure C.2. Plasmid map of pPdR (catalog numbers #85083) (Suzuki, 2014).

pPdX sequence 5657 bps:

```

TGGCGAATGGGACGCGCCCTGTAGCGGCGCATTAAAGCGCGGGCGGGTGTGGTGGTTAC
GCGCAGCGTGACCGCTACACTTGCCAGCGCCCTAGCGCCCGCTCCTTTTCGCTTTCTTC
CCTTCCTTTCTCGCCACGTTTCGCCGGCTTTCCCCGTCAAGCTCTAAATCGGGGGCTCCC
TTTAGGGTTCCGATTTAGTGCTTTACGGCACCTCGACCCCAAAAACTTGATTAGGGTG
ATGGTTCACGTAGTGGGCCATCGCCCTGATAGACGGTTTTTCGCCCTTTGACGTTGGA
GTCCACGTTCTTTAATAGTGGACTCTTGTTCCAAACCTGGAACAACACTCAACCCTATCT
CGGTCTATTCTTTGATTTATAAGGGATTTTGCCGATTTTCGGCCTATTGGTTAAAAAAT
GAGCTGATTTAACAAAAATTTAACGCGAATTTTAAACAAAAATATTAACGTTTACAATTC
AGGTGGCACTTTTCGGGGAAATGTGCGCGGAACCCCTATTTGTTTATTTTTCTAAATAC
ATTCAAATATGTATCCGCTCATGAATTAATCTTAGAAAACTCATCGAGCATCAAATG
AAACTGCAATTTATTCATATCAGGATTATCAATACCATATTTTGA AAAAAGCCGTTTCTG
TAATGAAGGAGAAAACTCACCGAGGCAGTTCCATAGGATGGCAAGATCCTGGTATCGG
TCTGCGATTCCGACTCGTCCAACATCAATACAACCTATTAATTTCCCCTCGTCAAAAAT
AAGGTTATCAAGTGAGAAATCACCATGAGTGACGACTGAATCCGGTGAGAATGGCAA
AGTTTATGCATTTCTTTCCAGACTTGTTC AACAGGCCAGCCATTACGCTCGTCATCAA
ATCACTCGCATCAACCAACCGTTATTCATTCGTGATTGCGCCTGAGCGAGACGAAATA
CGCGATCGCTGTTAAAAGGACAATTACAAACAGGAATCGAATGCAACCGGCGCAGGAA
CACTGCCAGCGCATCAACAATATTTTCACCTGAATCAGGATATTTCTTAATACCTGGA
ATGCTGTTTTCCCGGGGATCGCAGTGGTGAGTAACCATGCATCATCAGGAGTACGGAT
AAAATGCTTGATGGTTCGGAAGAGGCATAAATTCGGTCAGCCAGTTTAGTCTGACCATCT
CATCTGTAACATCATTGGCAACGCTACCTTTGCCATGTTTCAGAAACAACTCTGGCGCA
TCGGGCTTCCATACAATCGATAGATTGTCGCACCTGATTGCCCGACATTATCGCGAGC
CCATTATAACCATATAAATCAGCATCCATGTTGGAATTTAATCGCGGCCCTAGAGCAAG

```

ACGTTTCCCGTTGAATATGGCTCATAACACCCCTTGTATTACTGTTTATGTAAGCAGAC  
AGTTTTATTGTTTCATGACCAAAATCCCTTAACGTGAGTTTTTCGTTCCACTGAGCGTCAG  
ACCCCGTAGAAAAGATCAAAGGATCTTCTTGAGATCCTTTTTTTCTGCGCGTAATCTGC  
TGCTTGCAAACAAAAAACACCGCTACCAGCGGTGGTTTGTGGCCGATCAAGAGC  
TACCAACTCTTTTTCCGAAGGTAACGGCTTCAGCAGAGCGCAGATACCAAATACTGTC  
CTTCTAGTGTAGCCGTAGTTAGGCCACCACTTCAAGAACTCTGTAGCACCGCCTACATA  
CCTCGCTCTGCTAATCCTGTTACCAGTGGCTGCTGCCAGTGGCGATAAGTCGTGTCTTA  
CCGGGTTGGACTCAAGACGATAGTTACCGGATAAGGCGCAGCGGTCCGGGCTGAACGG  
GGGGTTCGTGCACACAGCCCAGCTTGGAGCGAACGACCTACACCGAACTGAGATACCT  
ACAGCGTGAGCTATGAGAAAAGCGCCACGCTTCCCGAAGGGAGAAAAGGCGGACAGGTA  
TCCGGTAAGCGGCAGGGTCCGAAACAGGAGAGCGCACGAGGGAGCTTCCAGGGGGAAA  
CGCCTGGTATCTTTATAGTCCTGTCGGGTTTCGCCACCTCTGACTTGAGCGTCGATTTT  
TGTGATGCTCGTCAGGGGGGCGGAGCCTATGGAAAAACGCCAGCAACGCGGCCTTTTT  
ACGGTTCCTGGCCTTTTTGCTGGCCTTTTTGCTCACATGTTCTTTCTGCGTTATCCCCTG  
ATTCTGTGGATAACCGTATTACCGCCTTTGAGTGAGCTGATACCGCTCGCCGACGCCG  
AACGACCGAGCGCAGCGAGTCAGTGAGCGAGGAAGCGGAAGAGCGCCTGATGCGGTA  
TTTTCTCCTTACGCATCTGTGCGGTATTTACACCGCATATATGGTGCACCTCTCAGTAC  
AATCTGCTCTGATGCCGCATAGTTAAGCCAGTATACACTCCGCTATCGCTACGTGACTG  
GGTCATGGCTGCGCCCCGACACCCGCCAACACCCGCTGACGCGCCCTGACGGGCTTGT  
CTGCTCCCGGCATCCGCTTACAGACAAGCTGTGACCGTCTCCGGGAGCTGCATGTGTC  
AGAGGTTTTACCGTCATCACCGAAACGCGCGAGGCAGCTGCGGTAAGCTCATCAGC  
GTGGTCGTGAAGCGATTACAGATGTCTGCCTGTTTCATCCGCGTCCAGCTCGTTGAGT  
TTCTCCAGAAGCGTTAATGTCTGGCTTCTGATAAAGCGGGCCATGTTAAGGGCGGTTTT  
TTCTGTTTGGTCACTGATGCCTCCGTGTAAGGGGGATTTCTGTTTCATGGGGGTAATGA  
TACCGATGAAACGAGAGAGGATGCTCACGATACGGGTTACTGATGATGAACATGCCCG  
GTTACTGGAACGTTGTGAGGGTAAACAACACTGGCGGTATGGATGCGGGCGGGACCAGAG  
AAAAATCACTCAGGGTCAATGCCAGCGCTTCGTTAATACAGATGTAGGTGTTCCACAG  
GGTAGCCAGCAGCATCCTGCGATGCAGATCCGGAACATAATGGTGCAGGGGCGCTGACT  
TCCGCGTTTCCAGACTTTACGAAACACGGAACCCGAAGACCATTGATGTTGTTGCTCAG  
GTCGAGACGTTTTGAGCAGCAGTCGCTTACGTTTCGCTCGCGTATCCGGTATTGATT  
CTGCTAACCAGTAAGGCAACCCCGCCAGCCTAGCCGGTCTCAACGACAGGAGCAGC  
ATCATGCGCACCCGTGGGGCCGATGCCGGCGATAATGGCCTGCTTCTCGCCGAAAC  
GTTTGGTGGCGGGACCAGTGACGAAGGCTTGAAGCGAGGGCGTGCAAGATTCCGAATA  
CCGCAAGCGACAGGCCGATCATCGTCGCGCTCCAGCGAAAGCGGTCTCGCCGAAAAT  
GACCCAGAGCGCTGCCGGCACCTGTCCTACGAGTTGCATGATAAAGAAGACAGTCATA  
AGTGCGGCGACGATAGTCATGCCCCGCGCCACCGGAAGGAGCTGACTGGGTTGAAG  
GCTCTCAAGGGCATCGGTGAGATCCCGGTGCCTAATGAGTGAGCTAACTTACATTA  
TTGCGTTGCGCTCACTGCCCGCTTTCCAGTCGGGAAACCTGTCGTGCCAGCTGCATTA  
ATGAATCGGCCAACGCGCGGGGAGAGGGCGGTTTGGTATTGGGCGCCAGGGTGGTTT  
TTCTTTTACCAGTGAGACGGGCAACAGCTGATTGCCCTTACCAGCCTGGCCCTGAGA  
GAGTTGCAGCAAGCGGTCCACGCTGGTTTGGCCAGCAGGCGAAAATCCTGTTTGATG  
GTGGTTAACGGCGGGATATAACATGAGCTGTCTTCGGTATCGTCGTATCCCCTACC  
AGATATCCGCACCAACGCGCAGCCGGACTCGGTAATGGCGCGCATTGCGCCAGCGC  
CATCTGATCGTTGGCAACCAGCATCGCAGTGGGAACGATGCCCTCATTGAGCATTGTC  
ATGGTTTGTGAAAACCGGACATGGCACTCCAGTCGCCTTCCCGTTCCGCTATCGGCT  
GAATTTGATTGCGAGTGAGATATTTATGCCAGCCAGCCAGACGCGACCGCGGAGAC  
AGAACTTAATGGGCCCGCTAACAGCGCGATTGCTGGTGACCCAATGCGACCAGATGC  
TCCACGCCAGTCGCGTACCGTCTTCATGGGAGAAAATAATACTGTTGATGGGTGCT  
GGTCAGAGACATCAAGAAATAACGCCGGAACATTAGTGCAGGCAGCTTCCACAGCAAT  
GGCATCCTGGTCATCCAGCGGATAGTTAATGATCAGCCACTGACGCGTTGCGCGAGA  
AGATTGTGCACCGCCGCTTTACAGGCTTCGACGCGGCTTCGTTCTACCATCGACACCAC  
CACGCTGGCACCCAGTTGATCGGCGCGAGATTTAATCGCCGCGACAATTTGCGACGGC  
GCGTGCAGGGCCAGACTGGAGGTGGCAACGCCAATCAGCAACGACTGTTTGGCCGCCA  
GTTGTTGTGCCACGCGGTTGGGAATGTAATTCAGCTCCGCCATCGCCGCTTCCACTTTT  
TCCCGGTTTTTCGCAGAAACGTGGCTGGCCTGGTTTACCACGCGGGAAACGGTCTGAT  
AAGAGACACCGGCATACTCTGCGACATCGTATAACGTTACTGGTTTACATTACCACC

CTGAATTGACTCTCTTCCGGGCGCTATCATGCCATACCGCGAAAGGTTTTGCGCCATTC  
GATGGTGTCCGGGATCTCGACGCTCTCCCTTATGCGACTCCTGCATTAGGAAGCAGCC  
CAGTAGTAGGTTGAGGCCGTTGAGCACCGCCGCCGCAAGGAATGGTGCATGCAAGGA  
GATGGCGCCCAACAGTCCCCCGGCCACGGGGCCTGCCACCATACCCACGCCGAAACAA  
GCGCTCATGAGCCCGAAGTGGCGAGCCGATCTTCCCCATCGGTGATGTCGGCGATAT  
AGGCGCCAGCAACCGCACCTGTGGCGCCGGTGATGCCGGCCACGATGCGTCCGGCGT  
AGAGGATCGAGATCTCGATCCCGCGAAATTAATACGACTCACTATAGGGGAATTGTGA  
GCGGATAACAATTCCCCTCTAGAAATAATTTTGTTTAACTTTAAGAAGGAGATATACCA  
TGGGCAGCAGCCATCATCATCATCACAGCAGCGGCCTGGTGCCGCGCGGCAGCCA  
TATGTCTAAAGTTGTTTACGTTTCTCACGACGGTACCCGTCGCGAACTGGACGTTGCGG  
ACGGTGTTCCTCTGATGCAGGCGGCAGTTTCTAACGGCATCTACGACATCGTTGGTGA  
CTGCGGTGGTTCTGCGTCTTGCGCGACCTGCCACGTGTACGTGAACGAAGCGTTCACC  
GACAAAGTTCGGGCTGCTAACGAACGTGAAATCGGTATGCTGGAATCTGTTACCGCGG  
AACTGAAACCGAACTCTCGTCTGTCTTGCCAGATCATCATGACCCCGGAGCTGGACGG  
TATCGTTGTTGACGTTCCGGACCGTCAGTGGTGAGGATCCGAATTCGAGCTCCGTCGA  
CAAGCTTGCGGCCGCACTCGAGCACCACCACCACCACCCTGAGATCCGGCTGCTAAC  
AAAGCCCGAAAGGAAGCTGAGTTGGCTGCTGCCACCGCTGAGCAATAACTAGCATAAC  
CCCTTGGGGCCTCTAAACGGGTCTTGAGGGGTTTTTTGCTGAAAGGAGGAACTATATC  
CGGAT

pPdR sequence 6602 bps:

TGGCGAATGGGACGCGCCCTGTAGCGGCGCATTAAAGCGCGGGCGGGTGTGGTGGTTAC  
GCGCAGCGTGACCGCTACACTTGCCAGCGCCCTAGCGCCCGCTCCTTTTCGCTTTCTTC  
CCTTCCTTTCTCGCCACGTTTCGCCGGCTTTCCCCGTCAAGCTCTAAATCGGGGGCTCCC  
TTTAGGGTTCCGATTTAGTGCTTTACGGCACCTCGACCCCAAAAACTTGATTAGGGTG  
ATGGTTCACGTAGTGGGCCATCGCCCTGATAGACGGTTTTTTTCGCCCTTTGACGTTGGA  
GTCCACGTTCTTTAATAGTGGACTCTTGTTCCAAACTGGAACAACACTCAACCCTATCT  
CGGTCTATTCTTTTGATTTATAAGGGATTTTGCCGATTTTCGGCCTATTGGTTAAAAAAT  
GAGCTGATTTAACAAAAATTTAACGCGAATTTTAAACAAAAATATTAACGTTTACAATTC  
AGGTGGCACTTTTCGGGGAAATGTGCGCGGAACCCCTATTTGTTTATTTTTCTAAATAC  
ATTCAAATATGTATCCGCTCATGAATTAATTCCTTAGAAAACTCATCGAGCATCAAATG  
AAACTGCAATTTATTCATATCAGGATTATCAATACCATATTTTTGAAAAAGCCGTTTCTG  
TAATGAAGGAGAAAACTCACCGAGGCAGTTCATAGGATGGCAAGATCCTGGTATCGG  
TCTGCGATTCCGACTCGTCCAACATCAATACAACCTATTAATTTCCCCTCGTCAAAAAAT  
AAGGTTATCAAGTGAGAAATCACCATGAGTGACGACTGAATCCGGTGAGAATGGCAAA  
AGTTTATGCATTTCTTCCAGACTTGTTCAACAGGCCAGCCATTACGCTCGTCATCAAA  
ATCACTCGCATCAACCAACCGTTATTTCATTCGTGATTGCGCCTGAGCGAGACGAAATA  
CGCGATCGCTGTTAAAAGGACAATTACAAAACAGGAATCGAATGCAACCGGCAGGAA  
CACTGCCAGCGCATCAACAATATTTTCACCTGAATCAGGATATTCTTCTAATACCTGGA  
ATGCTGTTTTCCCGGGGATCGCAGTGGTGAGTAACCATGCATCATCAGGAGTACGGAT  
AAAATGCTTGATGGTTCGGAAGAGGCATAAATTCGGTCAGCCAGTTTAGTCTGACCATCT  
CATCTGTAACATCATTGGCAACGCTACCTTTGCCATGTTTCAGAAACAACTCTGGCGCA  
TCGGGCTTCCCATACAATCGATAGATTGTCGCACCTGATTGCCCGACATTATCGCGAGC  
CCATTTATACCCATATAAATCAGCATCCATGTTGGAATTTAATCGCGGCCTAGAGCAAG  
ACGTTTCCCGTTGAATATGGCTCATAACACCCCTTGTATTACTGTTTATGTAAGCAGAC  
AGTTTTATTGTTTCATGACCAAAATCCCTAACGTGAGTTTTTCGTTCCACTGAGCGTCAG  
ACCCCGTAGAAAAGATCAAAGGATCTTCTTGAGATCCTTTTTTTCTGCGCGTAATCTGC  
TGCTTGCAACAAAAAAACCACCGCTACCAGCGGTGGTTTGTGTTGCCGGATCAAGAGC  
TACCAACTCTTTTTCCGAAGGTAACCTGGCTTCAGCAGAGCGCAGATACCAAAACTGTG  
CTTCTAGTGTAGCCGTAGTTAGGCCACCCTTCAAGAACTCTGTAGCACCAGCCTACATA  
CCTCGCTCTGCTAATCCTGTTACCAGTGGCTGCTGCCAGTGGCGATAAGTCGTGTCTTA  
CCGGGTTGGACTCAAGACGATAGTTACCGGATAAGGCGCAGCGGTCCGGGCTGAACGG  
GGGGTTCGTGCACACAGCCAGCTTGAGCGAACGACCTACACCGAACTGAGATACCT  
ACAGCGTGAGCTATGAGAAAGCGCCACGCTTCCCGAAGGGAGAAAGGCGGACAGGTA

TCCGGTAAGCGGCAGGGTTCGGAACAGGAGAGCGCACGAGGGAGCTTCCAGGGGGAAA  
CGCCTGGTATCTTTATAGTCCTGTCGGGTTTCGCCACCTCTGACTTGAGCGTCGATTTT  
TGTGATGCTCGTCAGGGGGGCGGAGCCTATGGAAAAACGCCAGCAACGCGGCCTTTTT  
ACGGTTCCTGGCCTTTTTGCTGGCCTTTTTGCTCACATGTTCTTTCTGCGTTATCCCCTG  
ATTCTGTGGATAACCGTATTACCGCCTTTGAGTGAGCTGATACCGCTCGCCGAGCCG  
AACGACCGAGCGCAGCGAGTCAGTGAGCGAGGAAGCGGAAGAGCGCCTGATGCGGTA  
TTTTCTCCTTACGCATCTGTGCGGTATTTACACCCGCATATATGGTGCACTCTCAGTAC  
AATCTGCTCTGATGCCGCATAGTTAAGCCAGTATACTCCGCTATCGCTACGTGACTG  
GGTCATGGCTGCGCCCCGACACCCGCCAACACCCGCTGACGCGCCCTGACGGGCTTGT  
CTGCTCCCGGCATCCGCTTACAGACAAGCTGTGACCGTCTCCGGGAGCTGCATGTGTC  
AGAGGTTTTACCGTTCATCACCAGAAACGCGCGAGGCAGCTGCGGTAAGGCTCATCAGC  
GTGGTTCGTGAAGCGATTACAGATGTCTGCCTGTTTCATCCGCGTCCAGCTCGTTGAGT  
TTCTCCAGAAGCGTTAATGTCTGGCTTCTGATAAAGCGGGCCATGTTAAGGGCGGTTTT  
TTCTGTTTTGGTCACTGATGCCTCCGTGTAAGGGGGATTTCTGTTTCATGGGGGTAATGA  
TACCGATGAAACGAGAGAGGATGCTCACGATACGGGTTACTGATGATGAACATGCCCG  
GTTACTGGAACGTTGTGAGGGTAAACAACCTGGCGGTATGGATGCGGCGGGACCAGAG  
AAAAATCACTCAGGGTCAATGCCAGCGCTTCGTTAATACAGATGTAGGTGTTCCACAG  
GGTAGCCAGCAGCATCCTGCGATGCAGATCCGGAACATAATGGTGACAGGGCGCTGACT  
TCCGCGTTTTCCAGACTTTACGAAACACGGAACCGAAGACCATTTCATGTTGTTGCTCAG  
GTGCGCAGACGTTTTGAGCAGCAGTCGCTTACGTTTCGCTCGCGTATCCGGTATTTCATT  
CTGCTAACAGTAAGGCAACCCCGCCAGCCTAGCCGGGTCTCAACGACAGGAGCACG  
ATCATGCGCACCCGTGGGGCCCGCATGCCGGCGATAATGGCCTGCTTCTCGCCGAAAC  
GTTTGGTGGCGGGACCAGTGACGAAGGCTTGAGCGAGGGCGTGCAAGATTCCGAATA  
CCGCAAGCGACAGGCCGATCATCGTCGCGCTCCAGCGAAAGCGGTCTCTCGCCGAAAT  
GACCCAGAGCGCTGCCGGCACCTGTCCTACGAGTTGCATGATAAAGAAGACAGTCATA  
AGTGCGGCGACGATAGTCATGCCCCGCGCCACCGGAAGGAGCTGACTGGGTTGAAG  
GCTCTCAAGGGCATCGGTTCGAGATCCCGGTGCCTAATGAGTGAGCTAACTTACATTA  
TTGCGTTGCGCTCACTGCCCGCTTTCCAGTCGGGAAACCTGTCGTGCCAGCTGCATTA  
ATGAATCGGCCAACGCGCGGGGAGAGGGCGGTTTGGCGTATTGGGCGCCAGGGTGGTTT  
TTCTTTTACCAGTGAGACGGGCAACAGCTGATTGCCCTTACCAGCCTGGCCCTGAGA  
GAGTTGCAGCAAGCGGTCCACGCTGGTTTTGCCCGAGCAGGCGAAATCCTGTTTGATG  
GTGGTTAACGGCGGGATATAACATGAGCTGTCTTCGGTATCGTCGTATCCCCTACC  
AGATATCCGCACCAACGCGCAGCCCGGACTCGGTAATGGCGCGCATTGCGCCAGCGC  
CATCTGATCGTTGGCAACCAGCATCGCAGTGGGAACGATGCCCTCATTACGATTTGC  
ATGGTTTGTGAAAACCGGACATGGCACTCCAGTCGCCTTCCCGTTCCGCTATCGGCT  
GAATTTGATTGCGAGTGAGATATTTATGCCAGCCAGCCAGACGCGAGACGCGCCGAGAC  
AGAACTTAATGGGCCCGCTAACAGCGCGATTTGCTGGTGACCCAATGCGACCAGATGC  
TCCACGCCAGTCGCGTACCGTCTTCATGGGAGAAAATAATACTGTTGATGGGTGTCT  
GGTCAGAGACATCAAGAAATAACGCCGGAACATTAGTGACAGGCAGCTTCCACAGCAAT  
GGCATCCTGGTTCATCCAGCGGATAGTTAATGATCAGCCCACTGACGCGTTGCGCGAGA  
AGATTGTGCACCGCCGCTTTACAGGCTTCGACGCCGCTTCGTTCTACCATCGACACCAC  
CACGCTGGCACCCAGTTGATCGGCGCGAGATTTAATCGCCGCGACAATTTGCGACGGC  
GCGTGCAGGGCCAGACTGGAGGTGGCAACGCCAATCAGCAACGACTGTTTGCCCGCCA  
GTTGTTGTGCCACGCGGTTGGGAATGTAATTCAGCTCCGCCATCGCCGCTTCCACTTTT  
TCCCGCGTTTTTCGCAGAAACGTGGCTGGCCTGGTTTACCACGCGGGAAACGGTCTGAT  
AAGAGACACCGGCATACTCTGCGACATCGTATAACGTTACTGTTTACATTACCACC  
CTGAATTGACTCTCTTCCGGGCGCTATCATGCCATACCGCGAAAGGTTTTGCGCCATT  
GATGGTGTCCGGGATCTCGACGCTCTCCCTTATGCGACTCCTGCATTAGGAAGCAGCC  
CAGTAGTAGGTTGAGGCCGTTGAGCACCGCCCGCAAGGAATGGTGATGCAAGGA  
GATGGCGCCCAACAGTCCCCCGGCCACGGGGCCTGCCACCATACCCACGCCGAAACAA  
GCGCTCATGAGCCCGAAGTGGCGAGCCCGATCTTCCCATCGGTGATGTGCGCGATAT  
AGGCGCCAGCAACCGCACCTGTGGCGCCGGTATGCCGGCCACGATGCGTCCGGCGT  
AGAGGATCGAGATCTCGATCCCGCGAAATTAATACGACTCACTATAGGGGAATTGTGA  
GCGGATAACAATTTCCCTCTAGAAATAATTTGTTTAACTTTAAGAAGGAGATATACCA  
TGGGCAGCAGCCATCATCATCATCACAGCAGCGCCCTGGTGCCGCGCGGCAGCCA  
TATGAACGCAACGACAACGTGGTGATTGTTGGCACTGGTCTGGCTGGCGTTGAAGTT

GCGTTTGGTCTGCGTGCAAGCGGCTGGGAAGGTAACATCCGCCTGGTGGGTGATGCGA  
CTGTTATTCCGCACCACCTGCCGCCGCTGTCTAAAGCGTACCTGGCGGGCAAGGCGAC  
TGCGGAGTCTCTGTACCTGCGCACTCCGGATGCTTACGCGGCTCAGAACATCCAGCTG  
CTGGGCGGTACCCAGGTTACCGCGATTAACCGTGACCGTCAGCAGGTGATTCTGTCTG  
ATGGCCGTGCACTGGATTATGATCGTCTGGTGTGGCAACTGGCGGTCGTCGCCGTCC  
GCTGCCGGTGGCTAGCGGCGCTGTTGGTAAAGCAAACAACCTCCGTTATCTGCGTACC  
CTGGAAGACGCAGAATGCATCCGTCGCCAGCTGATTGCGGACAACCGTCTGGTTGTTA  
TCGGTGGCGGCTACATCGGTCTGGAGGTTGCTGCTACTGCGATCAAAGCGAACATGCA  
CGTGACTCTGCTGGACACTGCTGCGCGTGTCTGGAACGTGTGACTGCTCCGCCGGTG  
AGCGCATTCTACGAGCATCTGCACCGGAAGCTGGTGTGGACATTCGTAAGGTACTC  
AGGTTTGGCGCTTTGAAAATGTCTACCGATCAGCAGAAAAGTTACTGCGGTTCTGTGCGA  
AGACGGCACTCGTCTGCCGGCTGATCTGGTTATTGCGGGTATTGGCCTGATCCCGAAC  
TGCGAACTGGCATCCGCAGCGGGCCTGCAGGTTGACAACGGCATCGTGATCAACGAGC  
ACATGCAGACTAGCGATCCGCTGATTATGGCAGTGGGCGATTGTGCGCGTTTCCACTC  
TCAGCTGTATGACCGTTGGGTTTCGCATCGAAAGCGTGCCGAACGCGCTGGAACAGGCG  
CGTAAAATCGCAGCAATCCTGTGCGGTAAGTTCCGCGTGACGAGGCGGCTCCGTGGT  
TTTGGAGCGACCAGTATGAAAATCGGCCTGAAAATGGTGGGCCTGTCCGAAGGTTACGA  
CCGTATCATCGTTCGTGGCTCTCTGGCGCAGCCGACTTCTCTGTTTTCTATCTGCAGG  
GTGATCGCGTTCGTCAGTTGACACTGTGAACCGTCCGGTGGAAATTAACCAGTCTAA  
ACAGATCATTACTGATCGCCTGCCGGTTGAGCCGAACCTGCTGGGTGACGAATCTGTG  
CCGCTGAAGGAGATCATCGCGGCTGCAAAAGCTGAACTGTCTTCTGCGTGAGGATCCG  
AATTCGAGCTCCGTCGACAAGCTTGCGGCCGCACTCGAGCACCACCACCACCCT  
GAGATCCGGCTGCTAACAAAGCCCGAAAGGAAGCTGAGTTGGCTGCTGCCACCGCTGA  
GCAATAACTAGCATAACCCCTTGGGGCCTCTAAACGGGTCTTGAGGGGTTTTTTGCTG  
AAAGGAGGAACTATATCCGGAT



## **VITA**

Akbota Kakimova entered Eurasian National University named after L.N.Gumilev, Astana, Kazakhstan, in September 2010 and in July 2014 received the degree of Bachelor of Science in Biotechnology. In July 2016 she received the degree of Master of Science in Biotechnology from Eurasian National University named after L.N.Gumilev.